UNIVERSITY OF SASSARI

DOCTORAL THESIS

The role of forests in soil protection: root reinforcement and slope stability evaluation at different analysis scales.

Author:
Ilenia MURGIA

Tutor:
Gian Franco CAPRA

A thesis submitted in fulfillment of the requirements for the degree of Doctor of Philosophy

in the

Department of Architecture, Design and Urban Planning

July 6, 2022

La borsa di dottorato è stata cofinanziata con risorse del
Programma Operativo Nazionale Ricerca e Innovazione 2014-2020 (CCI 2014IT16M2OP005),
Fondo Sociale Europeo, Azione I.1 “Dottorati Innovativi con caratterizzazione Industriale”

UNIONE EUROPEA
Fondo Sociale Europeo

Ministero dell'Università e della Ricerca

Declaration of Authorship

I, Ilenia MURGIA, declare that this thesis titled, "The role of forests in soil protection: root reinforcement and slope stability evaluation at different analysis scales." and the work presented in it are my own. I confirm that:

- This work was done wholly or mainly while in candidature for a research degree at this University.
- Where any part of this thesis has previously been submitted for a degree or any other qualification at this University or any other institution, this has been clearly stated.
- Where I have consulted the published work of others, this is always clearly attributed.
- Where I have quoted from the work of others, the source is always given. With the exception of such quotations, this thesis is entirely my own work.
- I have acknowledged all main sources of help.
- Where the thesis is based on work done by myself jointly with others, I have made clear exactly what was done by others and what I have contributed myself.

Signed: 

Date: 06 July 2022

Acknowledgements

I thank the School of Architecture and Environment, particularly Prof. Fabio Bacchini and Prof. Vincenzo Pascucci.

A special thanks go to those who have followed me step by step during this journey. In particular, to Filippo Giadrossich for having made me passionate about this research field and for having constantly stimulated and motivated me. To Massimiliano Schwarz and Denis Cohen for having allowed me to be part of their ideas and projects and welcomed me into their research group. To Marco Niccolini for having patiently followed me and explained the company's world, for having contacted me in the realization of the forestry plans. To all of you, I cannot thank you enough!

I thank Irene, Antonio, Simone, Ludmilla, and Elisa, essential consultants, colleagues, and friends.

I thank Romain, Nicolas, Elena, Barbara, Denise, Giorgio, Serena, and all my *ladies* for making this travel full of wonderful new friendships.

I thank my mom for being the strongest and most courageous woman I know.

I thank Andrea for having been fundamental and always supporting and stimulating me.

I thank all the people who were there and are still there to remind me that I can count on each of them every day.

To Ilenia

UNIVERSITY OF SASSARI

Abstract

Department of Architecture, Design and Urban Planning

Doctor of Philosophy

The role of forests in soil protection: root reinforcement and slope stability evaluation at different analysis scales.

by Ilenia MURGIA

Rainfall-induced shallow landslides are natural hazards with potential high impact to the human and natural environment. Since the frequency and intensity of critical rainfall events are expected to increase in the future due to climate change, the escalation of these critical events will produce expected consequences. For this reason, mitigation strategies must be identified to protect natural and man-made environments. There is worldwide interest in developing reliable slope stability models capable of locating areas most susceptible to landslides, and identifying the correct management of direct protection forest in order to optimize their function. To adequately evaluate the effect of vegetation on soil stability, root reinforcement models must be able to provide values applicable and integrable into the slope stability models.

This work promotes the use of applications developed from recent scientific studies, available for both academic and professional fields. After analyzing state of the art concerning slope stability and root reinforcement models, three case studies are presented showing different spatial scale analyses and based on the use of three software: RBM++ for tree scale, SOSlope for local scale, and SlideforMAP for regional scale.

Contents

List of Figures

List of Tables

List of Acronyms

BRR Basal Root Reinforcement

DEM Discrete Element Method

DTM Digital Terrain Model

DSM Digital Surface Model

FAIR Findability, Accessibility, Interoperability, and Reuse

FBM Fiber Bundle Model

FDEM combined Finite-Discrete Element Method

FEM Finite Element Method

FInT Find Individual Trees

FoS Factor of Safety

GIS Geographic Information System

GUI Graphical User Interface

ISM Infinite Slope Method

LA Limit Analysis

LEMs Limit Equilibrium Methods

LRR Lateral Root Reinforcement

MS Method of Slices

NMs Numerical analysis Methods

PFA Piano Forestale Aziendale

PMs Physically-based models

RBM Root Bundle Model

RBMw Root Bundle Model with Weibull survival function

RR Root Reinforcement

RRMs Root Reinforcement Models

SIFRAP Landslide Phenomena Information System of Piedmont

SL Shallow Landslide

SLs Shallow Landslides

SSDMs Slope Stability Physically-based Deterministic Models

SSPMs Slope Stability Physically-based Probabilistic Models

SSM Slope Stability Model

SSMs Slope Stability Models

TRAMM Triggering of RApid Mass Movements

WWM Wu-or-Waldron Method

USCS Unified Soil Classification System

Chapter 1

Introduction

Rainfall-induced Shallow Landslides (SLs) are among the most common gravitational mass movements on natural and artificial slopes, acting as landscape agents of sediment transfer and erosion. However, SLs are also potential hazards with well-known consequences that affect both the human environment, causing loss of life and damage to structures and infrastructures (Schwarz et al., 2010; Askarinejad, 2013; Dorren and Schwarz, 2016; Ran et al., 2018), and the natural environment, shaping many landscapes worldwide (Istanbulluoglu, 2005) and affecting the agro-forestry production in general (Jones et al., 2008) (Figure 1.1). Since the frequency and intensity of critical rainfall events are expected to increase in the future due to more unstable air masses and significant magnitude storms associated with climate change (Gariano et al., 2017), the escalation of previously mentioned SLs-induced consequences is also expected (Crozier, 2010). As such, mitigation strategies must be identified to protect natural and man-made environments.

Shallow Landslide (SL) susceptibility depends on several environmental factors such as terrain and soil physical properties, hydrological regimes, and land use. Among these factors, land use dramatically influences landslide susceptibility, showing a crucial stabilizing effect due to the Root Reinforcement (RR) activation in case of vegetation presence (Glade, 2003; Sidle and Ochiai, 2006; Persichillo et al., 2017). In the specific case of forested areas, several studies confirm this effect, i.e., as the forested surface increases, the presence of unstable areas decreases and, consequently, the number of SL events (Montgomery et al., 2000; Reichenbach et al., 2014). However, considering that vegetation conditions may change rapidly in space and time, it is difficult to assess this positive effect over large areas and adequately consider its contribution to predicting potential SLs. Knowing and assessing land use changes, specifically in vegetation cover, is critical when using Slope Stability Models (SSMs).

There is worldwide interest in developing reliable SSMs capable of locating areas most susceptible to landslides in the context of urban, environmental, and landscape planning activities (Moos et al., 2018). The accessibility and detail of data required for slope stability assessment have improved significantly in recent decades, consequently refining the quality of Slope Stability Model (SSM) results based on appropriate assumptions and modeling approaches. One example is implementing detailed information of above-ground forest structure obtained by remote sensing

(A) Shallow landslide on the provincial road 310 of Pratovecchio-Stia village (Tuscany, Italy)

(B) Shallow landslide on the hill (Bitti village, Sardinia, Italy)

FIGURE 1.1: Shallow landslides affect human and natural environments. In the first picture (A), a shallow landslide occurred on the downslope side of a main infrastructure. This road tract was studied and presented at the EGU general assembly (Murgia et al., 2021). The second picture (B) shows some landslide events that occurred after heavy rainfall in a rural area.

techniques, for example, through aerial and terrestrial laser scanning or structure for motion (Camarretta et al., 2020; Neuville et al., 2021).

The application of SSMs has proven valuable and necessary in various contexts. One application is the development of hazard maps of SL susceptibility and quantifying the frequency with which they occur (scenario-based). A fundamental requirement for using such maps in the planning process is their constant updating in case of significant landscape changes, such as topography modifications due to human activities (construction of infrastructure, mining, etc.). However, the stability assessment in this type of analysis often neglects the vegetation presence and contribution. SSMs are also valuable in determining protective forest by identifying areas where direct protection for structures and infrastructure is evident (e.g., *Silvaprotect project in Switzerland* (2016), for the identification and management of direct protection forests). Additionally, combining the SL risk analysis and estimated RR values it is possible to evaluate which silvicultural measures are appropriate to improve and ensure the stabilizing effect of forests. The use of SSMs allows for detailed forest management on critical areas requiring priority action, e.g., on steep slopes or channels subject to detention and transport of large woody debris, or in forests subject to alteration caused by disturbance factors, e.g., forest fires, storms, pathogens (Vergani et al., 2016). At local scales, SSMs support the design and sizing of technical protection measures, as well as the cost-benefit analysis of soil bio-engineering measures (Bischetti et al., 2021).

All these applications demonstrate the central role of forests, and vegetation in general, in the mitigation of SL events (Stokes et al., 2014), defining SSMs as valuable tools for the management and, eventually, improvement of soil protection (Figure 1.2). Forest mitigation effects are central in slope stability, as well as to riparian ecosystems (Pollen and Simon, 2005; Hubble et al., 2010) and urban environments (Stokes et al., 2014; Mickovski, 2021), degraded lands (Ji et al., 2020; Zhu et al., 2017), and agricultural systems (Loades et al., 2010).

In order to adequately evaluate the effect of vegetation on soil stability, the Root Reinforcement Models (RRMs) realized for the RR estimation must be able to provide values that are applicable and integrable into the SSMs, as well as realistic. However, since they are generally complex computational models written in programming languages (e.g., R or MATLAB), they are not straightforward. For this reason, simplified RRMs are often preferred to complex ones even if the latter are much more able to provide accurate estimations. Therefore, in the case of RRMs, it is necessary to share and promote the use of appropriate ones by making them available to anyone through easily usable tools, such as software.

In this context, the international association for natural hazards risk management (ecorisQ) developed several tools for evaluating the management of natural hazards. One of the main objectives of this research group is to develop applications from recent scientific research results and make them available in both academic and professional fields. The complex mathematical models created to describe and analyze

(A) Shallow landslide on the forest (Pratovecchio-Stia village, Tuscany, Italy)

(B) Shallow landslide on the forest (Bitti village, Sardinia, Italy)

FIGURE 1.2: In the two pictures, it is possible to observe roots that have counteracted the landslide detachment in the upper part of the unstable soil mass. In particular, in picture (B) roots are still active and stretched to compensate for the further movement of the soil.

soil stability hydro-mechanical phenomena were converted into software equipped with an easy-to-use Graphical User Interface (GUI), aiming to achieve their primary goal. Following the ecorisQ approach and aim, this research project focused on upgrading, validating, and promoting innovative tools to support land planning and forest management, starting from a single tree scale to a regional scale of analysis.

The research project In order to provide an overview of modeling SLs, the chapter 2 shows a review of SSMs that consider the effect of vegetation by implementing different RRMs. This review is currently accepted for publication in Elsevier's Ecological Engineering journal as part of the special issue of the Soil, Bio- and Eco-Engineering conference (Murgia et al., Accepted). This framing provides a context for the research work described in subsequent chapters and the importance of developing and using innovative tools for slope stability analysis.

The following are three software applied to the three main case studies addressed in this research project:

- the development and application of RBM++ software to quantify values of RR mechanical parameters of the Japanese cedar (*Cryptomeria japonica*, (Thunb. ex L.f.) D.Don). This tree species is often placed in sloping areas and used as a nature-based solution for soil stability interventions;
- the application of SOSlope software for a back-analysis of an artificially induced SL in Rüdlingen (Switzerland), aiming to reconstruct the hydro-mechanical conditions that led to its triggering. Considering the availability of detailed measurements recorded during the experiment, it was possible to identify the potentials and limitations of SOSlope;
- the application of SlideforMAP software in the Monviso forestry plan (Italy), aiming to identify and validate a method to assess the SL probability and determine unstable areas where RR should or could be improved through silvicultural interventions.

These three case studies represent the three main scales of analysis (Figure 1.3) of the effect of roots on soil protection, allowing for an integrated analysis of their application.

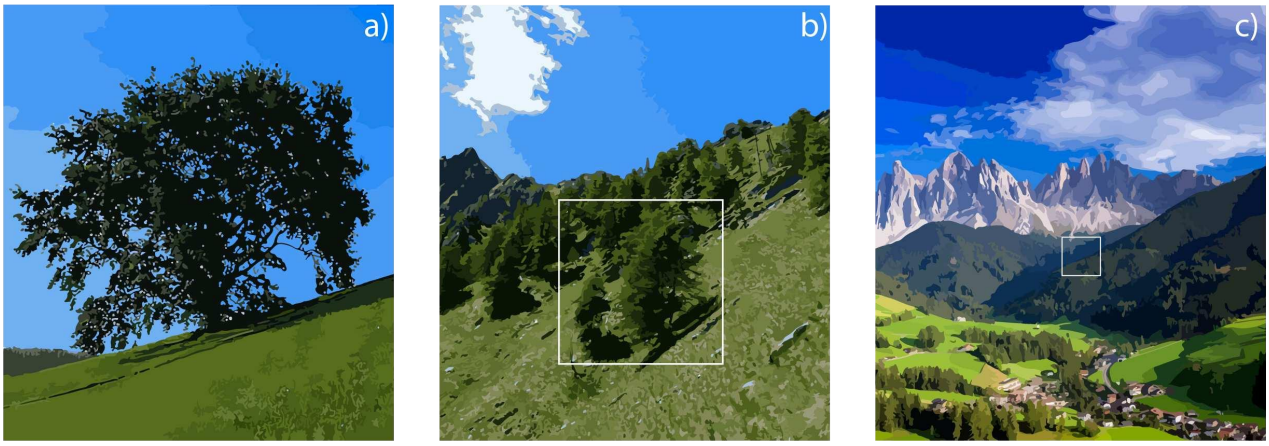

FIGURE 1.3: Figure shows the three analysis scale considered in the research project: a) tree analysis scale, to evaluate how the root reinforcement of a single tree changes in space; b) local analysis scale, to evaluate the influence of root reinforcement in the hydro-mechanical dynamics of slope stability; and c) regional analysis scale,to verify and identify forest areas that should acquire a direct soil protection function as a priority.

Chapter 2

The state of the art of slope stability and root reinforcement models

Landslide processes involve the downslope movement of soil or rock under the effect of gravity (*United State Geological Survey, USGS* 2004). Shallow landslides SLs are a subset of these processes that usually involve soil masses less than 2 m thick (Phillips et al., 2021), generally sliding translationally over the failure surface at or near discontinuities in the soil profile or the bedrock contact. SLs are of interest to several fields research related to soil science (Tofani et al., 2017) and this multidisciplinarity involves observing the same process from different perspectives.

Generally, slope stability is defined as an equilibrium condition of the soil mass able to resist its gravity-driven downslope movement that should be maintained despite changes in hydrologic and mechanical conditions (e.g., increased soil weight due to rainwater infiltration). The loss of stability describes the situation in which the equilibrium condition failed, favoring the SL triggering. However, also the slope stability definition takes on different meanings depending on the scope of study and the user's main aims (McColl, 2015). Generally speaking, it considers i) the disposition factors that determine the stability conditions of the slope; ii) how a triggering event (e.g., rainfall) changes initial stability conditions; and iii) how changes in soil properties promote the exceeding of the critical failure threshold and SL triggering. In slope stability analysis, boundary conditions are defined by considering environmental characteristics (i.e., morphology, lithology, pedology, and vegetation cover) and evaluating their influence on the triggering hydrological and mechanical processes (Sidle and Bogaard, 2016).

The most common indicator used to quantify slope stability is the Factor of Safety (FoS) obtained by the ratio of stabilizing forces (i.e., soil shear strength and root reinforcement) to destabilizing forces (i.e., the gravitational driving force of the soil mass). Slopes are typically considered stable when FoS is ≥ 1; slope failure occurs at FoS < 1. Temporal changes in the FoS are mainly influenced by factors acting over shorter or longer periods such as i) soil suction and pore water pressure during rainfall events that result in short-term changes in, ii) water content varying

due to seasonal conditions, specifically considering subsurface fluxes and water loss by evapotranspiration, iii) vegetation altering soil physicochemical characteristics through root growth and decay, and iv) soil depth influenced by the intensity of the pedogenesis process (Ziemer, 1981; Liang et al., 2007; Ghestem et al., 2011). Roots introduce complexity in evaluating vegetated slope stability and FoS calculations, affecting the accuracy of the analysis.

RR is defined as the additional force provided by roots opposing the soil mass deformation and displacement under gravity. RR can be distinguished according to the root stress experienced by orientation of the shear plane (i.e. horizontal or vertical). Field observations validated by field and laboratory tests have shown the activation of root stress in tension, compression, bending, and shear mechanisms (Zhou et al., 1998; Docker and Hubble, 2008; Schwarz et al., 2011; Cohen and Schwarz, 2017; Schwarz et al., 2015). These three types of stresses assume fundamental importance in the distribution of forces activated during SL initiation (Schwarz et al., 2015). The RR mechanism can distinguished in i) basal RR provided by roots growing through an horizontal shear plane (i.e. approximately parallel tot he soil surface) and ii) lateral RR, provided by roots growing through a vertical shear plane. It is relevant to highlight that the basal RR, if present, is the most efficient reinforcement mechanism (Cohen and Schwarz, 2017) since it guarantees a root anchoring effect to the deeper and stable soil layers. However, the activation and intensity triggered by the basal RR depend on both the root system morphology and the thickness of the rooted zone.

2.1 Empirical Knowledge

Critical information on understanding shallow landslide (SL) processes is briefly reviewed, developing the context to discuss their implementation in modeling approaches. The goal is to discuss the principal hydrologic processes that promote the initiation of SLs and the mechanical processes resulting from changes in soil water conditions.

2.1.1 Hydrological processes

In rainfall-induced SLs, hydrological processes are generally recognized as the leading causes of soil shear strength loss by increasing soil water content and pore water pressure (Lehmann et al., 2013). Hydrological effects depend strongly on the water content antecedent the triggering rainfall event and on seasonal evapotranspiration processes, thus are time-dependent (Chirico et al., 2013; Arnone et al., 2016a). For this reason, it is necessary to consider these dynamics in slope stability models for the factor of safety quantification.

It is well-known that the increase of soil water content can promote i) the development of subsurface water movement, e.g., infiltration and flows, which influence

both soil characteristics and hydrological behavior; and ii) the development of positive pore water pressures under saturated conditions (Bishop, 1955; Morgenstern and Price, 1965), and iii) decrease the negative pore water pressure (toward zero, or reduce the matric suction) under unsaturated conditions.

Rainwater infiltration causes changes in soil moisture conditions, which is strongly influenced by environmental variables such as soil porosity or transmissivity. Changes in soil moisture affect infiltration rate, generally fast at the onset of rainfall reducing as soil moisture increases, and the water movement through the soil. Water flow always in the negative pressure gradient, both in unsaturated and saturated conditions (i.e. Darcy's law), but in the particular case of saturated soils, water movement occurs mainly driven by the forces of gravity (Nimmo, 2009).

Reaching soil saturation occurs through subsurface flows, generally distinguished into the matric and preferential flows path. The unsaturated diffuse flow consists of water movement between pores, resulting in a uniform moisture condition throughout the soil. Gravity force and matric pressure gradients are the driving factors, and their effects depend on soil characteristics, such as soil permeability, porosity, etc. Additional water supply promotes water movement by overland flow or through preferential flows, developed in the macropores and spaces created by the pedofauna and plant roots. Nimmo (2009) pointed out the existence of three basic modes of preferential flow i) flow through macropores; ii) funneled flow, also called deflected or focused flow, consisting of flow deviation caused by the presence of obstacles that promotes water accumulation in adjacent areas; and iii) unsteady conductive flow. However, in some cases, preferential flow promotes soil drainage by limiting pore pressure development during storms (Penna et al., 2015; Bogaard and Greco, 2016).

Preferential flow development is crucial in SL initiation processes. For example, several studies have shown a central role for flows developed in the presence of shallow bedrock fractures (Reneau and Dietrich, 1987; Montgomery and Buffington, 1997). Exfiltration is the process in which the development of high pressures at the soil-bedrock interface is caused by the connection of some bedrock fractures to areas of hydraulic recharge (Montgomery et al., 2002; Askarinejad and Springman, 2021). This process is strongly influenced by rainfall duration and intensity, as well as by the morphological and geological characteristics of the area, promoting the occurrence of SLs on planar and convex slopes, as well as differences in the timing and mode of SL initiation in topographically similar areas (Montgomery et al., 2002).

As a result of water infiltration, the increase in soil weight, which is considered as mechanical loading (Lehmann et al., 2013), occurs. This new condition could be critical in very steep areas where the destabilizing loads promote the unstable mass sliding driven by the gravity force (Lepore et al., 2013; Shao et al., 2016).

Pore water develops a positive pressure, recognized as the main effect of rainfall-induced SLs. The main consequence of the positive pore pressures development is reducing the effective stresses in the soil resulting in a shear strength reduction.

Lehmann et al. (2013) observed that also hydrological connectivity is a critical process that can promote SLs triggering in large interconnected areas.

Roots influence infiltration processes by pores formed by plant roots and creating preferential drainage pathways (Beven and Germann, 1982). In addition, roots reduce soil moisture through evapotranspiration depending on the time scale of analysis (Arnone et al., 2016a). In the short term, when considering the influence of this process at the slope scale, it assumes less influence if compared to the magnitude of the root mechanical contribution to ensuring stability (Sidle and Bogaard, 2016). Roots hydrological effects are more influential in the hydrologic balance of an entire basin, draining and regulating flows over large areas (Cohen and Schwarz, 2017).

All hydrologic processes are influenced by soil depth, considered a critical control parameter for assessing how a saturated condition can be achieved. The combination with soil physico-chemical characteristics and the groundwater table height determine the water storage capacity. However, the measurement of soil depth still presents some difficulties, particularly in knowing its variability in space. To overcome this problem, some of the most popular hydrological models calculate flows considering surface topography and developing terrain indices based on the digital terrain model (Borga et al., 2004; Lanni et al., 2011), computed with algorithms in Geographic Information System (GIS) environment (e.g., Montgomery and Dietrich, 1994; Pack et al., 1998; Baum et al., 2005). Among these indices, the most widely used in slope stability modeling is the topographic wetness index introduced by Kirkby and Weyman (1972).

The evaluation of hydrological processes, mainly predicting through models how pore water pressure varies in response to precipitation events, is fundamental to evaluate their influence on mechanical processes and calculate the probability of SLs event.

2.1.2 Mechanical processes

The relationship between driving forces, such as gravity, soil particle friction, and pore water pressure, result in the local loss of shear strength and thus the initiation of SL. This central concept can be incorporated into the Mohr-Coulomb rupture criterion that defines the shear strength of saturated soils. Terzaghi, 1943, with his theory of effective stress, identifies the difference between total stress and positive pore water pressure as the leading cause of changes in soil mechanical behavior and the consequent movement of the unstable mass on the slip plane.

Through root reinforcement (RR), vegetation provides greater resistance to soil movement due to root-soil friction, greater cohesion, and stiffness of the soil mantle. The contribution of RR in increasing soil cohesion was highlighted since the 1970s (Gray, 1974). This effect was analyzed in both laboratory tests, using standard Casagrande shear box (Giadrossich et al., 2010), large machines reproducing the same principle (Yildiz et al., 2018), and field experiments (O'Loughlin, 1972; Ekanayake et al., 1997). Giadrossich et al., 2017 reviewed methods for evaluating

and quantifying RR, where the discriminant is the consideration of soil-root interaction and the behavior of the root itself in the final output. A key aspect discussed concerns the better accuracy of data measured in the field than those obtained in the laboratory. Field tests preserve the complexity of the soil-root system, which is partly lost in laboratory reconstructions.

The geometry and conceptual representation of SL have led to a distinction between Basal Root Reinforcement (BRR) and Lateral Root Reinforcement (LRR). BRR acts on the basal shear surface of the SL and would be the most effective reinforcement mechanism if uniformly distributed along with the profile (Cohen and Schwarz, 2017). However, the progressive reduction in root number, with increasing soil depth, affects the intensity of RR (Swanson and Swanston, 1977; Schmidt, 2001; Rickli and Graf, 2009; Giadrossich et al., 2019). Some studies (Schmidt, 2001; Montgomery et al., 2009; Schwarz et al., 2010) highlighted the need to also consider LRR as a stabilizing mechanism that can be activated in the lateral sides of potential the SL and able to influence their size (Reneau and Dietrich, 1987; Schmidt et al., 2001; Roering et al., 2003; Schwarz et al., 2010). The magnitude of the LRR depends on the spatial distribution of the roots (Cohen and Schwarz, 2017; Giadrossich et al., 2020) and the sliding mass deformation (Zhou et al., 1998; Giadrossich et al., 2019), activating simultaneously along all sides in case of the soil mass rigid behavior (Zhou et al., 1998; Giadrossich et al., 2019), or progressively in case of differential deformation.

Schwarz et al. (2015) have schematically reconstructed the progressive triggering of rainfall-induced SLs and the corresponding activation of the RR. Due to the increase in pore water pressure and subsequent reduction in soil suction, a local loss of shear strength occurs, resulting in downslope movement of the sliding mass. This condition is evident in the field with the development of a tension crack at the top and sides, where tension-activated roots can be observed to counteract the failure. Simultaneously, lateral compressive stresses develop in the downslope zone due to root compression and passive earth pressure. If the cumulative lateral stress exceeds the critical value, the soil gives way by developing a failure surface. This condition is similar to the passive soil pressure conditions (Kramer, 1996). Considering the root compression, this study observed that it does not affect overall soil strength but increases stiffness and acts as a delay factor in the initiation of SLs (Schwarz et al., 2015).

Passive soil pressure is still poorly considered in stability assessment. Most geotechnical parameter studies in the literature focus on soil shear strength, while few consider passive wedge of shearing soil. Field observations have shown that the triggering mechanisms of SLs are characterized by differential deformations that show localized activation of zones in tension, shear, and compression (Schwarz et al., 2015; Cohen and Schwarz, 2017; Cislaghi et al., 2019). In our knowledge, the study of Burroughs (1985) is the first effort to integrate ground water response, soil shear strength, and root strength in slope stability modeling.

Assessing how soil mechanical processes, and in particular RR, change over

space and time is still complex and nowadays done based on a limited number of samples which are averaged according to the reference scale of the analysis (Montrasio et al., 2011; Baum and Godt, 2010).

2.2 Slope stability modeling approaches

Slope stability models (SSMs) are based on three main approaches for quantifying stability conditions: conceptual, statistical, and Physically-based models (PMs), which can be more specifically divided into Slope Stability Physically-based Deterministic Models (SSDMs) and Slope Stability Physically-based Probabilistic Models (SSPMs). Studies on shallow landslide (SLs) triggering based on conceptual and statistical approaches are still few, according to a review by Reichenbach et al., 2018. The analysis of stability in vegetated slopes, thus considering root reinforcement (RR), is generally performed through the physically-based approach (Figure 2.1).

However, to provide a complete picture of the current state of SSMs, the conceptual and statistical approaches will also be briefly described in 2.2.1 and 2.2.2.

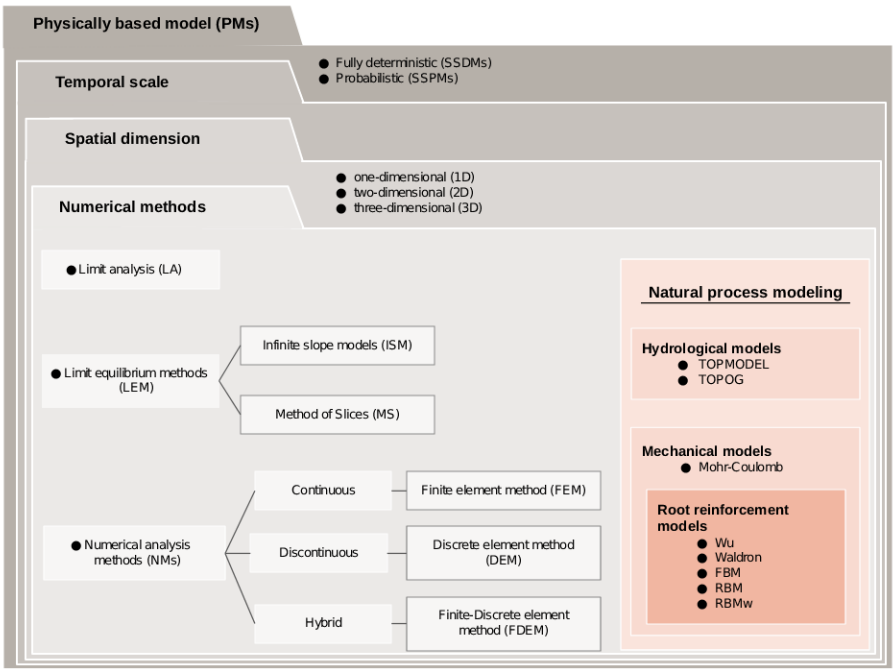

FIGURE 2.1: Physically-based models, both fully deterministic and probabilistic, can implement temporal scale combined with different spatial dimensions and numerical methods to simulate main hydrological and mechanical processes, including the root reinforcement.

2.2.1 Conceptual approaches on slope stability analysis

Conceptual models aim to provide a simplified methodology for estimating the FoS changes in space and time (Piegari et al., 2006), identifying *ad hoc* empirical combinations of factors determining instability dynamics (Segre et al., 1995), and using simplified mathematical equations adapted to real data that cannot always be measured

(D'Ambrosio et al., 2003). Studies have demonstrated the ability of some models to reproduce complex dynamics that occur in large and medium-sized SLs, for example, through the cellular automaton model. The original cellular automaton model (Segre et al., 1995) aimed to solve the overestimating problems of the frequency of large SLs events highlighted by the use of power-law statistics. This approach does not consider the temporal resolution and hence different timing of triggering small events, tending instead to merge them into a single large event. A solution has been proposed by the model of Bak et al. (1988), better known as the sandpile model, by developing cellular automatons based on the self-organized criticality approach. This simple method considers progressive slope failure, with scalable results for more realistic analysis. The main features of the sandpile model are the discretization of the system into elements identified by two- or three-dimensional cells, and the application for each cell of specific evolution rules (i.e., triggering, movement, and stopping). Hergarten (2003) identified some critical issues of this model related to the scalability of the obtained results, proposing a solution through the use of the spring-block model of Olami et al. (1992) (Hergarten, 2013). The spring-block model discretizes the slope into blocks based on the digital terrain model grid (Bak et al., 1988). Each block represents the unit of FoS estimation and is connected to neighboring blocks and a rigid guide plate through elastic bonds that simulate the activated forces on the slope. When a block loses stability, it is displaced, causing the neighboring blocks to move. This model implies dissipation, i.e., the potential energy stored gradually in the elastic bonds is partly transferred to the guide plate and partly lost by the system (Liucci et al., 2017). The development of new cellular automatons has continued over the years: Pelletier et al. (1997) and Piegari et al. (2006) have produced a model that considers topography and soil water content; Segre et al. (1995), Avolio et al. (2000), and D'Ambrosio et al. (2003) have developed alternatives to cellular automaton models with self-organized criticality approach.

2.2.2 Statistical approaches on slope stability analysis

The statistical models are based on two key assumptions i) future SLs may occur in the same areas susceptible to landslides in the past, and ii) the parameters needed for stability analysis, i.e., mechanical and hydrological information, are derived from the digital terrain model (Guzzetti et al., 2000; Ruette et al., 2011). Environmental variables considered include slope gradient and curvature, contributing area and curvature, soil and bedrock types, and, only in a few cases, the effect of vegetation. Ruette et al. (2011) consider four explanatory variables of which the vegetation type is a binary choice between grassland and forest. In statistical models, vegetation is considered a variable that includes all direct and indirect effects on slope stability.

In order to quantify the correlation between precipitation duration-intensity and the probability of SLs occurrence, inventories (Malamud et al., 2004; Ruette et al., 2013), and global case studies (Guzzetti et al., 2008) are considered. The statistical coefficient representing this correlation is estimated by different methods, the best

known of which are: i) bivariate and multivariate analysis (Carrara, 1983; Süzen and Doyuran, 2004b), also called logical regression (Hosmer and Lemeshow, 2000; Süzen and Doyuran, 2004a), through the consideration of explanatory variables classified in some discrete classes (e.g., classes of soil types, ranges of slope angles, etc.), ii) classification and regression trees (Nefeslioglu et al., 2009; Yeon et al., 2010) and random forests (Breiman et al., 1984), recursively analyze information through the graphical realization of a decision tree that allows the identification of values that best represent a given attribute (Nefeslioglu et al., 2009; Felicísimo et al., 2013); iii) support vector machines (Vapnik, 2013) proceeds through nonlinear transformations of variables and binary identification of the probability SLs occur (Brenning, 2005); iv) artificial neural networks (Brenning, 2005; Falaschi et al., 2009; Arnone et al., 2014; Koopialipoor et al., 2019) based on complex interactions between units, also called neurons, through rules that simulate SLs dynamics. Some studies have demonstrated good accuracy of logistic regression (Süzen and Doyuran, 2004b; Ayalew and Yamagishi, 2005; Nandi and Shakoor, 2010), comparable to more complex neural network methods (Nefeslioglu et al., 2008; Yilmaz, 2009; Rossi et al., 2010). In conclusion, Ruette et al. (2011) argued for the possibility, through statistical methods, of identifying key factors controlling the triggering of SLs to be considered in more detailed analyses with physically-based models.

Physically-based models PMs generally combine a hydrological module to quantify the pore soil water pressure varying over space and time and a mechanical module to evaluate soil mechanical parameters changing due to hydrological response (Capparelli and Versace, 2011). The combined analysis of the processes provides numerical values indicative of the slope stability condition and its failure probability.

PMs analyze morphological, hydro-mechanical, and meteorological information that influence SLs triggering (Kim et al., 2014). For example, these models evaluate the susceptibility of SLs by extrapolating the following data from the digital terrain model: i) slope and altitude (Kim et al., 2014); ii) soil properties, depth, and soil water flows.

PMs mainly consist of i) fully deterministic models, entirely based on measured or estimated parameters, and ii) probabilistic models, which consider a probability distribution, both in terms of spatial distribution and uncertainty of the parameters considered.

The reliability of the analysis performed with PMs depends strongly on the type of input parameters measured or estimated, but also on the degree of complexity implemented in PMs for the simulation and modeling of the interactions of underlying processes. In particular, in the stability analysis on vegetated slopes, adding a fixed value of root cohesion to soil cohesion is potentially less plausible than an analysis based on estimating the variability of diameter and number of root-bundles in the soil. However, another aspect of evaluating the accuracy is the objective of the analysis.

PMs are based on numerical models for the reconstruction and evaluation of the

investigated slope, considering a spatial and, in some cases, temporal dimension for stability assessment.

2.2.3 Physically-based modeling approaches

Physically-based models PMs generally combine a hydrological module to quantify the pore soil water pressure varying over space and time and a mechanical module to evaluate soil mechanical parameters changing due to hydrological response (Capparelli and Versace, 2011). The combined analysis of the processes provides numerical values indicative of the slope stability condition and its failure probability.

PMs analyze morphological, hydro-mechanical, and meteorological information that influence SLs triggering (Kim et al., 2014). For example, these models evaluate the susceptibility of SLs by extrapolating the following data from the digital terrain model: i) slope and altitude (Kim et al., 2014); ii) soil properties, depth, and soil water flows.

PMs mainly consist of i) fully deterministic models, entirely based on measured or estimated parameters, and ii) probabilistic models, which consider a probability distribution, both in terms of spatial distribution and uncertainty of the parameters considered.

The reliability of the analysis performed with PMs depends strongly on the type of input parameters measured or estimated, but also on the degree of complexity implemented in PMs for the simulation and modeling of the interactions of underlying processes. In particular, in the stability analysis on vegetated slopes, adding a fixed value of root cohesion to soil cohesion is potentially less plausible than an analysis based on estimating the variability of diameter and number of root-bundles in the soil. However, another aspect of evaluating the accuracy is the objective of the analysis.

PMs are based on numerical models for the reconstruction and evaluation of the investigated slope, considering a spatial and, in some cases, temporal dimension for stability assessment.

2.2.4 Numerical methods for slope modeling

The factor of safety (FoS) calculation can be made by models based on different analysis methods, from limit analysis to the widely used limit equilibrium methods, and finally, more complex numerical or analytical approaches (finite element method; discrete element method).

Limit analysis Limit Analysis (LA) assumes that the soil mass has a perfectly plastic stress-strain relationship (Drucker and Prager, 1952) and can be represented empirically by two theorems: upper bound or lower bound plasticity (Chen, 2007). These theorems are shown to be helpful when both lower and upper solutions can

be estimated, considering the collapse load enclosed between edges from below and above (Yu et al., 1998).

The lower bound plasticity theorem assumes that the external loads are not more significant than the collapse loads and that the material failure criterion is not exceeded at any point in the soil mass. The equilibrium is satisfied by the stresses on the entire soil mass. This theorem does not consider deformations and displacements, and the stress state is not necessarily the actual state at collapse (Leshchinsky and Ambauen, 2015).

The upper bound plasticity theorem considers a set of external loads acting on a failure mechanism, and their work on a displacement increment is equal to that from the internal stresses (Yu et al., 1998). When the work rate along a kinematically allowable collapse surface due to the external loads is greater than or equal to the work done by the internal stresses, the external load cannot exceed the effective collapse load.

Lower bound and upper bound analyses support the exact solution (Leshchinsky and Ambauen, 2015; Yu et al., 1998), a necessary consideration when applying these approaches to slope stability.

The LA fundamentals applied to rigid-perfectly plastic material are i) the soil mass reaches the breaking point though without yielding if in the lower limit the stress is at equilibrium; and ii) the soil mass moves past internal dissipation if plastic deformation develops in the upper limit. Liu et al. (1995) pointed out some problems in the formulas used in the LA, such as the complexity of the computational formulation, low efficiency for problem-solving, and limited scope. The applications of LA are mainly with plane stress-strain and asymmetric plate/shell analyses and assumes the effect of pore water pressure by reducing soil strength (Camargo et al., 2016). Recently updated versions of LA-based methods are emerging as effective slope stability assessment techniques, e.g., the 3D numerical limit analysis of Camargo et al. (2016).

Limit Equilibrium Methods Limit Equilibrium Methods (LEMs) are among the most widely used solutions for slope stability assessment, the spread of which has been aided by the ability to analyze complex soil profiles and different loading conditions (Yu et al., 1998; Lepore et al., 2013; Arnone et al., 2016a). For these reasons, LEMs are used to evaluate both two- and three-dimensional systems. In addition, simple analyses of two-dimensional systems can be used to preliminary assess the slope stability conditions. Space discretization assumptions allow for more or less complex solutions. The simplest leads in the Infinite Slope Method (ISM), while more complex is the Method of Slices (MS). For example, ISM assumes the slope as a rigid block, homogeneous in its mechanical and hydrological characteristics, and calculates the FoS required to reach a state of limiting equilibrium.

ISM is the oldest, simplest, and most widely used among LEMs (Selby, 1993; Pack et al., 1998; Montgomery and Dietrich, 1994; Burton and Bathurst, 1998; Borga

et al., 2002; Arnone et al., 2011; Lepore et al., 2013). Its main feature is modeling the slope failure considering it as planar and parallel to the slope surface. This approach allows verifying the equilibrium either by considering a single point on the slope or assessing the stability of a soil block by knowing width and length dimensions and the fixed profile thickness of soil. The latter assumption is considered reasonable because SLs are generally characterized by shallow depths relative to the length of the failure surface. The ISM assumes homogeneous or average soil properties along the soil profile to make the model statically determinate, analytically tractable, and computationally effective. Both of the former assumptions favor the application of ISM at a large scale even when the model domain is finely discretized. However, researchers aimed to establish a threshold value of approximate length-to-depth ratio to avoid significant errors due to oversimplification. Griffiths et al. (2011) proposed a threshold value of sixteen, based on a series of numerical experiments using a continuum mechanics model. Milledge et al., 2012 extended these experiments using the same model to examine thousands of slope scenarios covering the range of conditions expected for natural and found that the FoS was in error by less than 5% when length/depth ratios exceeded twenty-five.

The ISM root reinforcement is usually implemented as additional values of fixed cohesion representing the combined soil-root combination in the Mohr-Coulomb equation, both for deterministic and probabilistic approaches. This is the simplest assumption considering that most studies do not have spatially explicit controls on root reinforcement's spatial density or depths. Variable value of root cohesion in ISM is implemented by using the Root Bundle Model with Weibull survival function (RBMw) (Schwarz et al., 2013; Dazio et al., 2018; Gehring et al., 2019), or the Fiber Bundle Model (FBM) (Pollen and Simon, 2005).

The MS discretizes the slope into vertical slices, and calculates the forces and/or moments acting on each slice. Several methods were proposed, differing on how the interaction between the various slices is considered (Chen et al., 2017), and whether equilibrium is calculated for forces and/or moments. As a result, the value of the obtained FoS may be different. Considering that the number of available equilibrium equations is less than the number of unknowns in slope stability problems, MS relies on assumptions to make the problem controlled (Duncan, 1996). Some of these assume i) the absence of deformation on the boundaries between the slices (Morrison and Greenwood, 1989), ii) the influence of different inter-slice forces (Chen and Shao, 1988; Zheng et al., 2014) or pore water pressures acting on the inter-slice boundaries (Morrison and Greenwood, 1989). Duncan (1996) observed that when all equilibrium conditions are satisfied (the equilibrium of forces and moments), no effect of these assumptions was observed in the FoS calculation, while when only the equilibrium of forces is satisfied, the FoS is significantly affected by the slope set for the lateral forces between slices. For this reason, they stated that force equilibrium methods offer a reduced degree of accuracy compared to methods that satisfy all equilibrium conditions. In the MS approach the RR is implemented as fix value

(Greenwood, 2006) calculated by using the Wu-or-Waldron Method (WWM) (Wu et al., 1979; Waldron and Dakessian, 1981).

LEMs are still widely used and generally preferred to complex numerical models because of their simplicity (Chen et al., 2003).

Numerical analysis methods Numerical analysis Methods (NMs) were implemented to simulate the spatial complexity of geotechnical and hydrological parameters considered in slope stability analysis. NMs consider deformation, subsidence, pore pressure, and soil suction changes after an intense rainfall event. For this reason, NMs are more descriptive and accurate, but they need high computational costs and detailed input data (Rossi et al., 2013; Milledge et al., 2014). The most currently used NMs modeling can be divided into three main groups: i) continuous, ii) discontinuous, and iii) hybrid.

The Finite Element Method (FEM) belongs to continuous NMs and is commonly used to evaluate condition changes of elements subjected to stress and deformation arising from resisting and driving forces. FEM was adopted to solve oversimplification in modeling through ISM, where variations in soil mechanical behavior caused by the heterogeneity of physical characteristics and lateral interactions/deformations are neglected. The basic FEM approach is partitioning complex structures, characterized by infinite degrees of freedom, into a set of simpler elements connected to form a single mesh at specific points called *nodes* (Rajapakse, 2016). In the case of slope modeling, parameters related to displacements, velocities, and balance of forces are attributed to each node while material properties defining the stress-strain behavior are attributed to elements consisting of polygons composed of nodes. This discretization approach allows the calculation of active forces through simple algebraic equations (Rapp, 2017), providing more realistic modeling of progressive soil deformations.

Applications of FEM consider several approaches. Some are based on the Mohr-Coulomb concept of elastic-plastic soil, to which a value of apparent cohesion representing root reinforcement is added. These applications involve meshing the root model and soil matrix by nodes and considering contact near the soil-root interface using kinematic conditions (Dupuy et al., 2005). Other applications of FEM consider the development of new material models for rooted soil. The study of Świtała et al. (2018) and Świtała et al. (2019) proposed a coupled hydro-mechanical model to assess the root effect on soil's mechanical and hydrological behavior. Root reinforcement, considered as uniform parameter which change depending on vegetation type (Świtała, 2016), is combined with the Cam-clay model for unsaturated soils (Tamagnini, 2004) and implemented through a finite element code (Sanavia et al., 2006; Sanavia et al., 2008). Further FEM applications consider root as geogrid discrete element into the soil mesh (Mickovski et al., 2011; Mao et al., 2014b). These recent studies assume that all roots have same properties: their basic constitutive material

is isotropic and strength and modulus of elasticity are equal in case of compression and tension loadings.

Despite the significant advances in slope stability modeling made by FEM, there are some significant limitations. For example, difficulties in modeling the development of soil cracks consequent to the SLs initiation can be addressed by applying the material point method of Sulsky et al. (1994), able to deal with large material deformation. The material point method involves i) a continuum discretized into a finite number of material points, representing the volume of an element (Abe et al., 2014) and characterized by mass, velocity, acceleration, stress, strain, and other properties (Lagrangian description of the material) (Andersen and Andersen, 2010), and ii) an empty computational mesh in which the stability equations are solved and iteratively updated during the analysis (Eulerian grid) (Conte et al., 2020). From the combination of these two methods, the model was implemented simulating the reaction of an elasto-plastic material when subjected to significant deformations (Andersen and Andersen, 2010). However, to the best of our knowledge, there are no applications of this modeling approach in rooted soils.

As alternative solutions to continuous approaches, discontinuous methods have been developed for slope stability assessment. The Discrete Element Method (DEM) is the most widely used, developed to address engineering problems in granular, discontinuous, heterogeneous, anisotropic, and nonelastic materials. The DEM, like the FEM, is used to evaluate the effect of roots on different analysis scales. For example, Cundall and Strack (1979) and Bourrier et al. (2013) applied this method to study roots influence on the shear resistance, while Cohen and Schwarz (2017) implemented the DEM in the development of a new SSM, SOSlope.

The studies of Cundall and Strack (1979) and Bourrier et al. (2013) propose a modeling approach that discretizes the soil into locally deformable individual spherical elements and the roots as flexible cylinders embedded in the soil matrix. This model considers the root tensile loading until breakage, the root bending loading, the root-soil adhesive links until adhesion breakage, the root slippage associated with a frictional resistance at the root-soil interface (Bourrier et al., 2013). Under the influence of loading forces, elements move through space and interact with neighboring elements. At each time step, the contact forces between the particles are calculated for each displacement and recursively summed before the next time step.

The study of Cohen and Schwarz (2017) proposes the use of DEM for slope modeling and analysis using SOSlope. In this model, the DEM is combined with the spring-block model of Olami et al. (1992) (a subset of the self-organized criticality approach of Bak et al. (1988)) to consider forces redistribution on the slope and recursive computation of equilibrium. Starting from raster information of the digital terrain model, the slope is discretized into a series of blocks connected by links that simulate the mechanical forces of roots and soil (Cohen et al., 2009). In this way, in quantifying the factor of safety, derived from the ratio between resistive and active forces, the effect of the basal root reinforcement is considered a resistive force, while

the lateral root reinforcement as an active force. Like the previous method, the loss of block stability caused by the increase of the soil water content causes its movement, affecting lateral bonds and positions of the adjacent blocks. Depending on the movement direction of the block, the bonds simulate tension or compression forces.

Finally, hybrid NMs modeling was also developed combining FEM and DEM and obtaining the combined Finite-Discrete Element Method (FDEM). FDEM allows simulating a solid region as a set of deformable finite elements, by FEM, that may be subjected to progressive fracturing, by DEM (Munjiza et al., 1995).

2.2.5 Dimensional systems of slope stability analysis

Currently available SSMs have been realized in one, two, and three dimensional systems (1D, 2D, and 3D), providing different solutions depending on the final analysis purpose, data, and tools availability. Implementing a complex multidimensional system requires detailed data availability regarding the starting stability condition with a certain degree of precision and variability (uncertainty and spatial distribution). With the increase of spatial dimension, also the computational time increases due to a large number of freedom degrees necessary to solve.

The most commonly used models are those in 2D, generally based on ISM, which allow making assessments either in planimetric terms, as in the case of most SSMs, or considering the vertical section of the slope, such as SLIP4EX (Greenwood, 2006). The advantage of 2D SSMs is the low number of data inputs required, and lower computational time, allowing wider use in both engineering and scientific research (Pollen-Bankhead and Simon, 2010; Greenwood, 2006; Genet et al., 2010; Thomas and Pollen-Bankhead, 2010). More complex FEM- and DEM-based SSMs implemented in 3D require more input data, associated with greater inherent uncertainty, and a deeper understanding of processes, thus requiring more computational time.

Root reinforcement does not usually have the same spatial dimension as the respective SSM in which RR is implemented. In most PMs, the root contribution is considered in the force balance as a constant (static) value of uniformly distributed cohesion (Fig. 2.2a), and accounted for as basal cohesion. However, in both SSDMs and SSPMs, some models calculate the root reinforcement considering the spatial variability of RR. Among these, we can mention Mao et al. (2014a) which uses a homogeneous root cohesion for each soil layer, while it is set to zero in the case of non-vegetated areas. On the other hand, Arnone et al. (2016b) instead considers variations in basal root reinforcement (Fig.2.2b) based on the distribution of trees. More complex models consider the RR variability across multiple dimensions (Fig.2.2c), considering spatial variability of both lateral and basal RR. Among the SSPMs, Zadelhoff et al. (2021a) and Cislaghi et al. (2017) consider both basal and lateral RR. While among the SSDMs, Milledge et al. (2014) consider both lateral and basal root cohesion which decrease exponentially with increasing depth, identifying the critical depth and position of water table (Liucci et al., 2017). Cohen and Schwarz

(2017) consider basal and lateral RR spatially distributed based on the tree position and dimensions, including root -tensile and -compressive forces on the slope.

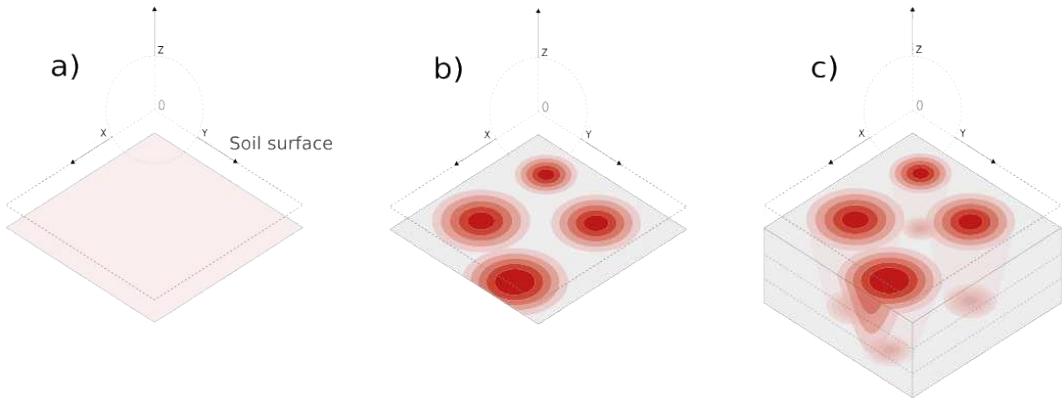

FIGURE 2.2: Root reinforcement a) uniformly distributed on horizontal layers, b) two dimension spatially variable on horizontal layers, and c) spatially variable both for horizontal and vertical surfaces.

Regarding the time dimension, only a few SSMs consider the progressive slope failure caused by the variation in the short time of the parameter values and thus the equilibrium conditions of the slope (Montgomery and Dietrich, 1994; Baum et al., 2002; Rossi et al., 2013; Cohen and Schwarz, 2017). For example, Bordoni et al. (2015) reported some studies where the TRIGRS model (Baum et al., 2002) was used to analyze timing and location of SL triggering considering local (Salciarini et al., 2008) and regional (Salciarini et al., 2006; Godt et al., 2008) scales.

Aiming to obtain a more complete analysis, parameters variability should be considered changing over time. Particular attention is focused on factors that, changing over short time periods, significantly influence in the triggering process, such as the increase of pore pressure (Montgomery and Dietrich, 1994; Baum et al., 2002; Rossi et al., 2013) and soil saturation (Montrasio and Valentino, 2008), or the activation of roots resistance forces (Schwarz et al., 2013). However, also changes over longer periods, such as soil depth (D'Odorico and Fagherazzi, 2003) or root decay (Vergani et al., 2016; Vergani et al., 2017b), should be considered allowing the stability assessment over years or decades (D'Odorico and Fagherazzi, 2003; Ciervo et al., 2017).

2.3 Root reinforcement modeling approaches

Although the contribution of RR is recognized as an influential factor in the hydro-mechanical dynamics that determine changes in slope stability conditions, quantifying their contribution is still difficult. Such estimation requires parameters that are often complex to measure, such as root geometry and size, but most importantly, it requires information on the mechanical characteristics determining the effective activation of RR during a SL event. Therefore, considering the difficulty of measuring and modeling the effect of roots, this factor is generally assumed as a constant and

uniform value of cohesion (Figure 2.2 a) added to the soil strength (Waldron, 1977; Wu et al., 1979), often calculated with the Mohr-Coulomb equation.

However, while this solution has shown practical advantages when used in SSMs, it does not allow quantifying and predicting the contribution of roots during soil deformation caused by the loss of stability (Michalowski and Zhao, 1996; Ekanayake and Phillips, 1999). Observations made by Fannin et al. (2005) showed the occurrence of two peaks during the slope failure process, the first due to soil shear strength and the second due to RR activation. In Figure 2.3, it is evident that these two peaks occur at different displacements, and the root contribution to soil stability is considered by adding it to the soil shear strength.

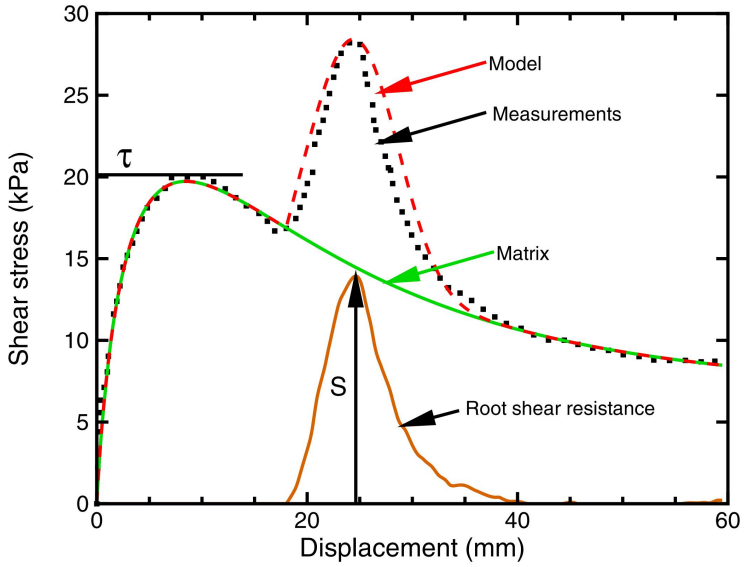

FIGURE 2.3: Picture from Cohen et al. (2011) showing an example of field pullout test dynamic from Fannin et al. (2005) study, highlighting the root's effects on soil stress-strain behavior. The graph shows three different curves: i) the curve with black squares and two different peaks shows soil matrix shear and roots tensile forces, ii) the green curve shows the only soil shear stress, and iii) the brown curve shows the root contribution.

For decades, and often still today, the estimation of apparent root cohesion is done with the models proposed by Waldron (1977) and Wu et al. (1979). These models consider roots as elastic fibers oriented perpendicular to the slip plane and affecting the soil's normal stress component. After losing soil stability, roots elongate subjected to tension forces developed due to downslope soil movement. The estimation of RR in these two RRMs does not consider the actual roots' diametric distribution, calculating the force as linearly proportional to the root area ratio. The root area ratio derives from the ratio between the area occupied by roots and a unit area of soil (Bischetti et al., 2005). The root inclination is also considered by becoming slightly negative in the case of roots not perpendicular to the cutting surface (Thomas and Pollen-Bankhead, 2010).

Waldron model Waldron (1977) proposed a first RRMs that considers the soil-root friction force, root diameters, and elastic modulus (estimated using Hooke's law). This model assumes that roots have identical properties and sizes. Since the shear strength value of each is inversely proportional to one-fourth of the root cross-sectional area or, similarly, to one-half of its diameter, small roots provide greater strength than coarse roots at an equal root area ratio.

Based on the concept of activated root length, the correlation between root tension and displacement and their progressive failure during soil deformation were exposed for the first time. However, this model showed the disadvantage of requiring parameters challenging to measure and estimate, e.g., soil depth, root length, and inclination.

Wu model After a few years, Wu et al. (1979) proposed a new simplified RRMs based on simultaneous activation and failure of all roots crossing the failure plane. This assumption shows an inevitable order-of-magnitude error in RR quantification (Schwarz et al., 2013) (Figura 2.4). Nevertheless, Gray and Ohashi (1983) proposed a further simplification of Wu's model by assuming that the average RR of the total rooted area is equal to the average of the product of root strength and root area. Again, the simplicity of the model's use influences its accuracy, producing an even more significant overestimation of the RR than the Wu model.

In general, both previous models consider i) maximum root resistance is additive to soil resistance, ii) RR is independent of displacement, and iii) simultaneous root activation and failure occur without accounting for their spatial variability in size. These assumptions are refuted by field and laboratory studies (Pollen and Simon, 2005; Docker and Hubble, 2008; Mickovski et al., 2007; Loades et al., 2010), which highlight the importance of considering diametric variability of roots in space and their progressive activation during SL initiation. The RR overestimation causes a potential underestimation of the slope stability in an investigated area (Montgomery et al., 2009; Schwarz et al., 2010).

However, the little information required, considering the critical root tensile strength and the cross-sectional area of roots crossing the failure surface, still favors the use of the Wu model (see Tables 2.1 and 2.2).

Fiber bundle model A first alternative to the previous RRMs was proposed by Pollen and Simon (2005) who, reconsidering the concept about progressive roots failure when subjected to a tension force (Waldron, 1977), developed a model in which roots, considered as a bundle of elastic fibers, are subjected to stress-step loading. The FBM and its updated versions (Pollen, 2007; Pollen-Bankhead and Simon, 2010; Thomas and Pollen-Bankhead, 2010) are widely used.

Although FBM has contributed to improving the estimation of RR, it still shows some limitations, mainly related to the roots' diametric distribution, geometry, and mechanical properties, due to the step-loading estimation approach. Considering

force dependence on load instead of displacement, it is not possible to estimate the residual tensile force remaining after the activation of maximum RR.

Root bundle model Following field observations that highlighted the importance of LRR in determining SL probability and size, it was considered necessary for RRMs to consider this effect. Therefore, Schwarz et al. (2010) created the Root Bundle Model (RBM) by implementing a strain-step loading approach. The RBM neglects the use of the correction factor for root inclination, assuming them to be oriented parallel to the sliding direction (Riestenberg and Sovonick-Dunford, 1983). This assumption is justified by the sampling method by which field measurements are made on lateral roots protruding from the vertical soil profile.

Unlike other models, the RBM considers the displacement and force ratio and estimates the RR by considering the root strength, the elastic modulus, geometric characteristics such as diameter, length, tortuosity, and branching points, and their density in the soil.

By considering RR as dependent on displacement instead of load, RBM allows for a complete force-displacement curve and redistribution of forces on each root, based on their geometric and mechanical properties (and not statistically imposed) (Schwarz et al., 2013).

RBM preserves the assumption of cumulative progressive activation of RR (introduced by Waldron (1977) and subsequently neglected by Wu et al. (1979) and FBM) along the activation area due to root-soil friction, assuming its measurement during pullout tests (Figure 2.3). Field pullout tests (Schwarz et al., 2010; Schwarz et al., 2011) showed a negligible influence of soil pressure and water content on the corresponding force and displacement, emphasizing the effect of root diameter and length instead.

Root bundle model with Weibull distribution function Considering the applicability of the Weibull function, Schwarz et al. (2013) have included this function in the RR quantification, considering the intrinsic variability of the mechanical properties of roots with similar diameters. This new version of the model, called RBMw, proposes a simplified mathematical formulation compared to the RBM, considering the "average" mechanical behavior of each root diameter class (Schwarz et al., 2013).

The figure 2.4 shows that, among the analyzed solutions, RBMw best fits the measured field values.

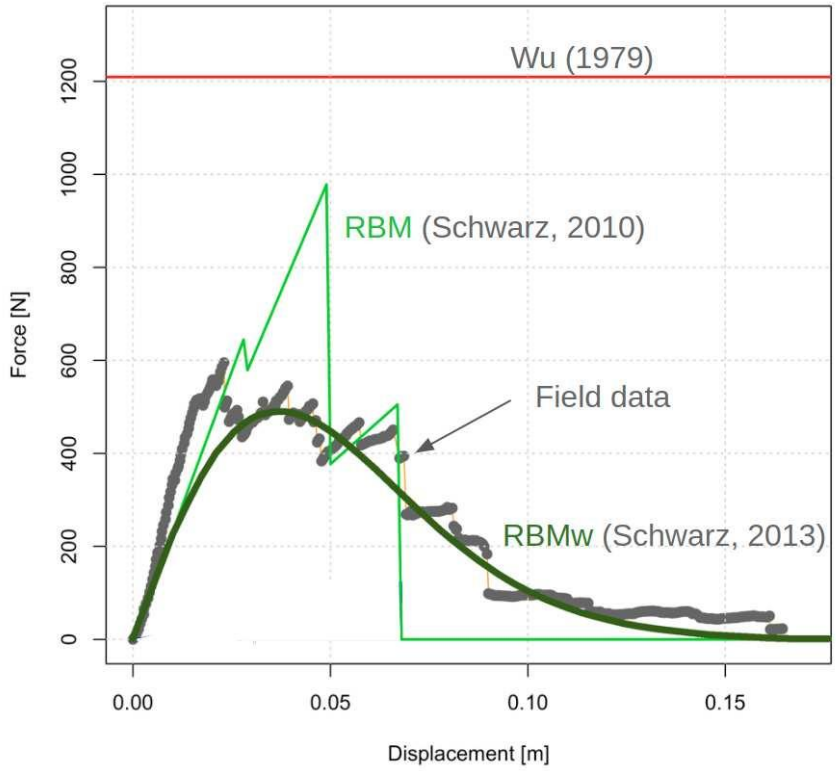

FIGURE 2.4: The graph from Schwarz et al. (2013) compares measured pullout force as a function of displacement (gray points) with the two versions of RBM and RBMw. It is immediately evident that the WU model provides a uniform and significantly greater RR value with respect to the other RRMs and to the measured values. The RBM (lightgreen line) overestimates the RR, while the RBMw (darkgreen line) better fits the measured data.

2.3.1 Numerical methods for root reinforcement modeling

The measurement of parameters required in analytical models still shows some general difficulties, e.g., related to the availability of instruments and time needed for field surveys and specific problems in estimating the geometrical and mechanical characteristics of the roots. The various measurement methods have been reviewed by Giadrossich et al. (2017) showing different approaches to quantify the force for single root, through tensile tests or pullout tests, or for rooted soils, through shear strength tests. Therefore, as an alternative solution to complex experimental methods, some studies proposed and validated complex numerical modeling methods for RR quantification based on the FEM and the DEM. Both methods, already widely used in slope stability analysis (section 2.2.3), have proved to be applicable also in the study of soil-root interaction during soil movement processes.

FEM has been applied in the analysis of wind-induced uprooting and anchorage mechanisms (Dupuy et al., 2007; Fourcaud et al., 2008), as well as root pullout analysis (Lin et al., 2010) and direct shear tests (Mickovski et al., 2011; Frydman and Operstein, 2001). These studies have highlighted that, although the model shows some difficulties in validating field measured data (Dupuy et al., 2007), FEM can be

considered as a valid numerical method (Mickovski et al., 2011; Mao et al., 2014b) able to provide data comparable to experimental tests.

Some examples of the FEM application have already been presented by Mickovski et al. (2011) and Mao et al. (2014b). In these studies, the investigated soil sample is modeled in 3D through a mesh made of tetrahedral deformable elements with four nodes. In contrast, the roots are modeled considering two different elements, beam, and truss. Beam type simulates the strength of roots in tension, compression, shear, bending, and torsion, while truss type exclusively simulates the strength in tension and compression (Spyrakos, 1994). This rooted soil sample was subjected to stress-strain until roots failure (figure 2.5).

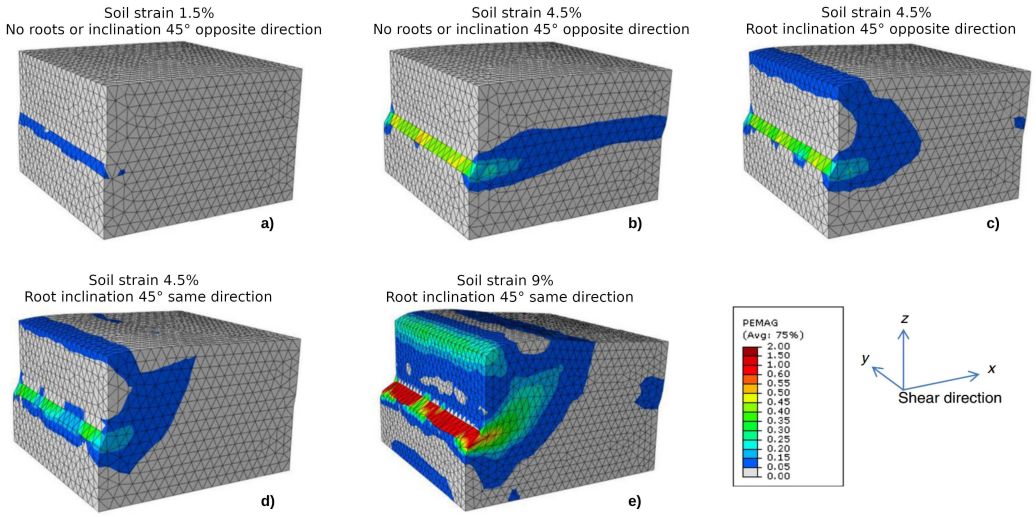

FIGURE 2.5: The picture, from Mao et al. (2014b), shows a modeled shear box test and the development of plastic zones on rootless and rooted soil samples, highlighting the influence of RR on soil mechanical properties. In the rootless soil, the plastic zone is verified on the left side (Figure a) and develops along the shear surface as soil strain increases (Figure b). In the rooted soil, the roots' effect is simulated by considering different inclinations: in Figure c, roots are inclined by 45°in the opposite direction of shear, while in Figures d and e, roots are inclined by 45°in the same direction. In these cases, the development of a plastic zone is evident perpendicular to the shear zone, differing in magnitude according to the two types of inclination (Figure c and Figure d).

Bourrier et al. (2013) proposed a new approach to modeling and evaluating soil-root interaction based on the DEM use. In this case, the soil is modeled by locally deformable rigid spheres and roots as deformable cylinders (figure 2.6). The set of spheres, uniformly distributed in space, simulates the soil particles and their interaction. The dimensions used for the spheres are equivalent to about 5 to 8 mm in diameter and, although larger than the real soil particles, Bourrier et al. (2013) justifies this decision as a necessary solution to model the evolution of soil movement under shear load. As for the roots, these are individually represented by deformable cylinders considered, as in the case of FEM, beam and truss elements (Mao et al., 2014b).

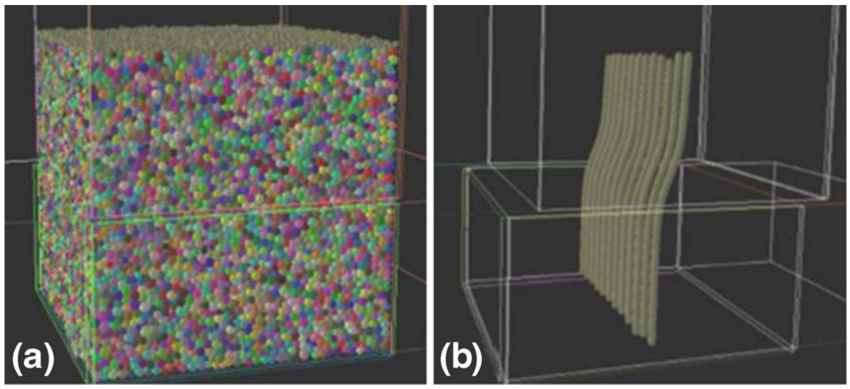

FIGURE 2.6: The two Figures show a shear box modeled by the DEM after Bourrier et al. (2013). Figures (a) is an example of modeled soil by locally deformable rigid spheres, while Figures (b) is an examples of root bundle modeled as deformable cylinders.

Through the DEM approach, it is possible to simulate the interactions between soil particles and between soil and roots, evaluating in detail forces developed at the soil-root interface.

The discussed RRMs are implemented on SSMs to consider the influence of RR in the assessment of slope stability in vegetated areas (Tables 2.1 and 2.2, specifically the column named *Root reinforcement model*).

2.4 Comparison of physically-based models

Twenty-one slope stability models (SSMs) are analyzed in this paper (Tables 2.1 and 2.2). Tables 2.1 shows the probabilistic model approaches, while table 2.2 shows the deterministic model approaches. The selection of models was made with objective criteria based on those models that consider the contribution of roots in the FoS calculation. In addition, some models among SSMs were selected with a subjective criterion, considering which, in our opinion, are the most used in the literature but which do not consider the RR. Models in both tables are sorted by date of publication. The main objective of each model is to meet the operational needs of stability analysis and assessment in specific applications. For this reason, it is difficult identifying the strengths and weaknesses of a SSM. However, it is more functional understanding in which environments and analysis scale the use of the SSM is most effective by considering methods and approaches implemented.

Starting from the evaluation of the modeling approach used to develop the SSM, it is evident from the Table 2.1 that all SSPMs are based on the ISM and consider a 2D dimensional space. Assuming its easy applicability and the request of few input data, often efficiently obtainable, the ISM allows to optimize the computational time for obtaining information about the stability conditions of the area. However, it especially encourages the application of SSPMs in analysis over extensive areas.

Differently, SSDMs aim to provide more detailed information about the processes promoting the SLs initiation. To do this, some SSDMs apply more complex modeling methods that allow for better implementation of soil-root interactions. Table 2.2 shows that the most recent SSDMs consider the slope through multidimensional systems based on the FEM and DEM. The complexity of these models requires more significant detail in the input data, resulting in longer modeling times that require consideration of smaller areas of extent.

The modeling approach generally influences the choice of the analysis scale, another essential criterion to evaluate the appropriate SSM. Their application ranges from regional scale to slope scale of analysis (Table 2.3). In particular, regional scales analyses aim to identify susceptible and more landslide-prone areas by investigating catchments, while slope scales analyses aim to understand in detail how variations in water content can determine the instability of sloping soils.

In large areas, the accuracy of the analysis depends on the SSM ability to simulate the spatial variability and uncertainty of environmental characteristics and physical parameters (e.g., soil depth and porosity, root cohesion), aiming at obtaining more realistic and plausible values through the probabilistic distribution of input parameters.

In the analysis of smaller areas, it is relatively easier to have detailed information, which can also be obtained by measuring required parameters in the field. In this context, parameters variability is reduced, consequently reducing the degree of uncertainty and allowing the assumption of uniform distribution relative, for example, to hydrological and mechanical soil properties or the rainfall distribution over the investigated area.

Based on this reasoning, SSPMs are preferred in regional analysis scales, as they better implement physical parameters and landscape variability. In contrast, SSDMs are generally preferred in local scales, providing detailed information about hydromechanical processes that favor SL triggering on a slope. However, the Table 2.3 shows that SSPMs can be used also for slope-scale analysis but obtaining less detailed results, while some SSDMs are valuable also for regional scale analysis, for example SHETRAN model can be applied to a single hillslope or to all subbasins in a large (e.g., 5,000 km^2) river basin (Ewen et al., 2000).

Modeling approach and analysis scale influence the analysis purpose of appropriate SSM application. The Table 2.3 shows that all SSMs allow for risk analysis, some even identifying SL trigger locations, sizes, and flow paths. Only a few have proven useful for assessing the effect of vegetation, and in particular, how the stability of the area changes as forest structure changes (Mao et al., 2014b; Arnone et al., 2016a; Cohen and Schwarz, 2017; Cislaghi et al., 2017; Zadelhoff et al., 2021a). In these cases, evaluating the actual vegetation's conditions and its influence on soil protection is necessary to identify appropriate management criteria aimed at preserving and improving the mitigation effect. Furthermore, considering changes to

which ecosystems and landscapes are and will be subjected in the future due to natural and human disturbances, assessing consequent changes in root reinforcement (Preti, 2013; Vergani et al., 2016; Vergani et al., 2017a) and landslide susceptibility is critical for accurate and effective land-use planning.

For this reason, it is crucial to focus on analyzing how SSMs consider the effect of vegetation in stability assessment. From both Tables 2.1 and 2.2, it is evident the use of different methods to quantify and implement the root reinforcement effect. In particular, in addition to SSPMs and SSDMs that neglect the effect of vegetation, other SSMs consider vegetation using either a spatially uniform value or a variable value of root reinforcement added to soil cohesion. Observing the temporal order used to illustrate the SSMs considered in the Tables 2.1 and 2.2, it is evident that in both cases, the most recent ones incorporate more carefully the root reinforcement, preserving its characteristic of spatial and temporal variability. This aspect is justified by the possibility of developing SSMs implemented with more complex modeling approaches, thanks to the improvement of technology and techniques for data collection and measurement. Focusing on the purpose of this article, the root reinforcement model and how SSMs consider this factor as input parameter is analyzed.

In the specific case of SSPMs, only two of the investigated models neglect the effect of vegetation, i.e., the method proposed by Park et al. (2013), for stability analysis in a GIS environment, and the HIRESSS model of Rossi et al. (2013), which analyze SL triggering conditions in real-time and on large areas. The decision to neglect vegetation effects could be justified by choice to find a simple and accessible method, as in the case of Park's method, or by the analysis purpose, as in the case of the HIRESSS model that aims to limit the processing complexity and get the result in the shortest possible time.

The remaining SSPMs that consider the root reinforcement contribution allow for more realistic evaluations of vegetated slopes. LISA (Hammond, 1992), SINMAP (Pack et al., 1998), STARWARS-PROBSTAB (Beek, 2002), and GEOtop-FS (Simoni et al., 2008) consider root reinforcement an additional uniform value of apparent cohesion calculated using the static model proposed by Wu et al. (1979) and Waldron and Dakessian (1981). In contrast, tRIBS-VEGGIE (Arnone et al., 2016a), PRIMULA (Cislaghi et al., 2017), and SlideforMAP (Zadelhoff et al., 2021a) consider root reinforcement variability over space. These consider variable or dynamic root cohesion are based on the fiber bundle model of Pollen and Simon (2005) (PRIMULA) and the RBMw of Schwarz et al. (2013) (tRIBS-VEGGIE and SlideforMAP). Another important aspect to highlight is that while tRIBS-VEGGIE considers only basal reinforcement, PRIMULA and SlideforMAP consider both basal and lateral reinforcement, improving the broad applicability of these models. These SSPMs are also appropriate for forest planning purposes, automatically reconstructing the hypothetical vegetation cover using probabilistic approaches applied to accessible information layers (e.g., comparisons between digital terrain and surface models, applications of

allometric equations to determine trees size) (Murgia et al., 2021).

MODEL APPROACH	MODEL NAME	AUTHORS	ROOT REINFORCEMENT PARAMETER	ROOT REINFORCEMENT MODEL	GEOTHECNICAL MODEL	HYDROLOGICAL MODEL	DIMENSION OF CALCULATIONS (Mathematical Spatial Dimension)	DIMENSION OF DISCRETIZATION (Physical Spatial Dimension)	TYPE OF OUTPUT	NOTE
Physically-based models Probabilistic approaches (SSPMs)	**LISA** (Level I, II, III Stability Analysis)	Hammond et al, 1992	Costant value of root cohesion	--	LISA II: LEM - ISM LISA III: LEM-MS	--	LISA II: 1D LISA III: 2D	2D	P(Fos) Map	Monte Carlo Regarding RR, the user can change the roots distribution considering timber stand
	SINMAP (Stability Index Mapping)	Pack et al, 1998	Costant value of root cohesion	--	LEM - ISM	TOPOG (O'Loughlin, 1986)	1D	2D	SI maps	Definition of SI classes Recommended for regional scales
	The coupled hillslope model **STARWARS - PROBSTAB**	van Beek, 2002	Costant value of root cohesion	WWM (Wu et al, 1979) *	LEM - ISM	STARWARS based on Richards eq	1D	2D	FoS P(FoS) Map Critical depth Map (+ Sensitivity maps of each input parameter)	Regional scale Root cohesion parameter introduced at the original version of the model by Kuriakose et al., 2006 *Schmidt et al. 2001 approach
	GEOtop-FS	Simoni et al, 2008	Costant value of root cohesion	--	LEM - ISM	GEOtop (Bertoldi et al, 2006), 3D richard's equations	1D	2D	P(Fos) Map	
	Park model	Park et al, 2013	--	--	LEM - ISM	TOPMODEL (Beven and Kirkby, 1979)	1D	2D	FOS and P(FoS) maps	Monte Carlo
	HIRESSS (High Resolution Slope Stability Simulator)	Rossi et al, 2013	--	--	LEM - ISM	Richard's equation	1D	2D	P(FoS) Map varying over time	Monte Carlo Real time monitoring
	tRIBS-VEGGIE (Triangulated Irregular Network (TIN)-based Real-time Integrated Basin Simulator-VEGetation Generator for Interactive Evolution) -Landslide model	Arnone et al, 2016a (Lepore et al, 2013)	Variable value of root cohesion*	RBMw (Schwarz, 2013) + Topological model (Arnone, 2016)	LEM - ISM	Richard's equation	1D	2D	P(FoS) map	*Basal root tensile force
	PRIMULA (PRobabilistic MUltidimentional shallow Landslide Analysis)	Cislaghi et al, 2017	Variable value of root cohesion*	FBM (Pollen and Simon, 2005)	LEM - ISM	TOPMODEL (Beven and Kirkby 1979)	1D	3D	P(FoS) map	*Basal and Lateral root tensile force
	SlideforMAP	van Zadelhoff et al, 2021	Variable value of root cohesion*	RBMw (Schwarz, 2013)	LEM - ISM	TOPMODEL (Beven and Kirkby, 1979)	1D	3D	P(FoS) map and several others maps about estimated parameters	Normal distribution of soil parameters *Basal and Lateral root tensile force

TABLE 2.1: Characteristics of slope stability physically-based probabilistic models

Considering SSDMs, also in this case there are models which neglect the effect of vegetation, such as the SHALSTAB model (Montgomery and Dietrich, 1994; Reginatto et al., 2012), the Lu and Godt model (Lu and Godt, 2008), and the SUSHI model (Capparelli and Versace, 2011). This choice may depend on their primary purpose, evaluating hydrological processes that promote SL initiation focusing on the analysis of pore pressure and suction variation in the investigated slope profile. Empirical knowledge regarding hydrological processes (Section 2.1.1) has shown that, at the local scale, the effect of roots in developing conditions predisposing SL initiation, such as increased pore pressure, is limited. In contrast, it assumes importance in subsurface water drainage at the basin level.

Most of the SSDMs presented in Table 2.2 show the use of constant values of root cohesion, generally calculated through the method Wu et al. (1979) and Waldron and Dakessian (1981). These SSDMs are dSLAM (Wu and Sidle, 1995), TRIGRS (Baum et al., 2002), TRIGRS-unsaturated (Savage et al., 2004) and Kokutse et al. (2006) model. In addition to the factor of safety quantification, TRIGRS and TRIGRS-unsaturated allow analyzing the spatial distribution of pore water pressure for a more complete understanding of the SL triggering process, while Kokutse et al. (2006) model consider a 3D model of root system.

The SSDMs that alternatively consider variable values of root cohesion are MD-STAB (Milledge et al., 2014), Ecosfix 1.0 (Mao et al., 2014a), and SOSlope (Cohen and Schwarz, 2017). These three SSDMs show different methods of estimating the root reinforcement, which thus affect the final result obtained. In particular, MD-STAB considers root cohesion as an exponential function of soil depth from Dunne (1991) and Benda and Dunne (1997) models, Ecosfix 1.0 considers Wu (1976) and Waldron (1977) models, and SOSlope considers the root bundle model Schwarz et al. (2013). The focus on considering the effect of root reinforcement more plausibly encourages their use in instability assessment analyses, in detailed forest management, and in identification of bio-engineering interventions, e.g., based on tree planting.

MODEL APPROACH	MODEL NAME	AUTHORS	ROOT REINFORCEMENT PARAMETER	ROOT REINFORCEMENT MODEL	GEOTHECNICAL MODEL	HYDROLOGICAL MODEL	DIMENSION OF CALCULATIONS (Mathematical Spatial Dimension)	DIMENSION OF DISCRETIZATION (Physical Spatial Dimension)	TYPE OF OUTPUT	NOTE
Physically-based models Deterministic approaches (SSDMs)	**SHALSTAB** (Shallow Landsliding Stability Model)	Montgomery and Dietrich, 1994 (version of Reginatto et al., 2012)	--	--	LEM - ISM	TOPOG (O'Loughlin, 1986)	1D	2D	Coefficient of instability degree map	Definition of coeff instability classes. High dependence on scale and resolution considered Using SHALSTAB with scale equalor smaller than 1: 50.000 are suitable only for preliminary studies
	dSLAM	Wu and Sidle, 1995	Costant value of root cohesion	--	LEM - ISM	The combined sub/surface kinematic modeling approach by Takasao and Shiiba (1988)	1D	2D	Maps of FOS distributions, landslide locations, debris flow paths, failure potential distributions, and other stability-related parameters	
	SHETRAN	Ewen, 2000	Costant value of root cohesion	--	LEM - ISM	Boussinesq equation for vertically averaged lateral flow and Richards equation for vertical flow	1D (2D)	2D	Singular value of FoS	Dual resolution: GISLIP and SHESLIP. Two coefficient are considered to simulate the soil erosion due by both raindrop impact and surface water flow.
	TRIGRS (Transient Rainfall Infiltration and Grid-based Regional Slope-stability analysis)	Baum et al, 2002	Costant value of root cohesion	--	LEM - ISM	Version of Richard's eq. proposed by Iverson (2000) and extended by Baum et al. (2002)	1D	2D	FoS map Pore Water Pressure Map	Regional scale Root cohesion in the revised models of Kim et al., 2014a; Saadatkhah et al., 2016
	TRIGRS unsatured	Savage et al, 2004	Costant value of root cohesion	--	LEM - ISM	Srivastava and Yeh (1991)	1D	2D	FoS map Pore Water Pressure Map	Regional scale
	Kokutse model	Kokutse et al, 2006	Costant value of root cohesion	WWM (Wu et al, 1979)	FEM	--	3D	3D	Singular value of FoS	3D model of root systems
	SLIP4EX	Greenwood, 2006	Costant value of root cohesion	WWM (Wu et al, 1979)	LEM - MS	--	2D	1D	Singular value of FoS	Preliminary analysis Fine roots are assumed to have no influence on cohesion
	Lu and Godt model	Lu and Godt, 2008	--	--	LEM - ISM	Steady unsaturated seepage conditions	1D	1D	Singular value of FoS	
	SUSHI (Saturated Unsaturated Simulation for Hillslope Instability)	Capparelli and Versace, 2011	--	--	LEM	Hydro-SUSHI module base on Richard equation	2D	1D	Soil suction variability along soil profile	SUSHI uses the FDM for mathematical solution.
	MD-STAB	Milledge et al., 2014	Variable value of root cohesion	Dunne, 1991; Benda and Dunne, 1997	LEM - ISM	Hydrostatic conditions	2D	3D	FoS map and SL size	Identification of critical depth and position of water table (Liucci_2017). Lateral and basal root cohesion decrease exponentialy with increasing depth
	Ecofix 1.0	Mao et al, 2014	Variable value of root cohesion	WWM (Wu et al, 1979)	FEM	--	2D	3D	FoS maps	FoS is determine by defining an upper threshold of nodal displacement. Root cohesion spatially variable; values don't consider the stiffness of the roots.
	SOSlope (Self-Organized Slope)	Cohen and Schwarz, 2017	Variable value of root cohesion*	RBMw (Schwarz, 2013)	DEM (Lu and Godt approach)	TOPMODEL (Beven and Kirkby, 1979)	3D	2D	FoS and several others maps about estimated parameters	RR is 3D-spatialy distributed based on the tree position and dimentions. Self-organized Critically approach *Basal and lateral reinforcement; tensile and compressive force

TABLE 2.2: Characteristics of slope stability physically-based deterministic models

This final aspect is also connected with another critical aspect of assessing the

applicability of an SSMs is the output data it is capable of producing. All SSMs considered providing information about stability by estimating the factor of safety or failure probability. Some SSMs produce additional information related, for example, to hydrological processes (pore water pressure, saturation, topographic index of humidity), or, as mentioned above discussing the analysis purpose, some produce information on the root reinforcement viewable on GIS environment. In particular, SOSlope for SSDMs and SlideforMAP for SSPMs produce output data related to basal and lateral root reinforcement over the investigated area, allowing to reason focusing on the actual mitigation effect of the forest, as well as the identification of silvicultural practices to improve this effect protection effect where ineffective. In this way, it will be possible to plan more accurately how to manage the forest to reduce the risk of triggering SLs.

MODEL APPROACH	MODEL NAME	APPLICABILITY								Note
		Modeling		Analysis scale		Analysis purpose		Output data		
		Complex numerical method	Multidimentional space	Regional	Slope	Risk assesment	Vegetation effect	Stability factor	Additional information	
SSPMs	LISA	*1			*2					*1: All SSPMs are implemented with LEM-ISM *2: All SSPMs can be used for slope-scale analysis, although they generally use and provide less detailed output data than SSDMs. *3: Stability Index
	SINMAP							*3		
	STARWARS - PROBSTAB									
	GEOtop-FS									
	Park model									
	HIRESSS									
	tRIBS-VEGGIE									
	PRIMULA									
	SlideforMAP									
SSDMs	SHALSTAB							*4		*4: Definition of coeff instability classes
	dSLAM									
	SHETRAN									
	TRIGRS									
	TRIGRS-unsatured									
	Kokutse model									
	SLIP4EX									
	Lu and Godt model									
	SUSHI									
	MD-STAB									
	Ecosfix 1.0									
	SOSlope									

TABLE 2.3: Applicability of slope stability models which consider root reinforcement. Models highlighted in orange consider the contribution of roots in calculating slope stability.

Finally, it is worth commenting on computation time. More complex models require geomorphological, geotechnical, and vegetational input data that sometimes may be difficult to access, either due to lack of instrumentation or measurement difficulties. Physically-based probabilistic models are a clear example of this, implementing statistical methods to reproduce parameter variability and proposing a reasonable alternative to conducting time-consuming and expensive parameter measurement campaigns in the field. In general, computational time depends on the level of detail in the spatial discretization and the input data required for models based on complex equations. This aspect is also related to the time required to obtain the result, which strongly depends on the availability of powerful computer

tools, showing a critical limitation in using some models.

2.5 Final remarks

Slope stability models are fundamental tools for understanding and quantifying the susceptibility to landslides of areas with critical environmental characteristics. As a mitigation factor in the shallow landslide initiation process, the focus on the protective role of vegetation has increased in slope stability models since the 2010s, considering the complexity represented by variability in root reinforcement.

The analyzed SSMs show various solutions applicable to different environments and scales, using hydro-mechanical soil and vegetation information to complete the stability analysis. However, it is difficult to make a rank of the most suitable models. The SSM choice depends on the context for which it has been realized, considering different aspects of the model such as dimensional space, computational scale, the purpose of the analysis, and output data. More recent SSM such as tRIBS-VEGGIE, PRIMULA, and SlideforMAP for SSPMs, and MD-STAB, Ecosfix 1.0, and SOSlope for SSDMs, highlight an increasing attention in considering root reinforcement as a variable factor in space and time. This type of model offers a more detailed output concerning the static ones. Moreover, all physically-based probabilistic models are more suitable than deterministic ones to perform regional-scale analysis.

Stability models may improve simultaneously as the techniques for data collection and measurement. The improvement of survey techniques, e.g., aerial and terrestrial laser scanning, is evident to obtain digital terrain and surface models used to estimate forest structure in spatial and dimensional terms. This improvement is not the same for techniques for acquiring data on root reinforcement. SSMs that consider root reinforcement need field measurements for their characterization and quantification. However, there are no shared standards in the specific case of root measurements, and hence aggregation of different sources is relatively ineffective. The proposal of standardized surveying methods and techniques will allow more systematic data collection implementation and improve the quality of root distribution and tensile strength data, particularly in the Findability, Accessibility, Interoperability, and Reuse (FAIR) perspective of Open-Science. The study of equations and models for reconstructing hydrological and mechanical processes will also need to evolve, accommodating this increased detail and then be implemented in increasingly advanced slope stability models.

Chapter 3

Software

All three software used in this research project were developed by or in collaboration with the international research group ecorisQ. Their application allows estimating the contribution of RR on soil stability considering three different scales of analysis (Figure 1.3), from the single tree scale using RBM++, to the local slope scale using SOSlope, and to the regional forest scale using SlideforMAP.

The only one currently available on the ecorisQ webpage is SOSlope, developed by Cohen and Schwarz (2017) and presently in the update phase for its second version. As for the remaining two software, RBM++ is currently in the first phases of application and GUI finalization, while SlideforMAP is still in the source code development phase and therefore usable only by code line via shell.

A fundamental aspect about the RR estimation is that all these software implemented the same standard values quantified for some tree species. These species are:

- tree of heaven (*Ailantus altissima*, (Mill.) Swingle);
- birch (*Betula pendula*, L.);
- chestnut (*Castanea sativa*, Mill);
- european beech (*Fagus sylvatica*, L.);
- spruce (*Picea abies*, (L.) H.Karst.);
- radiata pine (*Pinus radiata*, D.Don);
- black poplar (*Populus nigra*, L.);
- pubescent oak (*Quercus pubescens*, Willd);
- chinese windmill palm (*Trachycarpus fortunei*, (Hook.) H.Wendl.);
- gray alder (*Alnus incana*, (L.) Moench).

From the results of scientific research on RR of these tree species, standard values for the RR mechanical parameters were identified and made available for analysis with these software through the species choice option. The standardization process involves the steps described in sections 4.1.2 and 4.1.3 of this thesis, but requires

merging more data from locations with similar environmental conditions. In this way, it is possible to characterize the tree species well.

In the following sections, each software will be presented in detail.

3.1 The software RBM++ for root reinforcement estimation

RBM++ is a new software developed as part of this research project to estimate and evaluate the RR. The central part of the software development work involved rewriting the original R code of the Root Bundle Model with the Weibull survival function (RBMw) of Schwarz et al. (2013) in C++ programming language. This process allowed equipping the RBM++ with a GUI for easy use by researchers and professionals. RBM++ allows analyzing the displacement strength of root bundles and their spatial variability at different soil depths and distances from tree stems.

The beta version of the software (Figure 3.1) still depends on preliminary analysis through the original R code for quantifying the standard mechanical parameters of RR.

3.1.1 Input data

Using RBM++ requires specific information necessary to proceed with RR estimation:

1. the *Roots distribution* file, containing the root density recorded for each diameter class. The file should be created similar to the example in Table 3.1, considering 1 mm of increase of each diameter class. In this file:
    - *Id_Trench* corresponds to the profile in which roots are counted;
    - *Id_Tree* corresponds to the trees in which roots are counted;
    - *Distance* (in m) expressed in meters is the distance between the tree stand and the soil profile;
    - *Depth* (in cm) can be or the whole soil profile, or different layers of soil. This choice is at the user's discretion and depends on the detail of the analysis to be obtained.
    - columns from 1 to *n* correspond to root diameter classes.
2. the *Trees* file should be like the example in the Table 3.2. In this file:
    - *Id_Tree* should correspond to the previous table. This allows to assign specific trenches to their own tree;
    - *X and Y coordinates* allow to identify the position of each tree investigated;
    - *Age* is the tree age and an accessory information which allows reasoning over different characteristics of the tree, that influence the reinforcement.

- *DBH* is the tree diameter at 1.30m and an accessory information which allows reasoning over different characteristics of the tree, that influence the reinforcement.
- *Stand* is the location of the investigated tree and an accessory information which allows over different characteristics of the tree, that influence the reinforcement.

TABLE 3.1: Example of root distribution input file in RBM++

Id_Trench	Id_Tree	Distance (m)	Depth (cm)	1	2	...	n
j	i	f	l	n_{ϕ_1}	n_{ϕ_2}	...	n_{ϕ_n}
...	...	...	...	...	...	...	...

TABLE 3.2: Example of tree file data input file in RBM++

Id_Tree	X_coord	Y_coord	Age	DBH	Stand
i	x	y	n	d	*place*
...	...	...	...	...	...

The RBM++ application allows proceeding by two modes of data sets: i) through the *User defined* mode (Figure 3.1), permitting the user to enter specific values of the RR parameters related to the tree specie investigated, or ii) by choosing the tree specie among those already available by default. The latter function is helpful in case it is not possible to perform field sampling and quantify the specific values (Figure 3.2).

The *User defined* option allows obtaining root reinforcement estimation for specific trees or case study. This application required proceeding with data collection in the field and pullout tests (Giadrossich et al., 2017). Field or laboratory data should be used with RBMw equations to obtain the values corresponding to the mechanical root parameters shown in Table 3.3. Equation implemented into RBM++ are very complex, we suggest to see Giadrossich et al. (2013) and Dazio et al. (2018).

TABLE 3.3: Mechanical roots parameters required in *User defined* method in RBM++

Parameter	**Symbol**
Force factor	F0
Force exponent	α
Weibull survival mean	μ
Weibull survival standard deviation	σ
Root stiffness slope	ks
Weibull survival shape factor	ω

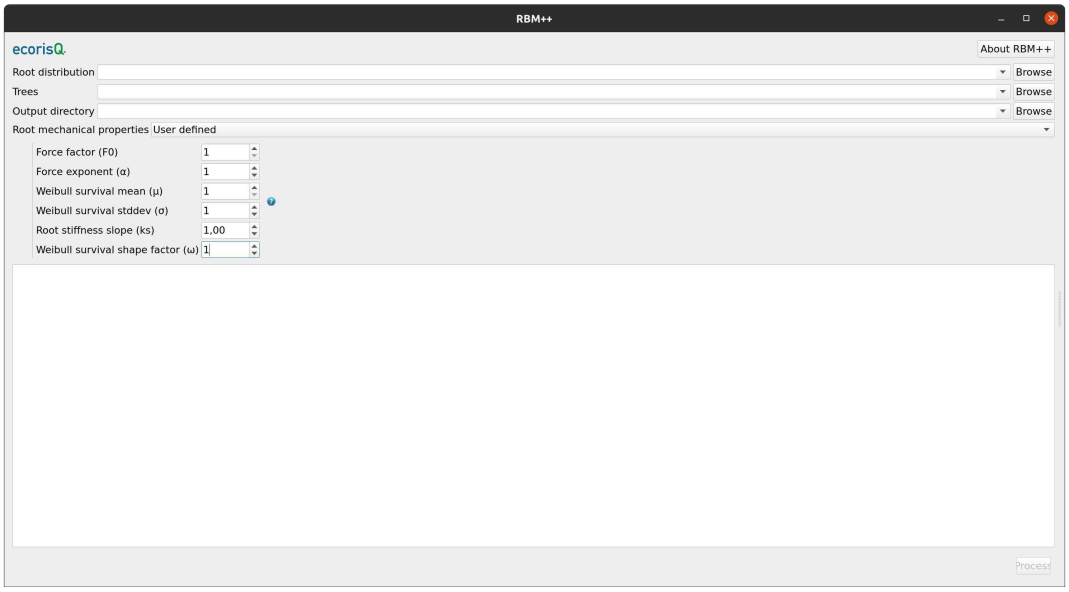

FIGURE 3.1: Graphical User Interface of RBM++ software showing the *User defined* option to estimate root reinforcement. This option allows the quantified values for the specific tree species investigated to be entered into the appropriate cells. However, input data on root distribution, measured for different soil depths and at different distances from the tree, and tree location, are common with the option of choosing the species from those already standardized. The software allows the user to indicate the folder to save the final processing results.

These mechanical parameters will be better discussed when showing the tree scale analysis in the Japanese cedar case study (section 5.1.1)

RBM++ allows to choose a tree species for RR estimation among the ones listed before. Considering the limited number of tree species available, it is possible to choose a tree species with characteristics more similar to the investigated one. In this way, the lack of data necessary to estimate the actual mechanical parameters in the Table 3.3 is overcome.

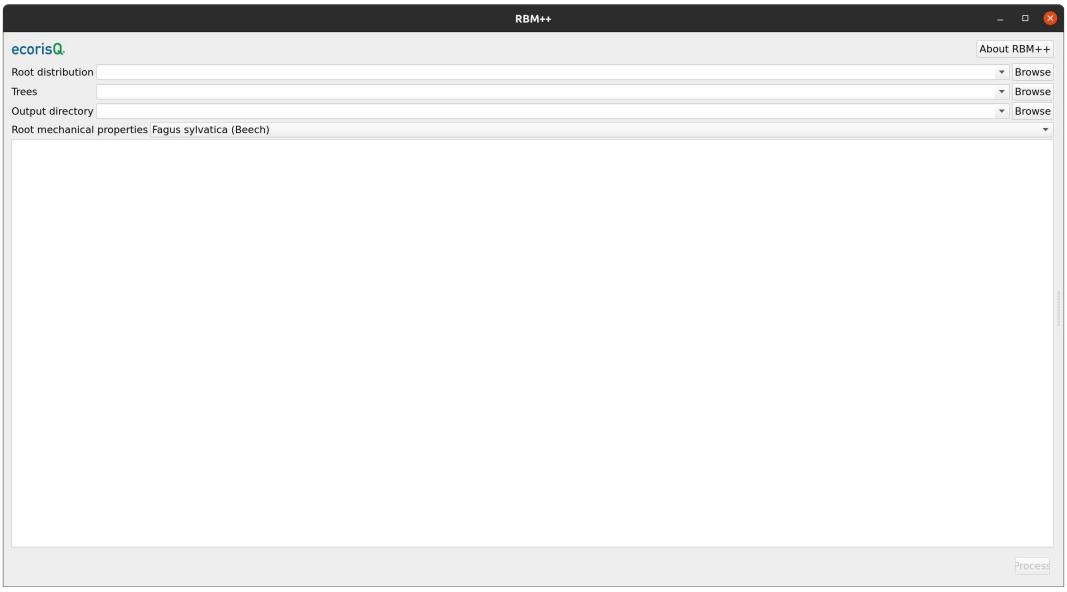

FIGURE 3.2: Graphical User Interface of RBM++ software showing the *Species choice* option to estimate root reinforcement. In the space referring to root mechanical properties, it is possible to view the already standardized tree species list and choose which one to use in estimating root reinforcement.

3.1.2 Output data

From the application of the RBM++ software, it is possible to obtain graphic results directly viewable in specific windows of the GUI and output files in text format. In fact, the same data displayed graphically are available in file format to allow for further analysis and processing.

Results displayed in the GUI are:

- the window of the *Map root reinforcement space distribution*, allowing the visualization of the estimated RR referred at each tree and different distances from the stem. This simplified visualization permits quick estimation and representation of RR for the investigated trees. It is also possible to query each element in the graph and visualize the maximum force values estimated for each trench.

- the window of *Displacement-Force Plot*, showing a technical plot of the force-displacement ratio for each trench. This window is also interactive, giving the possibility to turn the display of a specific trench on or off. Values shown in this graph represent the total RR that can be activated in case of SL on the entire depth profile along the longitudinal trench.

- windows of *Displacement-Force for each depth layer*, allowing to observe and analyze in detail the RR in a specific depth. The number of windows depends on the soil layers identified by the user.

All the windows will be shown describing the study case of Japanese cedar RR estimation (section 5.1.2).

3.2 The software SOSlope for local scale analysis

The software Self-Organized Slope (SOSlope) developed by Cohen and Schwarz (2017) was used in this research project for a local scale analysis. This software is based on a slope stability physically-based deterministic model (Table 2.2), which allows assessing the slope stability focusing on RR contribution on soil protection. We already discussed in the chapter 2 the main characteristics of this model when comparing with the other SSMs available.

Specifically, SOSlope is an hydro-mechanical model that allows calculating the Factor Of Safety (FoS) on a hillslope considering the effects of RR in tension, compression, and shear (Schwarz et al., 2015). Unlike other SSMs (described in Table 2.2), which consider only the BRR, SOSlope produces the analysis of LRR, in tension and compression, and the roots stiffness. Also in SOSlope, the calculation of RR is based on the RBMw by Schwarz et al. (2013).

3.2.1 Input data

SOSlope is developed with an intuitive GUI where the main parameters required must be inserted. Some of these data are in raster format, while others are entered directly into the GUI in number format or text files. Raster data required are:

- the digital elevation model (or digital terrain model) considers the area morphology. Furthermore, this data is also used for the spring-block model (Olami et al., 1992) implemented in SOSlope, allowing consideration of the progressive slope failure discretizing the slope in three-dimensional blocks considered as soil units. Each block contains soil physical parameter values and is connected by bonds to nearby blocks. Each bond represents mechanical forces, such as tension and compression of roots and soil.
- the contributing area (or catchment area) considers water flow movement on the soil. This data is estimated in GIS environment with different modules available.

Also in SOSlope, there is a double possibility to proceed with slope stability assessment. In this case, the *User defined* option regards soil physical parameters. Therefore it is possible to use:

1. the *User defined* application (Figure 3.3), where soil parameters from a specific area (i.e., cohesion, friction angle, density, porosity, initial water content, Van Genuchten parameters, soil depth, and slope) can be put in by the user.
2. choosing among default soil type (Figure 3.4), which allows to consider already standard soil parameters. In this case, the Unified Soil Classification System (USCS) is implemented in SOSlope and considers:
    - well-graded gravel, fine to coarse gravel soil type;

- poorly graded gravel soil type;
- silty gravel soil type;
- clayey gravel soil type;
- clayey gravel with many fines soil type;
- well-graded sand, fine to coarse sand soil type;
- poorly graded sand soil type;
- silty sand soil type;
- clayey sand soil type;
- silty sand with many fines soil type;
- clayey sand with many fines soil type;
- silt soil type;
- clay of low plasticity, lean clay soil type;
- clay of high plasticity, fat clay soil type;
- organic silt, organic clay soil type;
- organic clay, organic silt soil type;
- silt of high plasticity, elastic silt soil type.

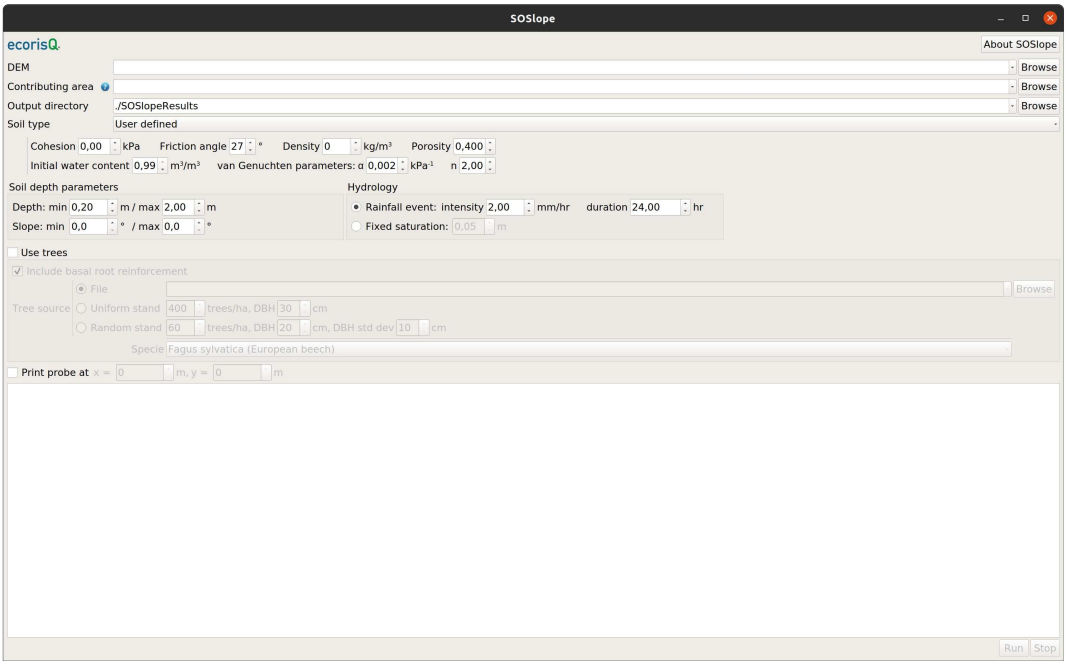

FIGURE 3.3: Graphical interface of SOSlope with *User defined* option for setting soil physical parameters. This option allows using the values of the main mechanical and hydrological parameters measured for the soil in the investigated area. These parameters are cohesion, friction angle, density, porosity, initial water content, and van Genuchten. Estimating the latter parameters is rather complex, but values already estimated by (Likos et al., 2014) for each USCS soil class are available in the literature. The other required parameters are standard for each calculation option.

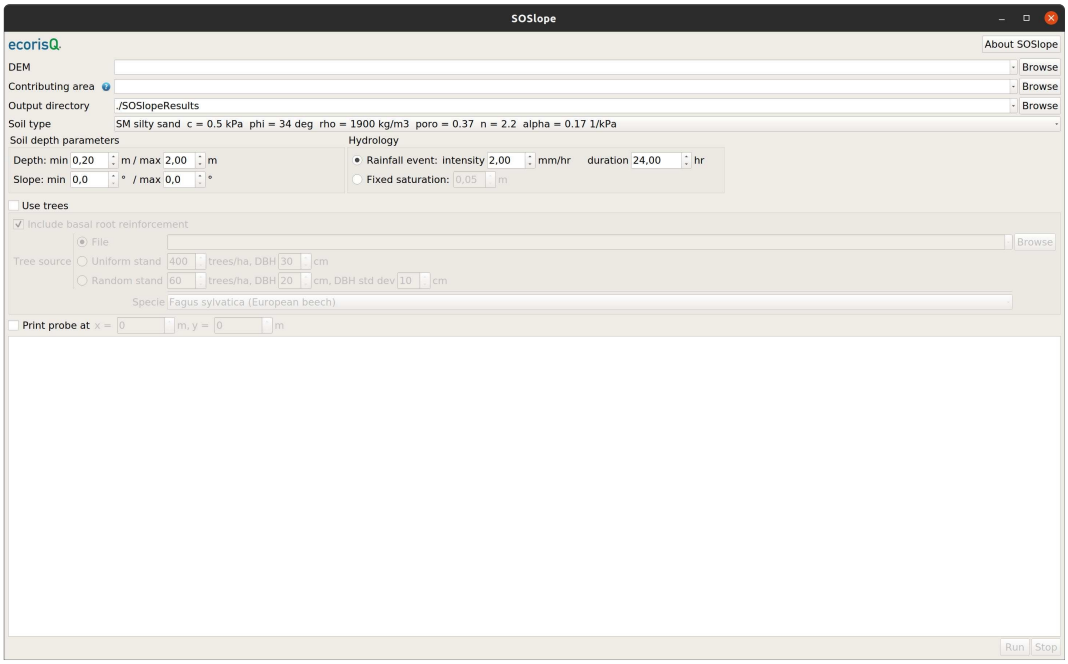

FIGURE 3.4: Graphical User interface of SOSlope with *Soil type* choice option for soil physical parameters data setting. Under soil type, it is possible to observe the list of USCS soil classes. Choosing the corresponding class of the investigated area allows using the standardized default parameters. The rest of the information required to perform the processing is identical to the *User defined* option.

Other necessary parameters regarding the morphology of the area are about minimum and maximum values of both soil depth and slope.

The advantage of using SOSlope is its strong focus when considering the spatial distribution of the forest and, consequently, RR. For this purpose, it is possible to consider tree presence in the investigated area and consider the forest by proceeding with three different options:

1. by using a text file with specific coordinates X and Y, and diameter at 1.3m of each trees;

2. by creating a virtual forest considering space structure and tree dimensions:

   - uniform forest, which regards to a regular structure built considering a tree density per hectare, and a uniform diameter at 1.3m. This application is helpful in the case of reforestation.
   - random forest, which considers random position identified considering a tree density per hectare, and random size based on average and standard deviations values of diameter.

As with RBM++, quantified standard reinforcement values can be used in SOSlope by choosing the tree species among available ones.

SOSlope allows simulating rainfall events by setting intensity and duration of the event. The simulated rainfall event increases the soil mass of the slope and decreases

the blocks' soil shear strength. FoS is calculated each time using a force balance, and if one or more blocks show FoS minor of 1, they are moved downslope by a predefined amount (usually 0.1 mm), and the FoS is recalculated for each one. This relative motion triggers instantaneous force redistributions across the entire hillslope similar to a self-organized critical (SOC) system of which the spring-block model (Bak et al., 1988; Hergarten and Neugebauer, 1998; Cohen et al., 2009) is a subset. FoS estimation and blocks' movement in case of instability are done in a loop and repeated every time until a new equilibrium is found. However, if all blocks are stable, whit a FoS greater than or equal to 1, the slope is stable, while if some blocks failed with displacements more significant than the set value (usually a few meters), the SL occurs.

The equation used for FoS estimation on SOSlope (Cohen and Schwarz, 2017) is:

$$F_oS = \frac{F_s + F_r}{\left|\left|F_d + \sum_4^{j=1} F_j\right|\right|} \tag{3.1}$$

where F_s is the soil basal resistive force including soil cohesion and friction, F_r is the basal root resistance, F_d is the driving force of gravity, and F_j, j=1,..., 4, simulate soil and root tension or compression.

3.2.2 Output data

The stability analysis carried out through the SOSlope software allows obtaining different output data in raster and text format (Table 3.4).

Output data	Data type	Description
Basal_root_reinforcement.asc	raster	BRR activated over space expressed in newton.
Displacement.asc	raster	Soil movement expressed in meters.
FOS.asc	raster	FoS values over space.
Landslides.asc	raster	Number and sequence of triggered SLs.
Landslides.dat	text	SLs information its location (X and Y coordinates of barycenter), the number of failed cells, area and volume.
Max_root_compression_mobilized.asc	raster	Activated LRR in compression expressed in newton.
Max_root_tension_potential.asc	raster	Potential LRR in tension expressed in newton.
Max_soil_compression.asc	raster	Soil compression values over space expressed in pascal.
Max_suction.asc	raster	Soil suction values over space expressed in pascal.
Max_water_pressure.asc	raster	Soil pore water pressure values over space expressed in pascal.
results.dat	text	All values of computed variables during the simulation.
rootdensity.dat	text	Root density values over space.
run.log	text	Log file of the run.
Secant_root_stiffness.asc	raster	Soil stiffness by roots expressed in newton.
Soildepth.asc	raster	Variability of soil depth over space expressed in meters.

TABLE 3.4: Output data information and type obtained from SOSlope

An essential point to mention is the result referred to the pore water pressure. The application of the Dual-Porosity model (Cohen and Schwarz, 2017) allows to estimate the evolution of this factor, distinguishing it in water pressure in macropores and soil fractures, and water pressure in the soil matrix. Obtaining these two separate data is allowed only by using SOSlope on the shell by command line. The raster-format data denoted *Max_water_pressure.asc*, in the Table 3.4 above, provides information on the spatial distribution of maximum pore water pressure without reporting any distinctions.

All of this information obtained from SOSlope provides a complete picture of the dynamics leading to the eventual triggering of SLs.

3.3 SlideforMAP model for regional scale analysis

The software used for regional scale analysis is SlideforMAP (Zadelhoff et al., 2021b), a physically-based probabilistic model (SSPMs) that predicts SL probability on a raster by calculating the ratio of failed hypothetical landslides over the total number of hypothetical landslides. Hypothetical SLs are randomly located on the raster and have an elliptical shape. The area of each hypothetical SLs is randomly selected from a Gamma distribution function (Malamud et al., 2004). The FoS is calculated

using the limit equilibrium approach (Table 2.1) and evaluates the ratio of resistance to gravitational active forces over the area of the SL. Also in this case, a value of the FoS less than 1 indicates a failed SL. Calculation of forces along the slip surface take into account the effect of water pressure on soil strength, where the water pressure is computed from the saturation index obtained using the TOPOG model (Vertessy et al., 1996). Force calculation requires values of soil cohesion, friction angle, hydraulic conductivity, and porosity. Wet soil density is calculated assuming a solid and water density of 2600 and 1000 kg m^3, respectively. LRR is added to the resistive forces on over half the circumference of the SL, while BRR is added over the area of the SL. LRR is calculated using the model of Moos et al. (2016) at the center of a triangulated tree configuration which gives the lowest value of reinforcement. The distance from this center to the triangulated trees is estimated based on an average tree density over the landslide area and transformed into a distance between tree trunks. Details of the calculations can be found in Zadelhoff et al. (2021b). This version of SlideforMAP includes the effect of soil compression at the toe over half of the circumference of the landslide.

Currently, SlideforMAP does not have a GUI, so its application was made through the source code run in the shell and by using a configuration file with all the parameter values.

3.3.1 Input data

The data required for analysis with SlideforMAP are:

- the digital elevation model (or digital terrain model) in raster format, to model the area morphology and estimate slopes;
- the contributing area (or catchment area) in raster format, to model the upslope catchment area, evaluate the soil water movement, and verify the soil saturation index;
- soil physical characteristics in text file format, such as cohesion, friction angle, hydraulic conductivity and porosity;
- average and standard deviation of soil depth values in text file format;
- the presence, structure, size, and species of trees in text file format, to quantify RR values and estimate its spatial distribution.
- information about rainfall intensities of different return period, to evaluate SL failure probability considering extreme rainfall events.

It is evident that input parameters required by SlideforMAP are very similar to those of SOSlope, being based on very similar SSMs. The main difference between the two software is that SlideforMAP, being part of SSPMs requires mean values and standard deviations of physical soil and hydrological parameters. Because of this, the software considers the spatial variability of these values.

3.3.2 Output data

SlideforMAP results are all in raster format and, in general, similar to SOSlope ones. Besides the information about the different types of RR (BRR and LRR), and the soil pore water pressure, SlideforMAP produces a fundamental output data about the failure probability estimated for the investigated area. This main information allows knowing the probability of SL occurring in case of specific rainfall intensity and duration.

SlideforMAP output data are reported in Table 3.5

Output data	Description
LargeWoodVolume.tif	The effective volume of large wood mobilized expressed in cubic meters.
Number_ls_per_cells.tif	The number of SLs simulated in each cell.
PotLWVolMobil.tif	The potential volume of large wood mobilized expressed in cubic meters.
Prob_failure.tif	The failure probability estimated in the study area.
Prob_runnout.tif	The runnout probability estimated in the study area
Root_basal.tif	The BRR activated expressed in newton.
Root_lateral.tif	The LRR in tension activated expressed in newton.
Slope.tif	The slope gradient estimated for the investigated area.
Soil_thickness.tif	The variability of soil depth over space expressed in meters.
TreesInCell.tif	The number of trees in each cell.
Trees_weight.tif	The estimated weight of the trees expressed in kilos.
Water_pressure.tif	The soil pore water pressure expressed in pascal.
Wetness_index.tif	The wetness index variability over space.

TABLE 3.5: Output data information and type obtained from SlideforMAP

The SlideforMAP application case study proposes a methodology for land analysis based primarily on failure probability assessment (section 4.3.2).

Chapter 4

Methodologies

In this chapter, three methodologies applied for the analysis in different scales and contexts are described, all based on the use of a software previously described. Applying the three methodologies in the same study area was impossible because of the necessity to adapt the work to the different phases planned in the research project. Therefore, while tree and local scales of analyses are carried out in Switzerland (Zollikofen and Rüdlingen) during the abroad period at the Bern University of Applied Science, the regional scale analysis is carried out in Italy (Monviso region) in collaboration with the company D.R.E.Am Italia.

4.1 Analysis on tree scale

Quantifying root reinforcement (RR) requires an upscaling process starting from forces measured from a single root, estimating the force procured by a bundle of roots, and finally quantifying the total reinforcement activated from the tree to contrast the soil movement (Schwarz et al., 2010). This upscaling process requires the elaboration of data collected in the field with two different sampling methods: i) a method for collecting the number and size of roots in the soil (subsection 4.1.2), and ii) a method for measuring the tensile force activated by individual roots through pullout tests (subsection 4.1.2). Considering that in this work, the quantification of RR was performed through the RBMw proposed by Schwarz et al. (2013), data were collected directly in the forest. Field measurements allow obtaining a more realistic quantification of root strength, which is also the result of interactions with several complex factors depending on the tree's environment (e.g., root-soil bond strength, water content, stoniness). Tests in natural soil allow considering essential aspects such as root tortuosity, generally neglected in laboratory tests. Tortuosity and elasticity characterize the force-displacement behavior and thus the force peak of a bundle of roots (Giadrossich et al., 2017).

Therefore, quantifying the number of roots and measuring their size allows for assessment of the RR spatial variability, both in vertical (BRR) and horizontal (LRR) directions. On the other hand, pullout tests allow the measurement of force-displacement values necessary for RR upscaling.

In this study, the RR of Japanese cedar (*Cryptomeria japonica*, (Thunb. ex L.f.) D.Don) is quantified. This tree species is widely used in East and Central Asia, and temperate climate countries for reforestation, so its importance for this research project depends on its common location in slope areas and its use in nature-based engineering. The Japanese cedar has been investigated in other studies, e.g., Genet et al. (2006) and Yamase et al. (2019), but no study deals with the biomechanical characterization of RR in the field.

The present study and analysis have provided three main steps:

1. the fieldwork to collect data about root density and forces;
2. the application of the original R code of the RBMw to quantify standard mechanical parameters of this species;
3. the application of the RBM++ software (section 3.1), realized within this research project, for RR estimation on different distances and soil depth layers.

The last step allowed us to observe and evaluate the spatial variability of RR of the two investigated Japanese cedar trees in Switzerland.

4.1.1 Zollikofen study area

For this analysis, two Japanese cedar trees were individuated in the didactic forest located behind the building of the Bern University of Applied Science in Zollikofen village (Bern, Switzerland; Figure 4.1). This forest is mainly composed by conifers, as in Japanese cedar, and broadleaf trees, such as Sycamore maple (*Acer pseudoplatanus*, L.).

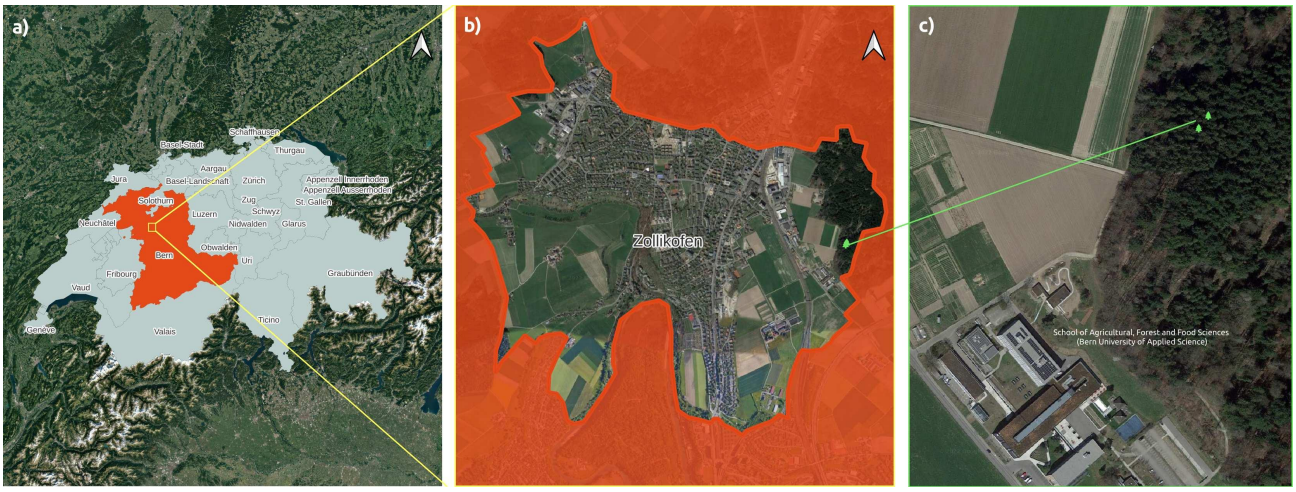

FIGURE 4.1: Figures show the framing of the study area. Zollikofen is a Swiss village belonging to the canton of Bern. The two plants investigated (Figure c) are located in the forest behind the School of Agriculture, Forest, and Food Science (HAFL) of Bern University of Applied Science (BFH).

From the web page of the Federal Swiss Confederation Office of Topography (swisstopo webpage), it is possible to observe that the forested area presents an almost flat morphology (Figure 4.2).

FIGURE 4.2: Zollikofen study area visualized from swisstopo webpage. The forested area presents an almost flat morphology

From the digital map of the Swiss soils, edited by the Federal Office of Agriculture and viewable directly on the geoportal web page, it is possible to observe the presence of medium-deep soils with little skeleton, developed on a geological substrate of moraines, with a good capacity of water storage.

4.1.2 Field measurements and data collection

Field data collection involved quantifying and measuring roots from different distances to the tree stem and different soil depths, and pullout tests to measure force-displacement for different root samples. Field-collected data related to soil root density and force-displacement ratio were processed through the original RBMw code written in R (Schwarz et al., 2013), aiming to verify the data quality and calculate the values of mechanical parameters needed to estimate the Japanese cedar RR.

Root distribution measurements

Root density in soil was measured close to two Japanese cedar trees using the method described by Schwarz et al. (2012b). As shown in Figure 4.3 (a), semicircular-shaped trenches were dug around each tree, developing four longitudinal soil profiles at distances from the tree of 1.5m, 2.5m, 3.5m, and 4.5m. In each profile, root density was investigated along lengths varying from a minimum of 5m for the innermost profile (1.5m distant) to about 9m for the outermost profile (4.5m distant). Finally, the soil depth investigated arrived generally until 60 cm. For each longitudinal profile, modular sectors 1m wide were identified, like shown in the Figure 4.3 (a). The

number of roots and their diameters were measured for different soil layers, each one identified with a thickness of 15cm (Figure 4.3 b), paying attention to consider only roots corresponding to the investigated species.

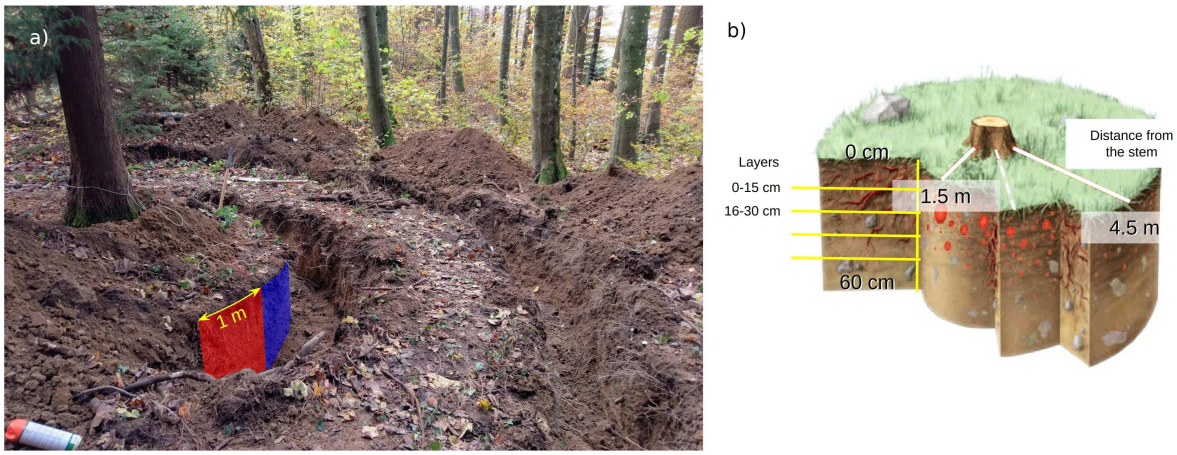

FIGURE 4.3: Figure (a) shows the two trenches dug around tree 1, which identify the four soil profiles at 1.5, 2.5, 3.5, and 4.5 meters from the tree. In each profile, sampling was done by systematically following the design presented in Figure (b) from Schwarz et al. (2010). By identifying sectors of 1m width and length equal to the maximum soil depth that could be investigated, layers of 15 cm each were identified in which the number and size of roots were recorded to quantify root density.

Root strength measurements

The pullout tests were carried out on 35 roots, distributed in several diameter classes ranging from a minimum of 1 mm to a maximum of 36 mm. This representative sample of data referring to different diameter sizes allows for a better root tensile strength upscaling. The importance of conducting field tests rather than laboratory tests is that field tensile tests consider the effect of the soil-root interface and all of the complex dynamics in the forest.

Following the methodology of Giadrossich et al. (2017), vertical trenches were dug to promote root escape from the soil. Carefully removing the soil to expose an adequate length and debarking the end of the root made it possible to anchor it to the pullout machine (Figure 4.4). The pullout machine has a complex structure consisting of a load cell for measuring the force activated by the root during the test and a wire displacement sensor for measuring the relative displacement. This means taking the root and elongating under tensile force until it breaks. It is possible to proceed with the root tensile tests through a constant tension guaranteed by a winch located in the final part of the machine. The test ends when the root, expressing its peak force, breaks. The root diameter is measured near the soil profile, i.e., the nominal diameter, and at the breaking point. In branching roots, it is possible to have multiple breakage diameters.

FIGURE 4.4: The Figure shows the pullout machine specially made to perform tensile tests on roots. This machine is equipped with a pulling system connected to a winch, a load cell to measure the force, a displacement sensor to measure the root displacement, and a datalogger for measuring data. In the anchoring process, the root, debarked, must be tied to a threaded bar with a ring to allow connection with sensors and the machine itself. The test begins when the root is subjected to tension force and proceeds until its complete failure.

4.1.3 Root Bundle Model with Weibull survival function

RBMw is a RRMs developed to quantify RR by considering the inherent variability in mechanical root properties, even in similar diameters. The model considers each root as a linear-elastic fiber that breaks when subjected to a tensile force and once it reaches a threshold displacement corresponding to its maximum force. Estimating the tensile force in a root using the fundamental equation of linear elasticity requires knowledge of its geometry (diameter, length, tortuosity) and mechanical properties (maximum tensile force, Young's modulus). In contrast to the original RBM (Schwarz et al., 2012b), RBMw implements a survival function, also known as a complementary cumulative distribution function, used to estimate the probability of failure of a complex system once a certain threshold is exceeded. The Weibull distribution is adaptable in the study of root failure (Pollen and Simon, 2005; Cohen et al., 2011).

The first step to calculating the RR is processing the raw data from the field-recorded pullouts to identify the equation for maximum reinforcement quantification (eq.5.1), minimizing the sum of the squared errors (Figure 5.2 c), and calculating

the equation for the secant spring constant (Figure 5.3). Both factors are estimated as a function of the root diameter (Dazio et al., 2018).

The equation 4.1 allows the quantification of maximum root reinforcement as a function of root diameter:

$$F_{max}(\phi) = F_0\phi^{\alpha} \tag{4.1}$$

where F_{max} is the maximum tensile force (in newton), ϕ is the root diameter (in meters), F0 is the constant, and α is the exponent.

However, the application of this equation can overestimate the maximum forces for root diameters $\leq$5mm, causing significant errors (Dazio et al., 2018). In order to improve the curve calibration for smaller roots, the equation 4.1 is modified by multiplying a cumulative normal distribution function:

$$C(\phi) = \frac{1}{2}[1 + erf(\frac{\phi_i - \phi_m}{\phi_s d\sqrt{2}})] \tag{4.2}$$

where ϕ_m and ϕ_{sd} are the coefficients that correspond to the mean and standard deviation of the cumulative normal distribution, respectively.

Considering the secant spring constant calculation, it is assumed that roots have a linear elastic behavior when subjected to a tension force (Schwarz et al., 2013). This constant varies with root diameter and is obtained from the ratio of the maximum root pull-out force to the respective displacement:

$$k(\phi_i) = k_0 + k_i\phi_i \tag{4.3}$$

where kϕ_i is the spring constant (in Nm^{-1}), ϕ_i is the root diameter (in meters), and k$_{0,i}$ are constant parameters.

Through the Weibull survival function, RBMw considers the intrinsic mechanical properties of roots (e.g., the ratio of lignin to cellulose or the root's moisture content) or the heterogeneity of soil mechanical properties. In the specific case of RBMw, the Weibull distribution, developed by Weibull (1939), is applied to calculate the failure time of roots (Pollen and Simon, 2005; Cohen et al., 2011). Therefore, the model assumes that the probability of root survival varies as a function of normalized displacement, which is obtained through the equation 4.4:

$$S(\Delta x^*) = exp[-(\frac{\Delta x^*}{\lambda^*})^{\omega}] \tag{4.4}$$

where Δx^* is the normalized displacement, ω is the Weibull shape factor, and λ^* is the Weibull scaling factor. The displacement normalization process is necessary to constrain the effect of the root diameter on the maximum displacement (Schwarz et al., 2013).

The quantification of the bundle root reinforcement (RR_{max}) referred to a specific

displacement (Δx) is obtained by summarizing the force of each root and multiplying by the survival function (S) as shown below:

$$RR_{max}(\Delta x) = \sum_{\Phi=1}^{\Phi_{max}} n_{\Phi} F(\phi_{\Phi}, \Delta x) S(\Delta x^*_{\Phi}) \tag{4.5}$$

where F_{tot} is the root reinforcement of a root bundle per linear width of the trench (in $Nm^{-}1$), Δx is displacement (i.e., the amount of root elongation under tensile force until the breaking point) (in meters), n is the number of roots corresponding of a root diameter class (ϕ), ϕ_{Φ} is mean root diameter of each root diameter class, Φ_{max} is maximum root diameter class considered, and Δx^*_{Φ} is normalized displacement of each root diameter class.

While key parameters for equations from 4.1 until 4.4 were obtained by applying the R code, values of RR were estimated in the RBM++ software by using the *User defined* option.

In the next chapter (section 5.1), data obtained from R elaboration and RBM++ application are shown and discussed.

4.2 Analysis on local scale

4.2.1 The TRAMM project

In this research project, SOSlope software (section 3.2) was used for a back-analysis of an artificially triggered SL during an experiment led in March 2009 with the Triggering of RApid Mass Movements (TRAMM) research project. TRAMM (WSL project webpage) was a multidisciplinary research project managed by the ETH Competence Centre of Environment and Sustainability to analyze and understand initiation and evolution processes of rapid mass movements, and the application of numerical and analytical methods to assess slope stability. The objectives set by this project were: i) understanding the mechanisms of SL initiation, ii) investigating the cause of changes in the soil mass velocity after its failure, and iii) analyzing the influence of hydrological conditions on slope stability.

Rüdlingen study area

The study area is located near the village of Rüdlingen, precisely on the east bank along the Rhine River (Figure 4.5). In the past, this area already showed a high predisposition to landslides. Askarinejad et al. (2012) reported the event occurred in May 2002 when, after intense rainfall lasting 42 minutes and with intensity of 100mm, 42 SLs were activated in the surrounding area (Fischer et al., 2003).

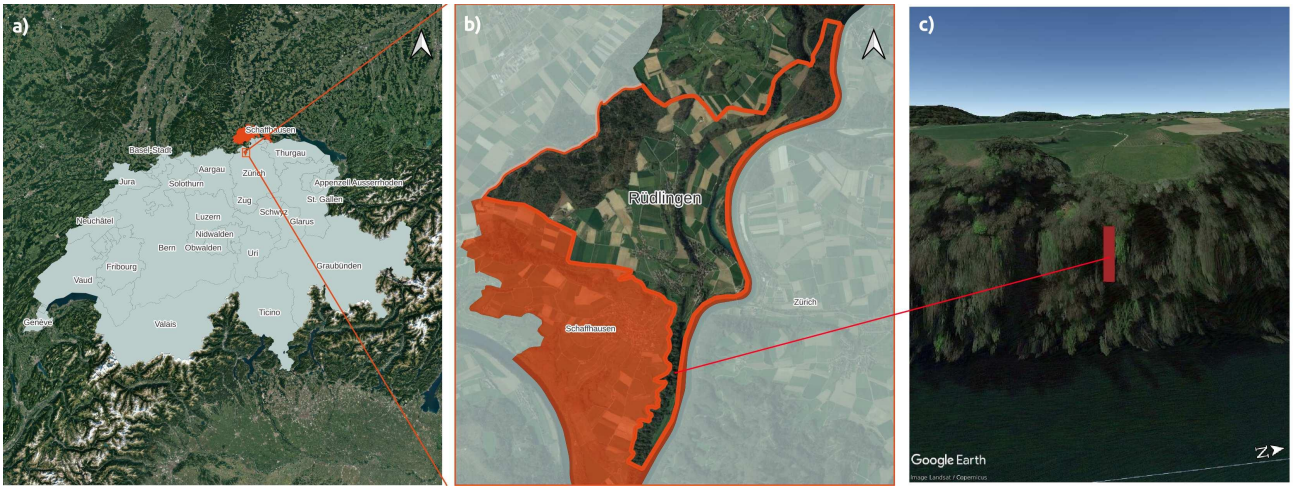

FIGURE 4.5: The figures show the framing of the study area. Rüdlingen is a Swiss village belonging to the canton of Schaffhausen. The instrumented area (Figure c) was realized on a forested slope on the left bank of the Rhine River.

The morphology can be considered as a predisposing factor to the SL risk, showing a gradient of slope ranging from a minimum of 37°to a maximum of 43°(Springman et al., 2009).

Field geological analysis showed an irregular substrate of Molasse, with alternate depositions of seawater Molasse and freshwater Molasse. Observations before the experiment revealed porous layers and fissures several centimeters wide in the

latter substrate. Soil depth, estimated by identifying the bedrock layer using the dynamic probing light method, was measured between 0.7 and 5.6 (Lehmann et al., 2013). Following the USCS, the soil was classified as a medium-low plasticity silty sand (Askarinejad et al., 2012). The presence of bedrock fissures and the high macroporosity of the soil, mainly due to root growth (Askarinejad et al., 2012; Schwarz et al., 2012a), allowed the development of preferential drainage paths, influencing the degree of soil saturation during the tests, as well as the general stability conditions of the slope (Askarinejad et al., 2012).

The forest is classified as *Aceri-Fraxinetum* and composed by three layers: i) a tree layer (about 80% coverage, 5–20 m high) in which Ash (*Fraxinus excelsior* L.) prevailed, ii) a lower layer of shrubs (1–5 m), and iii) a grass layer (Schwarz et al., 2012a). For each trees, the position and dimension were measured, allowing for the root reinforcement estimation.

Experimental setup

The project involved the installation of an extensively instrumented area, 35 m long and 7.5 m wide, equipped with several sensors for data collection (Figure 4.6 from Askarinejad et al. (2018)). The sensors used were tensiometers, time-domain reflectometry sensors, piezometers, soil temperature sensors, slope deformation sensors, earth pressure cells, acoustic sensors, and rain gauges, divided into three functional groups and placed in different strategic locations in the instrumented area.

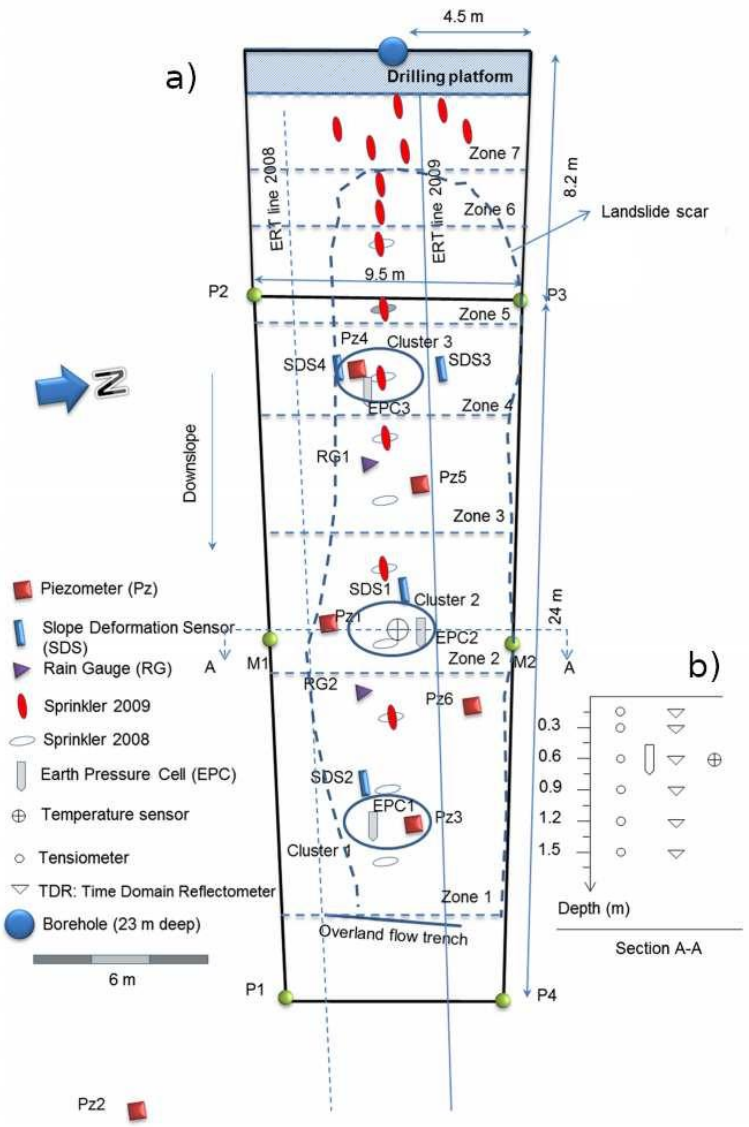

FIGURE 4.6: The experimental design from the paper by Askarinejad et al. (2018) shows the instrumentation and different rain zones at the Rüdlingen test site. Figure (b) details the depths at which the tensiometer nodes and time-domain reflectometry sensors are located. This arrangement is provided in each of the three clusters circled in blue.

Measurements of soil deformations were made from the soil surface, through photogrammetric methods (Akca et al., 2011), and from inside the soil mass, using slope deformation sensors. The slope deformation sensors were equipped with strain gauges and two-axis inclinometers placed on top of the instrumented area (Askarinejad and Springman, 2017). Indeed, to detect the presence of bedrock cracks capable of altering soil water movement, electrical resistivity tomography analysis was applied (Gambazzi and Suski, 2009).

Hydrological effects were measured at different locations and soil depths on the slope (Lehmann et al., 2013). Pore water pressure data were obtained by installing one tensiometer per functional group. Each node of the tensiometer was placed at different soil depths (Figure 4.6 b). Time-domain reflectometry sensors were used to measure soil moisture and installed at different depths (Figure 4.6 b). Hydrological

data recording during the experiments was done every 5 min.

Finally, in addition to sensors for parameter measurements, the area was provided with sprinklers necessary to simulate rainfall artificially. The number and position of sprinklers in the analysis area were modified following the results obtained from a first test.

The experiments In the first test, conducted in October 2008, after applying artificial rainfall for 4.5 days, with an average intensity of 15 mmh^{-1} for the first 2.5 days and 30 mmh^{-1} for the last two days, only minimal downslope soil movement occurred. Although the cumulative amount of artificial precipitation during the test (1700 mm) was similar to the total average precipitation for two years in this region (Askarinejad et al., 2011) and even though an increase in pore water pressure was observed (Askarinejad et al., 2012; Lehmann et al., 2013), no relevant surface movement occurred. The stable condition was maintained due to the development of rapid drainage flows through interconnected bedrock fissures and soil macropores, thereby preventing the initiation of SL.

Based on the observation in this first test, the experimental design was subjected to some modifications before proceeding with the second test in March 2009. Specifically, the number and location of sprinklers were changed to simulate greater precipitation intensity in the upper part of the instrumented area (see Figure 4.6 where the white oval symbol represents the sprinklers of the test in 2008, while the red oval symbol represents those of the test in 2009). The new sprinkler location, designed to increase the volume of water delivered to the soil in the upper part of the study area, resulted in the triggering a 130 m^3 SL after 15 h of artificial rainfall with an average intensity of about 10 mm/h (specifically around 20 mm/h on the upper part and around 5mm/h in the lower part). Soil deformation sensors and photogrammetric images recorded the progressive slope failure, which began with slight soil movement approximately 2 hours before the effective failure, and then continued with gradually increasing velocity over the next 30 minutes. The main factor of the progressive slope failure was the gradual activation of the RR driven mainly by their size (Schwarz et al., 2012a). In addition, water exfiltration phenomena were also observed at the back of the slope, confirming what was already observed in the previous experiment regarding the presence of preferential flow paths (Lehmann et al., 2013).

Hydrological and geotechnical observation The geotechnical and hydrological data collected during both experiments were analyzed to understand the dynamics that favored the loss of stability.

Regarding the hydrological behavior, variations of pore pressure and volumetric water content was analyzed in detail. After the second test, it was observed that the higher artificial rainfall intensity in the upper part of the area promoted the development of higher pore water pressure values. However, these values did not show

significant changes before or during the triggering (Askarinejad et al., 2018). Regarding the volumetric water content, volume increases of about 17% at depths of 0.6cm and 31% at 1.2m were recorded in the upper part of the instrumented area. The changes in water content along with the soil profile, as measured by the time-domain reflectometry sensors, were caused by different porosity in deep soil layers and, probably, by the presence of the water table at depths of 1.2m (Askarinejad et al., 2018). However, at about one hour before the slope failure, reductions were recorded both in the porosity, reaching in the upper part up to 0.7 kPa, and in the soil water content. Causes that explain these dynamics were either soil expansion at the failure surface due to increased pore pressure or the development of drainage flows through ongoing slope deformations.

Analysis of the data measured through the slope deformation sensors and strain gauges observed the presence of two slip surfaces, a shallow one at 0.5m, developed in the latter stages of slope failure, and a deeper one at 1.30m. This feature of the area affected the movement of water in the soil and caused different rates of movement of the unstable soil mass. From the photogrammetric images, it was observed that up to 23 min before failure, small movements occurred both downward and along the slope (Askarinejad et al., 2018). The upper part of the area began moving at a rate of 0.5 mm/s 22 min before the actual failure of the slope, then increasing to 140 mm/s 30 s before failure.

The root reinforcement observations Relative to the quantification of LRR potentially activated to counteract slope failure, the RBM from Schwarz et al. (2010) was used. Twenty-seven field pullout tests were performed on roots with diameters up to 5.5 mm using the methodology proposed by Schwarz et al. (2011). Root density and size data, necessary to upscale force values, were measured from an ash tree using the methodology proposed by Schmidt (2001). In addition, once the landslide occurred, the roots exposed on SL scarp were also mapped and measured. Root density was modeled and compared with the field measured one.

RR results showed values of 106 kN using the modeled root distribution and 83 kN using the field measured root distribution (Schwarz et al., 2012a). The difference of 23kN using RBM is due to overestimating the root number for diameter classes of 1, 2, and 3mm. However, RBM generally underestimates the braking forces of a bundle (of about 10% and 20%; Schwarz et al. (2011)). The calculated RR is reduced as a function of spatial variation in root density and size. Increasing the distance from the tree, root density and size decreases, affecting RR values over space. In conclusion, the progressive failure of the artificially triggered SL was caused by fluctuating variations in pore water pressure, the development of interacting unstable blocks along the failure area, bedrock and soil surface heterogeneity, and root failure near the upslope area and in shear zones lateral to the SL.

4.2.2 Methodology

The methodology applied for the reconstruction of triggering dynamics of the artificial SL is based on applying the SOSlope software. As mentioned above, SOSlope uses both information in raster format, specifically for the digital terrain model Digital Terrain Model (DTM), and the contributing area, and information in numerical format. It is essential to highlight that due to it being a complex deterministic model (section 2.2.4), the model application requires minimum resolutions of 1m per 1m, in order to obtain good results.

Calculation of the contributing area While the DTM was obtained online from the Swiss National Geoportal, the contributing area information was calculated in GIS environment using the *Catchment Area (Top-Down)* module of SAGA GIS (Module description sheet). This module provides several algorithms for estimating flow directions and calculating upslope areas using the rectangular grid of the DTM as base information. For this case study, among the algorithms made available, the Deterministic Infinity method of Tarboton (1997) was chosen, considering it more adequate to meet the needs of the analysis performed. In fact, because of the above condition related to the input data resolution, this method proved to be less sensitive than others to the resolution of the data (unlike the Multiple Flow Direction method of Freeman (1991) and the Triangular Multiple Flow Direction method of Seibert and McGlynn (2007)), although not overly accentuating the estimated runoff (as in the processing obtained with the Deterministic 8 method of O'Callaghan and Mark (1984) and the Rho 8 method of Fairfield and Leymarie (1991)) (Figure 4.7).

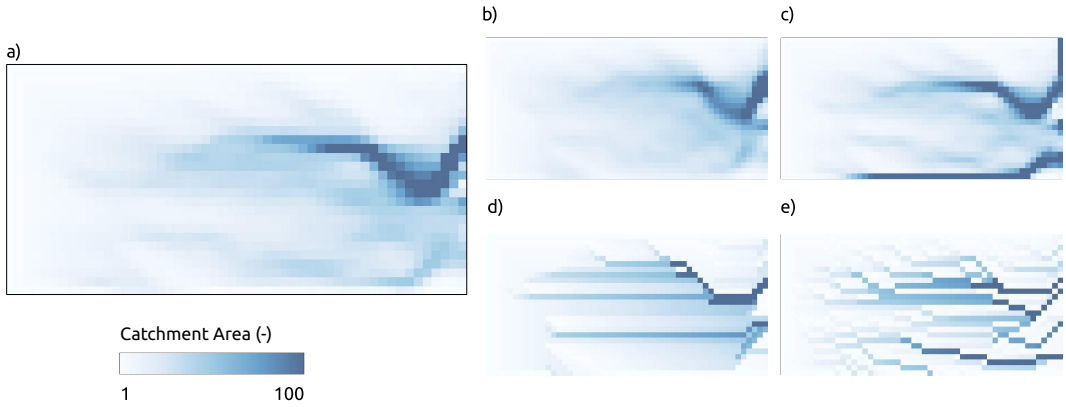

FIGURE 4.7: The four pictures show the results of applying five algorithms available for the calculation of the contributing area. Shown respectively are a) the Deterministic Infinity method, b) the Multiple Flow Direction method, c) the Triangular Multiple Flow Direction method, d) the Deterministic 8 method, and e) the Rho 8 method.

Identification of the others input parameters The remaining input data required in numerical format were collected through bibliographic analysis of papers published on the TRAMM project or chosen from those already provided by default in

SOSlope from the USCS. These values are reported in the following Table:

Parameters	Values	Unit	Source
Soil Type (USCS)	ML		Askarinejad (2013)
Friction angle	31.0-34.5	degree	Lehmann et al. (2013)
	29.5-32.5		Askarinejad and Springman (2017)
	29.3		Casini et al. (2009)
	33.0-34.0		Askarinejad (2015)
Dry density	1700	kg m^{-3}	Schwarz et al. (2012b)
Initial water content	*0.15-0.20*	m^3 m^{-3}	Schwarz et al. (2012b)
	0.15		Askarinejad (2015)
	0.27(depth 0.6-1.2m)		Askarinejad et al. (2012)
	0.35 (depth 0.9-1.5m)		Askarinejad et al. (2012)
van Genuchten parameters	α = 0.2	kPa^{-1}	Lu et al. (2010)
	α = 0.7	kPa^{-1}	Askarinejad (2015)
	n = 0.537	-	Askarinejad (2015)
Soil min depth	0.7	m	Lehmann et al. (2013)
Soil max depth	1.37	m	Askarinejad et al. (2018)
Slope min	37	degree	Springman et al. (2009)
Slope max	43 (middle slope)	degree	Springman et al. (2009)
	43 (middle slope)	degree	Askarinejad et al. (2012)
	40		Schwarz et al. (2012b)
Mean rainfall intensity	10	mm h^{-1}	Schwarz et al. (2012b)
Rainfall duration	15	hours	Askarinejad (2013)

TABLE 4.1: Values of input parameter from TRAMM project scientific papers

Pore pressure reconstruction An essential step in this methodology was to reconstruct the hydrological dynamics that favored the SL triggering, therefore taking into account the difference in simulated rainfall intensity between the upper and lower parts of the area due to the non-uniform sprinkler arrangement (Figure 4.6). However, in order to account for this process, it was necessary to find a solution to correct the main hydrological information required in SOSlope, i.e., the catchment area, and obtain a new *ad hoc* datum for this landslide event. Among the various hydrologic information available from the TRAMM project, measured pore pressure values at

different locations in the instrumented area (at 5m, 15m, and 25m from the upper boundary of the area (Lehmann et al., 2013)) were used to calibrate and correct the new catchment area values.

The reconstruction process then involved dividing the area into three sub-areas based on sprinkler density (red ovals in Figure 4.6). Next, each of these areas was assigned a corrective value calculated from the ratio of the pore pressure value measured during the test (Lehmann et al., 2013) with values estimated from processing with SOSlope at the same point (see Table 3.4 for output data Max_water_pressure.asc). Finally, by multiplying the original contributing area values (Figure 4.7 a) with the three correction coefficients (Table on Figure 4.8), it was possible to obtain a new catchment area data to be used for the dynamics reconstruction of Rüdlingen SL triggering.

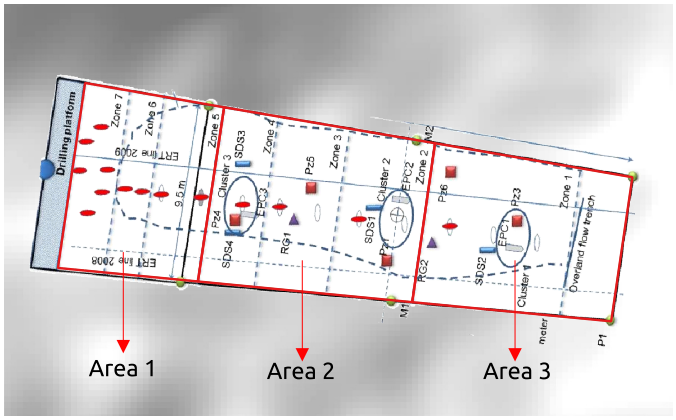

Area	Correction value
1	1.67
2	0.85
3	0.62

FIGURE 4.8: The Figure shows the three areas identified to make the contribution area correction. In reconstructing the slope's hydrological dynamics, it was necessary to quantify correction values to be applied in areas with different rainfall intensities. This difference depends on the number of sprinklers placed in each area during the March 2009 experiment (red ovals). The corrective values estimated from the ratio of pore pressure values measured in the field and obtained through a preliminary analysis with SOSlope are given in the table.

In SOSlope, several simulations were performed modifying the combination of parameters identified through the literature search (Table 4.1). Among the simulations performed, the one that best represents what happened during the second test in Rüdlingen was carried out with the input parameters shown in Table 4.2.

Parameters	Values	Unit	Source
Digital terrain model	-	Resolution 1x1	Swisstopo
Contributing area	Deterministic Infinity method	Resolution 1x1	Digital terrain model
Cohesion	0.5	kPa	default from SOSlope for ML soils
Friction angle	30	degree	Askarinejad and Springman (2017)
Dry density	1700	kg m^{-3}	Schwarz et al. (2012b)
Porosity	0.42	%	Calibrated
Initial water content	0.20	m^3m^{-3}	Schwarz et al. (2012b)
van Genuchten parameters	α = 0.130	kPa^{-1}	Default SOSlope
	n = 1.46	-	Default SOSlope
Soil min depth	1.1	m	Calibrated
Soil max depth	1.37	m	Askarinejad et al. (2018)
Slope min	37	degree	Springman et al. (2009)
Slope max	40	degree	Schwarz et al. (2012b)
Mean rainfall intensity	-	-	TRAMM measurements
Rainfall duration and intensity	-	-	TRAMM measurements
Tree size and position	-	-	TRAMM measurements

TABLE 4.2: Values of input parameter used on SOSlope simulation

For the evaluation of data quality and comparison with the results obtained from the TRAMM project, it is necessary to highlight that the rainfall data used in SOSlope simulation start one hour after the effective start of the field experiment. Looking at Figure 4.9 taken from Askarinejad et al. (2018), the data used in SOSlope excludes the rainfall provided on the soil before the first break, corresponding to about an hour. Data about this first simulated rainfall were not available for the simulations. Therefore, we chose to use the maximum value of initial water content reported in the literature (Table 4.2), which is 0.2 m^3m^{-3}, to simulate the water delivered to the soil in the time frame previous to the simulation.

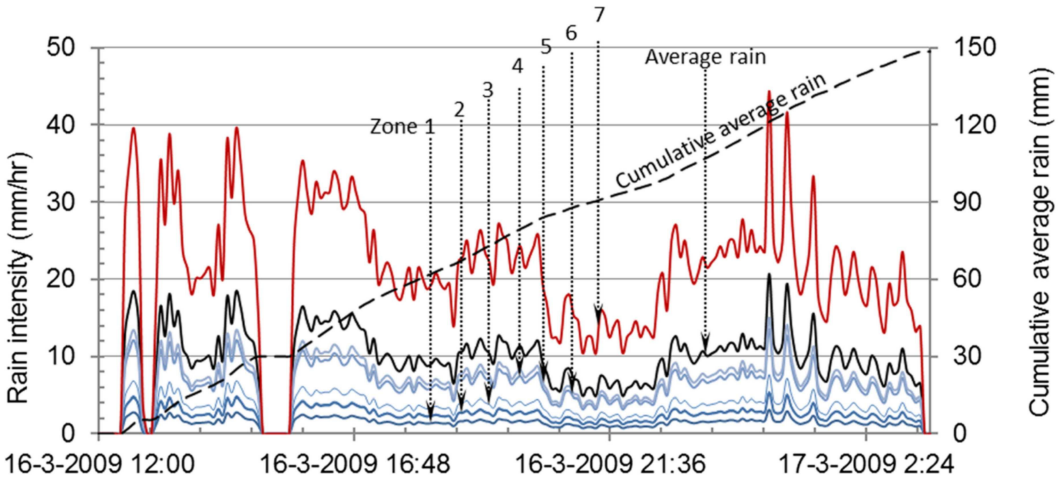

FIGURE 4.9: Variability of precipitation intensity in the experiment conducted in May 2009 (Askarinejad et al., 2018). Specifically, the lines with different shades of blue represent the rainfall intensity measured in the raining zones located centrally and in the lower part of the instrumented area, while the red line represents the intensity measured in the raining zone located in the upper part and provided with a more significant number of sprinklers (see Figure 4.6). Finally, the black line represents the average rainfall intensity and corresponds to the values used in the analysis with SOSlope.

Regarding the calibration of the porosity and minimum soil depth (Table 4.2), the values were calibrated based on the known ones, derived by default from SOSlope or the literature, and changed according to the results obtained from SOSlope simulations. Therefore, the porosity value was identified starting from the default value suggested by SOSlope for the sandy silt soil type (equal to 0.47) and gradually changed until finding a better combination with the values of the known parameters. On the other hand, soil depth was calibrated based on what Askarinejad et al. (2012) observed about the failure surface, placed at a depth between 0.8m and 1.3m. The value chosen for the simulation is the average between these two values.

4.3 Analysis on regional scale

The area under analysis is currently subject to renewal of the Piano Forestale Aziendale (PFA). The PFA is a detailed planning tool developed for planning silvicultural practices necessary for forest management (*Regione Piemonte website*).

Considering the typical alpine landscapes, characterized by steep areas, large valleys, and tributaries, in the past, this area has been shown to be susceptible to landslides, as reported by the Landslide Phenomena Information System of Piedmont (SIFRAP) (*website*). For this reason, a new methodology for the estimation of SL probability was applied, based on SlideforMAP software (section 3.3). This analysis allows evaluating the forest' protective effect currently present, and identifying points where it is necessary to intervene through silvicultural management and improve the protective effect.

4.3.1 Monviso study area

Morphology and slope The analyzed area is located in Piedmont, in the province of Cuneo (Figure 4.10), among the southern Cottian Alps, along the initial part of the Po river valley. It presents a highly variable morphology, with a wide central valley, where the Po River flows towards the flat area in the innermost part of the region. It is evident that also the altitude varies considerably, reaching maximum altitudes above 3500m asl, with the highest peak Monte Viso (3841 m asl), to the minimum altitude of 252 m a.s.l. in the plain. This morphology also determines a considerable variability of the slope, locally exceeding 100%, highlighting the presence of numerous tributaries that influence the water flow in the area under analysis.

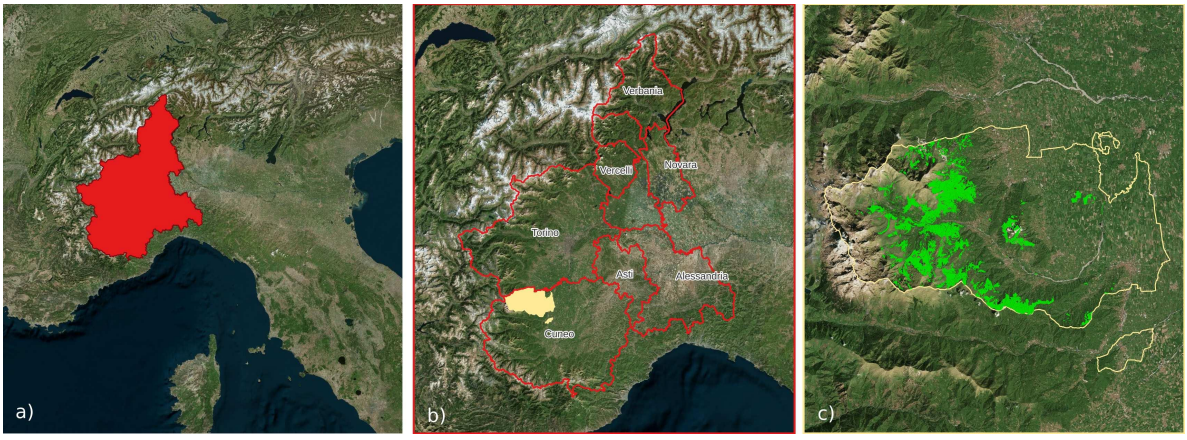

FIGURE 4.10: The figures show the framing of the study area. The area subject to planning is located in the Monviso valley, in the province of Cuneo, and involves the public part of the total forest cover.

Climate The morphology that characterizes the Monviso area has favored the presence of a climate with high continentality. Morphological and altimetric factors

cause a diversification of local climatic conditions, influencing temperatures, precipitation exposure, and intensity of rainfall events. In general, the area climate presents cold winters (average minimum temperature of Cuneo in January, with an average of 1.8°C) and mild summers (average maximum temperature of Cuneo in July of about 21.6°C) (data source *CentroMeteo*). Precipitations show an annual average of about 950 mm, with frequent snowfalls near the highest altitudes and favored by the effect of the Bora wind which is typical in alpine areas.

From the studies carried out by the Interreg ALCOTRA CCLIMATT (Climate Change in the Transboundary Territory project, 2014-2020), it was observed that the whole Piedmont region presents a rapid alternation of extreme events, which are becoming more intense and frequent. These effects are evident at high altitudes, affecting agro-silvopastoral activities, tourism, and, to some extent, the intensity and frequency of natural hazards. It has been shown that in the last 38 years, there has been an increase in maximum temperatures concentrated mainly in the summer and autumn seasons, while precipitation alternates between consecutive years of lower rainfall amount and periods of several years with significant rainfall average. Over the past 30 years, a precipitation deficit has been observed during the winter and summer seasons, with moderate precipitation during the spring period. In contrast, the fall period is characterized by a positive anomaly.

All of this information regarding the area' climate suggests the crucial role of its variation in the frequency and intensity of SLs.

Geology The geology of the area has seven major classes. The Po river flow valley and the flat area to the west consist of lowland and valley floor of alluvial deposits and represent the most significant extent (about 52% of the area). The other two most widespread geologic classes are represented by occhiadine gneisses (Monte Rosa and Val d'Ossola massifs) and minute gneisses (Dora-Maira, Sesia-Lanzo massifs), respectively 23% and 18% of the total area, located near the mid-elevations, between the plains and the Alps. The other less represented classes are serpentinites (Piamont zone, Jurassic-Cretaceous), with 4% of the surface localized near the alps. Less extensive surfaces, percentages less than 1, are represented by moraine deposits (Quanternary), dolomite and limestone (Mesozoic units), and calcareous (Piamont zone, Jurassic-Cretaceous).

Pedology Considering that 2% of the area is characterized by outcropping rock, the soil is present for the remaining 98% and includes four soil orders. The soil order which occupies a greater extent of area is the alphisols (about 35%), whose pedogenesis was favored by the transport action of soil particles deposited by the Po River. There are lowland alphisols, mountain alphisols, and a small part of alphisols of localized ancient terraces of the soil class level. The second order of soils diffusely present are inceptisols (about 30%), with mountain and lowland inceptisols. The following order is entisols (about 28%) and a small portion of spodosols (about 5%).

Vegetation Information on vegetation is only available for areas subject to planning (Figure 4.10 c). From the Figure 4.11, it is possible to observe the prevalence of thickets (BS, 41%) consisting mainly of upland and invasion birch. The vegetation cover represented by this category is concentrated on the mountain areas, forming extensive surfaces. The second category in terms of the surface is the forest category resulting from the association among maple, linden, and, ash forests (AF, 13%), spatially distributed. Next, there are the categories of chestnut, larch, green alder, and beech forests (CA 10%, LC 9%, OV 9%, and FA 8%, respectively). As in the case of maple-linden-ash forests, chestnut forests also cover spatially distributed areas, generally at lower elevations than other categories such as thicket and beech forests. On the other hand, larch forests, generally upland or grazing, are located near mountainous areas. Green alder stands are located at higher elevations and generally consist of invasive green alder stands associated with other broadleaf types. The beech forested area is mainly constituted by the area located south of the Monviso region and other smaller ones at higher altitudes, often shown in association with chestnut trees. Areas of reduced extension are still destined for reforested areas (RI 4%), generally consisting of mountain pine and mixed conifers. The remaining categories involve tiny vegetated areas. These are oak mixed with mesophyll broadleaf forest (QC 1%), black locust forests (RB 1%), and white willow forests (SP 0.1%). These three categories are predominantly related to lowland and riverine environments. Specifically, oak-carpine groves are located in lowlands, while black locust forest and willow forest are located near the flowing course of the Po River.

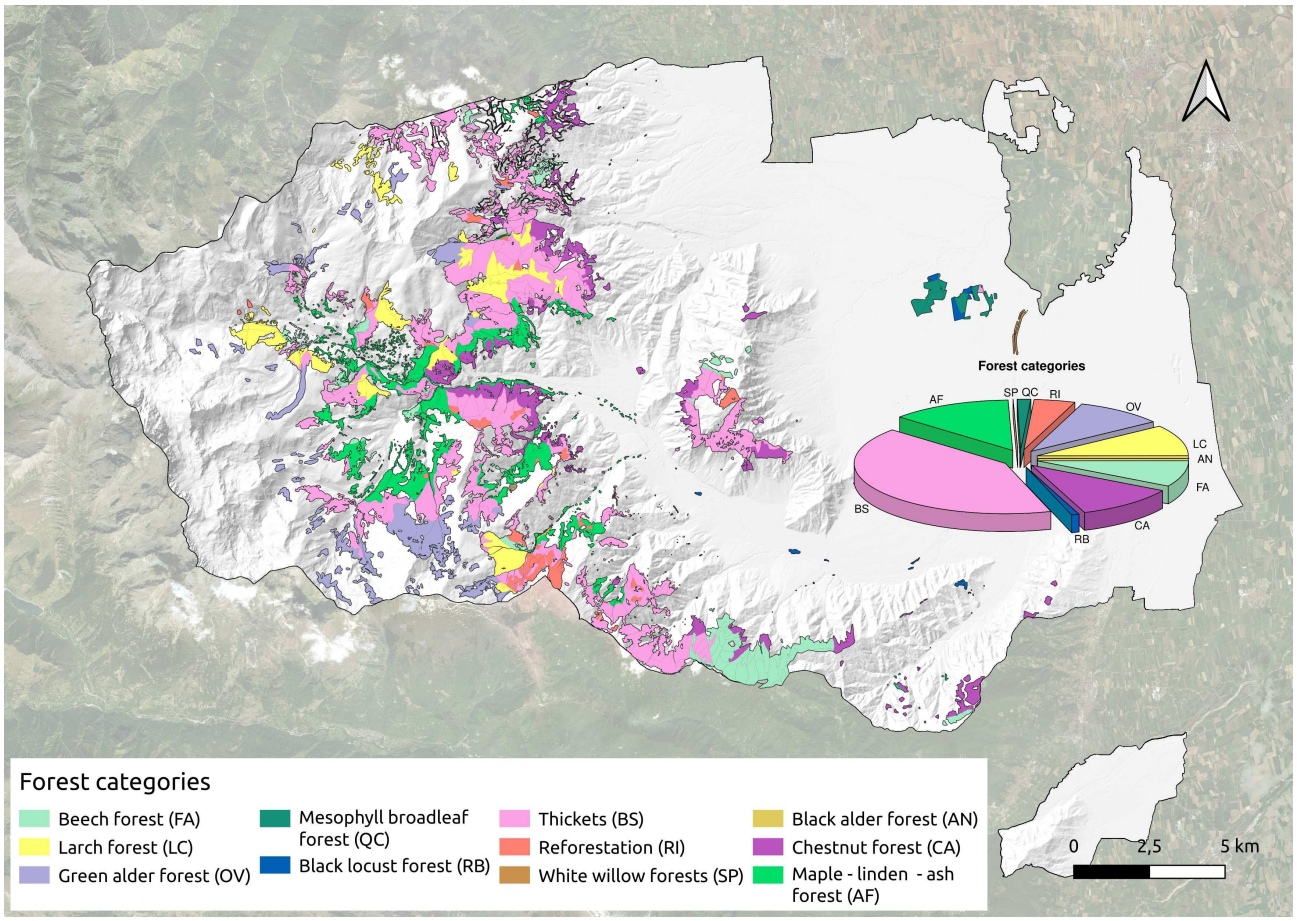

FIGURE 4.11: The map in the Figure shows the major forest categories identified in the area under planning.

The current functional destination of each forested areas is a central aspect of this study. The forest plan of Piedmont region defines forests with a direct protective function those directly involved in protecting structures and infrastructures or in vulnerable areas (steep slopes, old landslides areas, river strips). The management of thee forests mainly aims to preserve this protective role. In the whole area of Piedmont, 15% of the forests have a protective function, and 40% are public property. Considering silvicultural practices, on more than half of the surface involves monitoring process, while on 20%, improvement interventions can be carried out, e.g., conversions, and for 16%, renewal interventions, which mainly concern selective cuts in the forest.

The regional forestry plan also defines production-protection destination forests as located in mountains and hills with no direct protection and located in not particularly vulnerable stations. However, these areas are still subject to hydrogeological constraints. In these forests, it is possible to carry out sustainable silviculture aimed at wood production without compromising soil protection. In the Piedmont area in general, and in the area subject to planning in this study, the productive-protective destination is the most prevalent, with more than 45% of the regional surface. Most of it is managed through active short-term management, mainly through coppicing

and mixed management (more than 50%), improvements (37%), and forest regeneration cuts (10%).

In the specific case of the planning area, the currently assigned functional destinations are depicted in Figure 4.12.

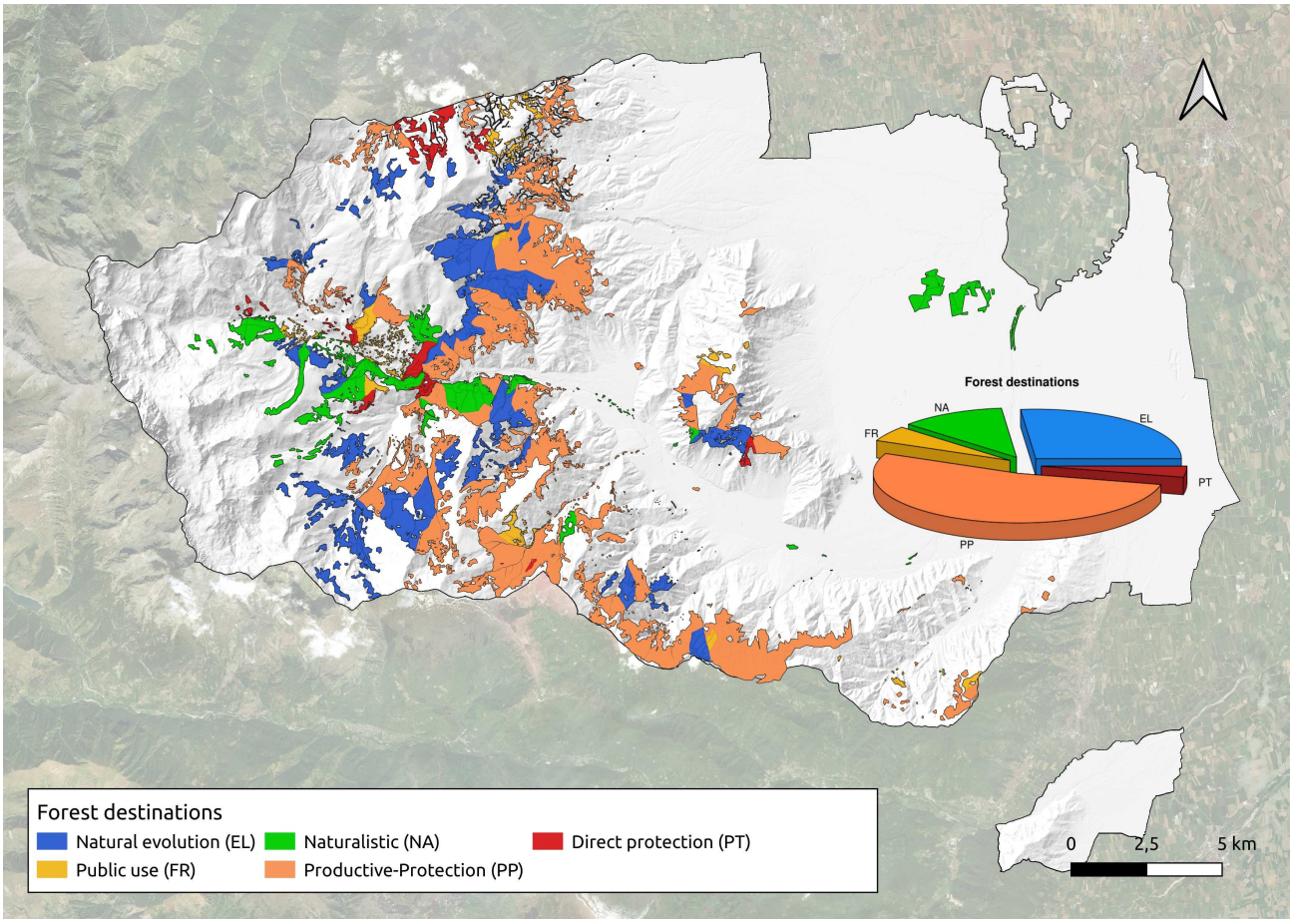

FIGURE 4.12: The map in the Figure shows the five functional destinations assigned to the different parts of the planning area. This assignment depends on their location, composition, structure, and characteristics. For example, in the case of direct protection forests, these are generally located near structures and infrastructures subject to the occurrence of natural hazards.

The pie chart in Figure 4.12 shows that a half of the planned area currently has a double function of production-protection (53%; PP in orange), assigned mainly to forest categories such as thickets, chestnut, maple-linden-ash forests, beech, and larch forests. Another large portion of the forest has been assigned to natural evolution (2%; EL in blue), without specific function, and naturalistic destination (12%; NA in green). Minor parts are dedicated to public use (5%; FR in yellow) and direct protection against potential natural hazards (4%; PT in red).

Observing in detail the composition of forested areas with direct protection, Figure 4.13 a) shows that 59% of the whole surface is composed of thickets (BS), while 32% is comped of maple-linden-ash forests (AF). This functional destination is also assigned to smaller surfaces of chestnut (5%; CA), larch (2%; LC), reforested areas

(1%; RI), and beech (1%; FA). The composition of forested areas with a productive-protective destination is different from the previous one. Since, also in this case, the most widespread forest category is thickets (38%; BS), the rest of the area is better divided among the other categories. Figure 4.13 b) shows almost equal surfaces of chestnut (18%; CA), maple-linden-ash forests (14%; AF), and beech (12%; FA). Smaller parts are composed of larch (8%; LC), reforested areas (5%), and green alder (5% OV).

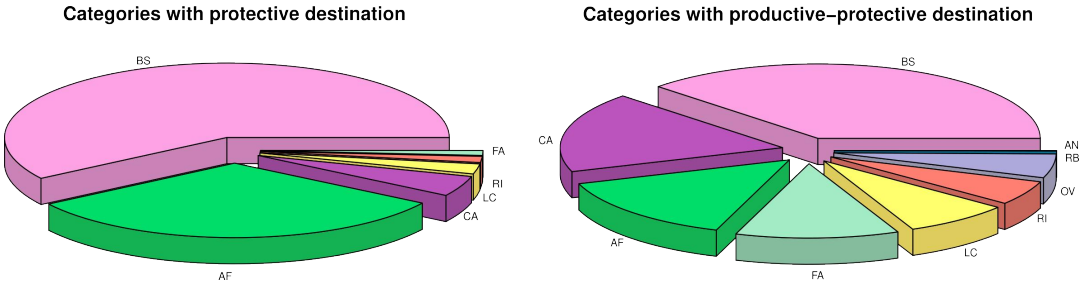

FIGURE 4.13: Forest categories composing direct protection and productive-protective destinations (BS: thickets, AF: maple-linden-ash forests; CA: chestnut; LC: larch; RI: reforested areas; FA: Beech; OV: green alder; RB: black locust: AN: black alder).

4.3.2 Methodology

Simulations of different rainfall events scenarios

The stability analysis performed using the method proposed in this research work compares four scenarios that differ in rainfall intensity and in the presence or absence of vegetation:

- analysis with rainfall intensity of 2-year return period with current vegetation (*2RT_Wa*), simulating the current scenario with common rainfall event;
- analysis with rainfall intensity of 100-year return period without vegetation (*100RT_W0*), simulating the worst-case scenario with exceptional rainfall event;
- analysis with rain intensity of 100-year return period with current vegetation (*100RT_Wa*), simulating the current scenario with exceptional rainfall event;
- analysis with rain intensity of 100-year return period with an ideal value of RR (*100RT_Wi*), simulating the ideal scenario with exceptional rainfall event.

Average hourly rainfall intensities derive from the inventory of intense precipitation available online from the Regional Agency for Environmental Protection of Piedmont (Inventory webpage). Among these simulations, analysis performed in *2RT_Wa* scenario was used to evaluate and calibrate input parameters to be used for next simulations.

Specific studies about rainfall intensity events and SLs occurrence showed that rainfall with return times of 1 or 2 years is unlikely to promote the initiation of SLs (Lu et al., 2010). For this reason, in the context of this analysis, the intensity referred

to 2 years return period cannot be considered an exceptional event. Therefore, to consider this fundamental aspect in the analysis, it is assumed as a parameters validation criterion that at least 98% of the investigated area must present a probability of SL occurrence lower than 10%.

The hourly rainfall value for different return periods is justified by observations from studies that stated this time frame is sufficient for achieving peak pore pressure and consequent changes in soil water movement (Lu et al., 2010).

Tree position and size estimation

In order to quantify and estimate the mitigation effect due to tree presence, and in particular root systems, another ecorisQ software was used, called Find Individual Trees (FInT) (Dorren, 2014). FInT allows estimating the location and size of trees based on DTM and Digital Surface Model (DSM). Once the position of the tree is identified and its height estimated, the software calculates the diameter at 1.3m using allometric functions.

In the specific case of this analysis, DTM and DSM with a resolution of 2m were used. Since the source data has a resolution of 5m, the use of the minimum resolution required by FInT to avoid further cell value re-sampling was preferred. The minimum height set for estimating tree size was 1m. Considering that most of the area belongs to the forest category of thickets, a minimum value of height was preferred. In addition, to consider the wide variability in size, a random processing value of tree diameter was set at 30%. Taking into consideration that forest structure variability is fundamental when analyzing extensive areas such as in this study.

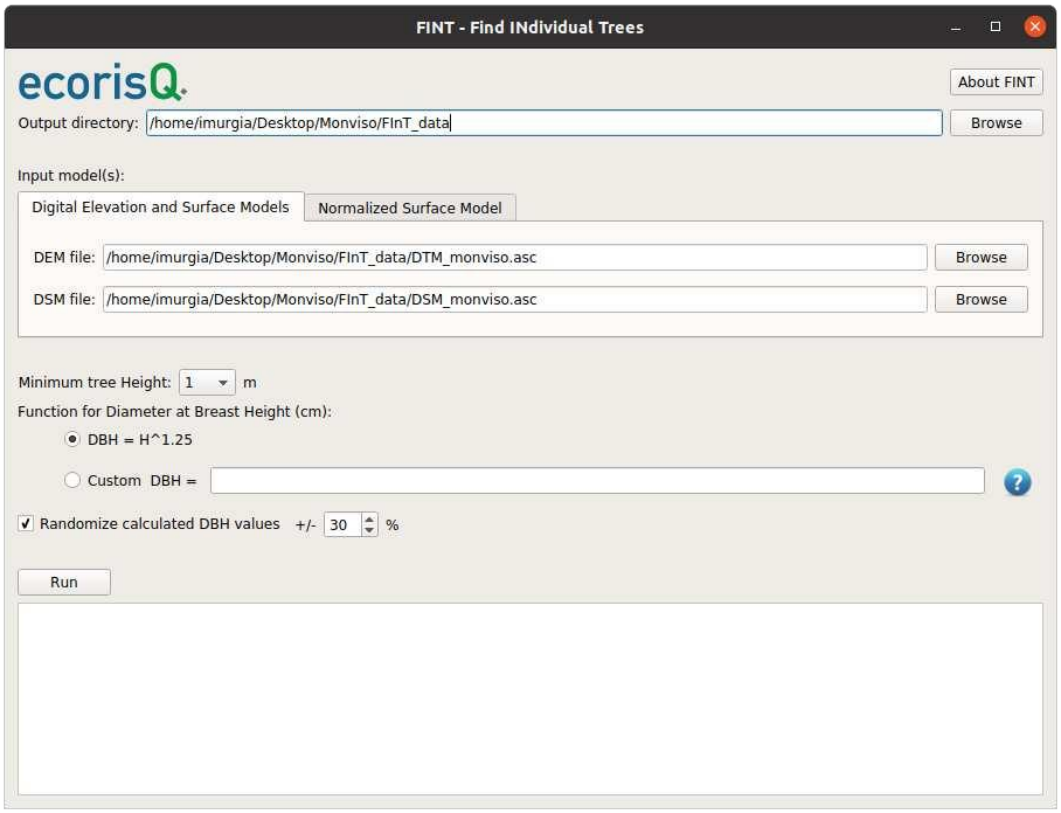

FIGURE 4.14: The Figure shows the Graphical User Interface of FInT software. This software estimates the tree's location and diameter based on input information such as the digital terrain model, the digital surface model, and the minimum plant height present in the area. Once the height of the identified hypothetical tree is estimated, FInT applies allometric equations to estimate its respective diameter. FInT makes it possible to reconstruct the hypothetical structure of the investigated forest virtually.

Once the tree data obtained from FInT had been verified and the outliers removed, the points relative to each tree were reported in the GIS to join the information relative to the forest category (Figure 4.11) with the QGIS module *Joint attributes by location*. This information is contained in the updated data of the new PFA version. In addition, to avoid the forest margin effect, trees located within a buffer of about 100m from the actual planning area boundary were also considered. In this case, the tree species was attributed to each point considering the nearest point-tree by using the QGIS *Join attributes by nearest* module. The assignment of the tree species is fundamental for the RR calculation and the assessment of SL probability in the scenario involving the actual forest (*100RT_Wa*).

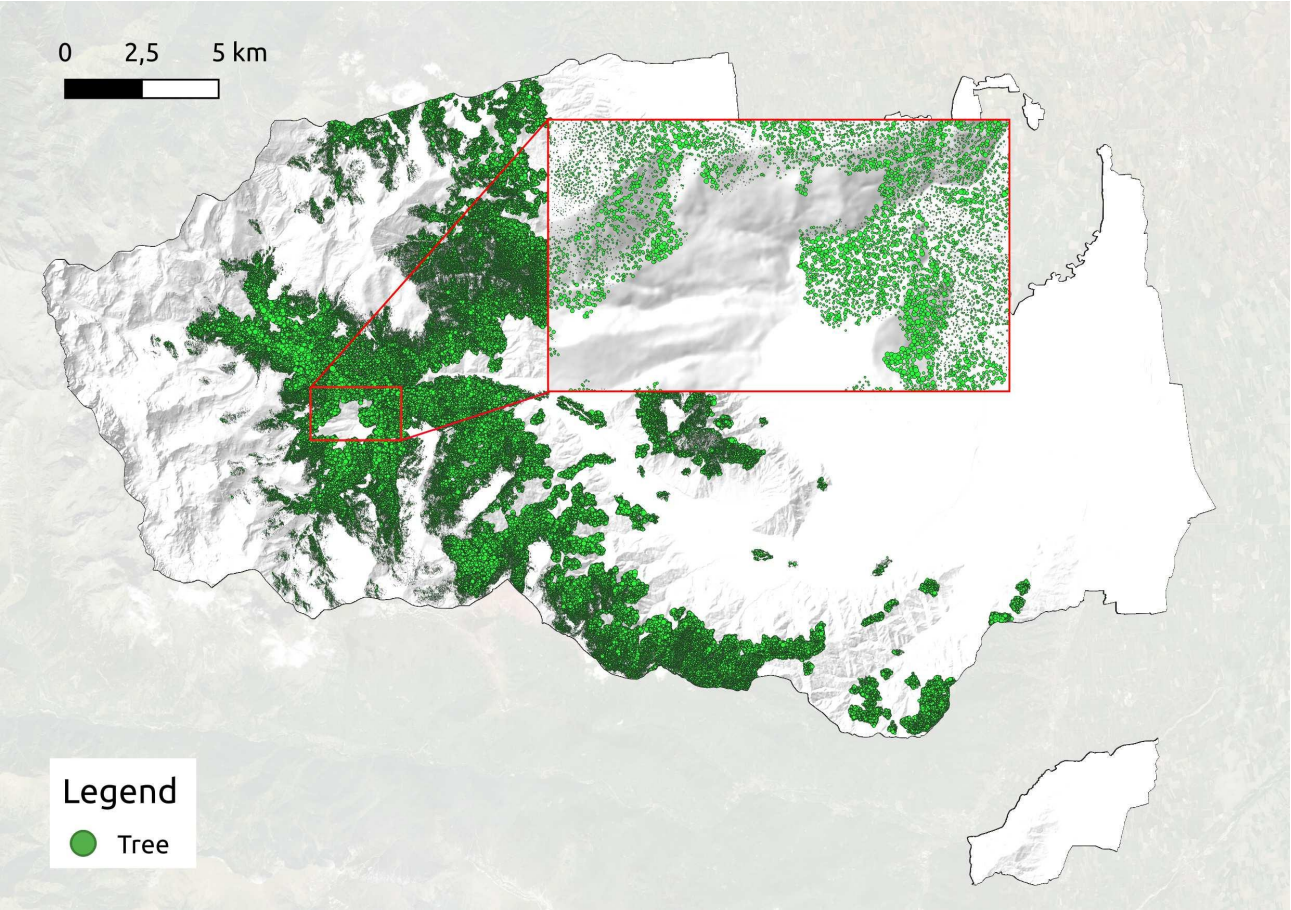

FIGURE 4.15: The Figure shows the location and diameter size at 1.30 m estimated for trees in the planning area. In the detail of the Figure in the red box, it is possible to observe the variability of the size of the green dots. i.e., the trees, based on the estimated diameter.

Chapter 5

Results and discussions

5.1 Tree scale analysis: the Japanese cedar root reinforcement

The tree scale analysis described in this study provides a first result related to the root reinforcement (RR) mechanical parameters of Japanese cedar. These mechanical parameters are necessary for the RR standardization of this tree species, as well as for the RBM++ software application for the RR spatial quantification.

5.1.1 Results from analysis using R

The values and information obtained from the elaboration performed with the R code of RBMw are similar to others published by previous studies on Japanese cedar reinforcement (Genet et al., 2008; Yamase et al., 2019). The results derived from these preliminary computations in R and the application of RBM++ will be discussed in more detail in the following subsections.

Root density values

The number and size of roots depend greatly on the tree species and by environmental characteristics such as soil type, area morphology, competition for space, and nutrients with neighboring trees that affect water and nutrient availability.

Figure 5.1 shows, for both Japanese cedar trees investigated, how the number of roots varies, increasing both the distance from the tree stem and the soil depth (each graph represents a distance to the corresponding tree, and each bar a soil depth layer). In general, it is possible to observe that this tree species has a strongly branched structure, with a substantial prevalence of small roots. However, significant differences are highlighted between the two investigated trees. Considering that the trees have an identical size in diameter at 1.30m of 27cm, these differences depend exclusively on the local conditions surrounding the tree. More precisely, in the specific case of Tree 2, there was strong proximity with neighboring trees, which could have created a competition condition for space and nutrients.

Root diametric class $\leq$2mm (yellow bars) prevails considerably in all distances and soil depth layers, confirming the strongly branched structure of the root system. The 2-5mm diametric class (red bars) is also well represented, generally reducing as

the distance increases, although in a different way for the two trees. While in Tree 2 the number of roots belonging to this diametric class reduces almost constantly, in Tree 1 the reduction shows a different root density trend, with roots belonging to this diameter class also in the furthest profile from the tree (Figure 5.1d). Roots belonging to the 6-10mm diametric class (orange bars), are infrequent and generally observed at distances close to the tree and in shallow soil layers. Their variability is similar to previous classes, but with quite smaller density. Also roots belonging to 11-15mm diametric class (green bars) were recorded, only in the distances closest to the stem and generally in the first 15cm of soil depth (Figure 5.1a, b, and e). Finally, only tree 1 presents roots with diameters belonging to the 16-30m class (blue bars; Figure 5.1a e b) and $\geq$30 mm class (purple bars; Figure 5.1a), on the shallow soil layer.

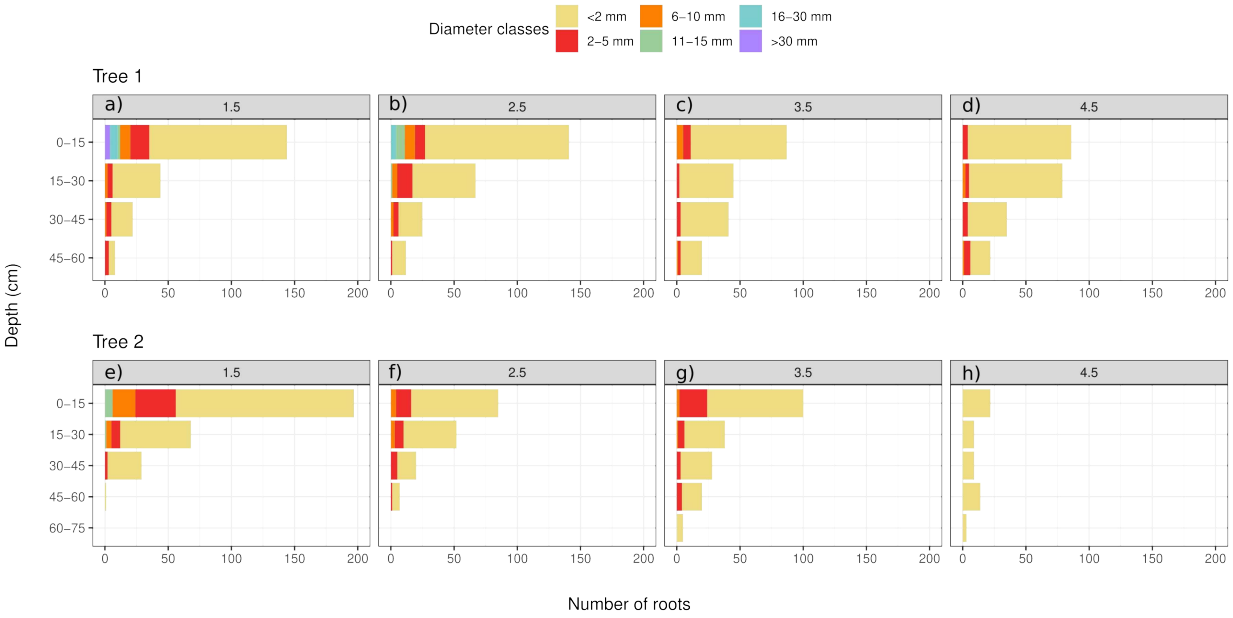

FIGURE 5.1: The graphs in this Figure show the measured root density in the two Japanese cedar trees considering soil profiles at different distances (each letter) and depth layers. Individual roots were grouped into diameter classes having a range of 5 mm. The distribution graph highlights the branching structure of the root system of this tree species.

In conclusion, results regarding root density confirm observations from previous studies of Fujimaki et al. (2007) and Genet et al. (2008). In particular, in the latter study they stated that part of the additional soil cohesion procured by roots is observed in the 0-15 cm depth layer, suggesting little contribution to the basal root reinforcement (BRR) for this tree species.

Root mechanical parameter values

The maximum tensile force measured through the multiplication of equation 4.1 and equation 4.2 is shown in the graph in Figure 5.2 (a and b). The mechanical RR parameters estimated are reported in the equation 5.1. The parameters F0, α, ϕ_m, and

ϕ_{sd} are the first four mechanical parameters necessary to characterize this species. As shown in the following equation: F0 = 701532.8N, α = 1.45, ϕ_m = 0.002m, and ϕ_{sd} = 0.004m:

$$F_{max}(\phi) = 701532.8\phi^{1.45} * \frac{1}{2}[1 + erf(\frac{\phi_i - 0.002}{0.004\sqrt{2}})] \tag{5.1}$$

This equation allows obtaining the green curve in Figure 5.2 (c), based on field data (red dots) and fitted values of diameter-pullout force ratio. The curve shows values greater than 5000N for roots with diameter size of about 0.03m. The values on the tensile strength for diameters smaller than 10 mm showed similar values compared to published data found in other studies on the Japanese cedar (Genet et al., 2006; Yamase et al., 2019).

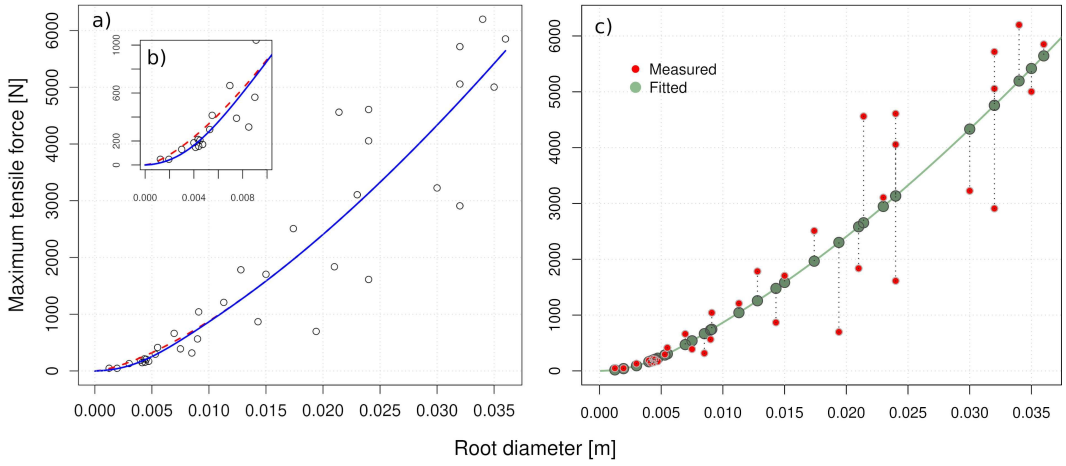

FIGURE 5.2: The Figure shows the processing and fitting steps of the field-measured reinforcement data. In Figure a, each white dot represents a tensile test performed. From the trend of these values, it was possible to construct the regression curve (red dashed line in Figure b) that best represents the relationship between tensile force and root diameter. However, the application of the equation 4.2 allowed for a better fit of the curve in roots with diameter leq10mm, identifying a new curve (solid blue line).
In Figure (c), the process of fitting the reinforcement values is depicted, i.e., the identification of the green points representing the force values obtained by applying the least squares method (Schwarz et al., 2013).

The two parameters of secant spring constant estimated for the equation 4.3 are kϕ_i = 0 and kϕ_i = 2074442.06. The Figure 5.3 shows the trend of the secant spring constant, representing the elasticity demonstrated by roots during pullout tests. In the RBMw, the secant Young's modulus is implemented, obtained from the ratio of root strength to strain at break as done by Waldron and Dakessian (1981). As mentioned earlier, this parameter summarizes the mechanical properties of the root-soil system under specific conditions (root diameter, tree species, stand, soil type, and moisture conditions) (Schwarz et al., 2013).

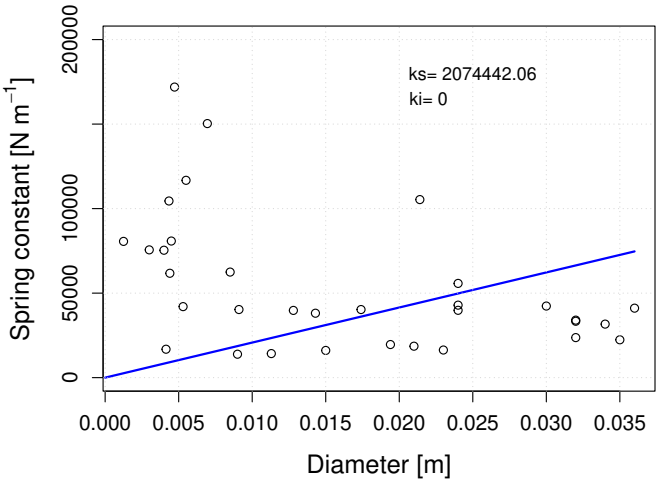

FIGURE 5.3: Graph of the spring constant

In the Figure 5.4, the survival probability as function of the normalized displacement (equation 4.4) is shown, with the data (gray dots) and best fit (dashed red line). R considers that the probability of a root to survive is a function of a normalized displacement. The two-parameter ω (shape factor) and λ (scaling factor) for Weibull survival function application are given by fitting the data (equation 5.4).

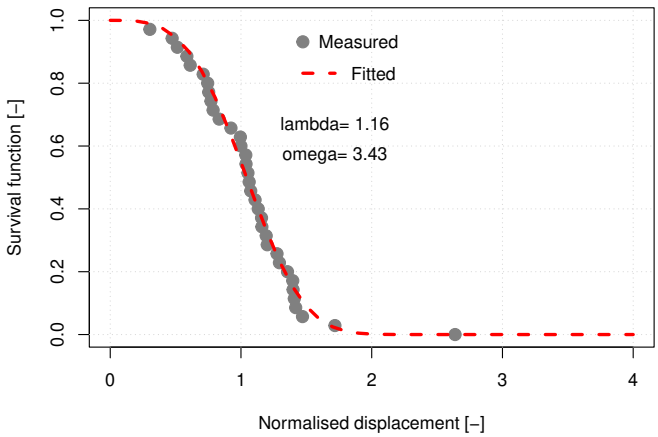

FIGURE 5.4: The Figure shows the survival probability distribution as a function of the normalized displacement. Gray points are the measured values, while the red dashed line represents the trend of these values. The displacement normalization process is necessary to eliminate the effect of root diameter on maximum root displacement and strength (Schwarz et al., 2013).

The RBMw considers the relative variability of root strength regardless of root diameter. Through this approach, this simplified model reduces the number of parameters needed to assess the RR, allowing to consider the roots' variability and reducing the source of errors (Schwarz et al., 2013). Furthermore, the variability in

mechanical behaviors is considered incorporated into the Weibull survival function (Dazio et al., 2018).

Finally, the quantification of the bundle root reinforcement obtained using the equation 4.5 is shown in the following Figure 5.5.

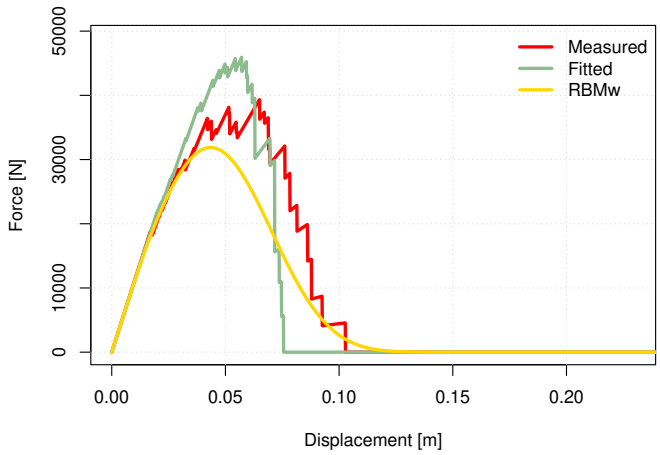

FIGURE 5.5: The graph in the Figure shows force-displacement curves considering measured data (red line), fitted data from the equation 5.1 (green line), and estimated data applying the RBMw (yellow curve).

The force-displacement curve in Figure 5.5 for the root bundle estimated through applying the RBMw (yellow curve) is shown to fit the curve representing the trend of the measured field data (red curve). The narrow and elongated shape of the curve demonstrates what was observed in the elasticity plot. The root bundle activates progressively, showing rapid force growth until it reaches a maximum value exceeding 30KN, corresponding to a displacement of about 0.04m. Subsequently to this peak, the force decreases gradually to 0 once the 0.10m displacement has been exceeded.

5.1.2 Root reinforcement estimation with RBM++

The estimated values for each RR mechanical parameter of Japanese cedar were processed in RBM++ software. The application of the software allows the estimated mechanical parameters to be applied to the real root distribution measured in the field (Figure 5.1). Through the *User defined* method, both the spatial distribution of reinforcement and the variation of force-displacement curves as a function of soil depths were quantified and evaluated.

Considering that in the graphs shown directly on the GUI there is no distinction between the trees or reference to the different distances, the Trench displayed are as follows:

- Trench 1 - Tree 1, linear profile at 1.5m distance;

- Trench 2 - Tree 1, linear profile at 2.5m distance;
- Trench 3 - Tree 1, linear profile at 3.5m distance;
- Trench 4 - Tree 1, linear profile at 4.5m distance;
- Trench 5 - Tree 2, linear profile at 1.5m distance;
- Trench 6 - Tree 2, linear profile at 2.5m distance;
- Trench 7 - Tree 2, linear profile at 3.5m distance;
- Trench 8 - Tree 2, linear profile at 4.5m distance;

Below, we report and discuss the main aspects observed from the results obtained via RBM++.

Map of root reinforcement space distribution The graph in Figure 5.6 allows evaluating how the RR estimated for the two trees is distributed in space. It is evident that although the two trees have the same diameter at 1.30m, the RR of Tree 2 is high in the trench closest to the tree. As far as the values referred to the other distances are concerned, the green color intensity clarifies no significant differences between the estimated reinforcement values. This observation is later confirmed by the displacement-force relationship plot shown in Figure 5.7.

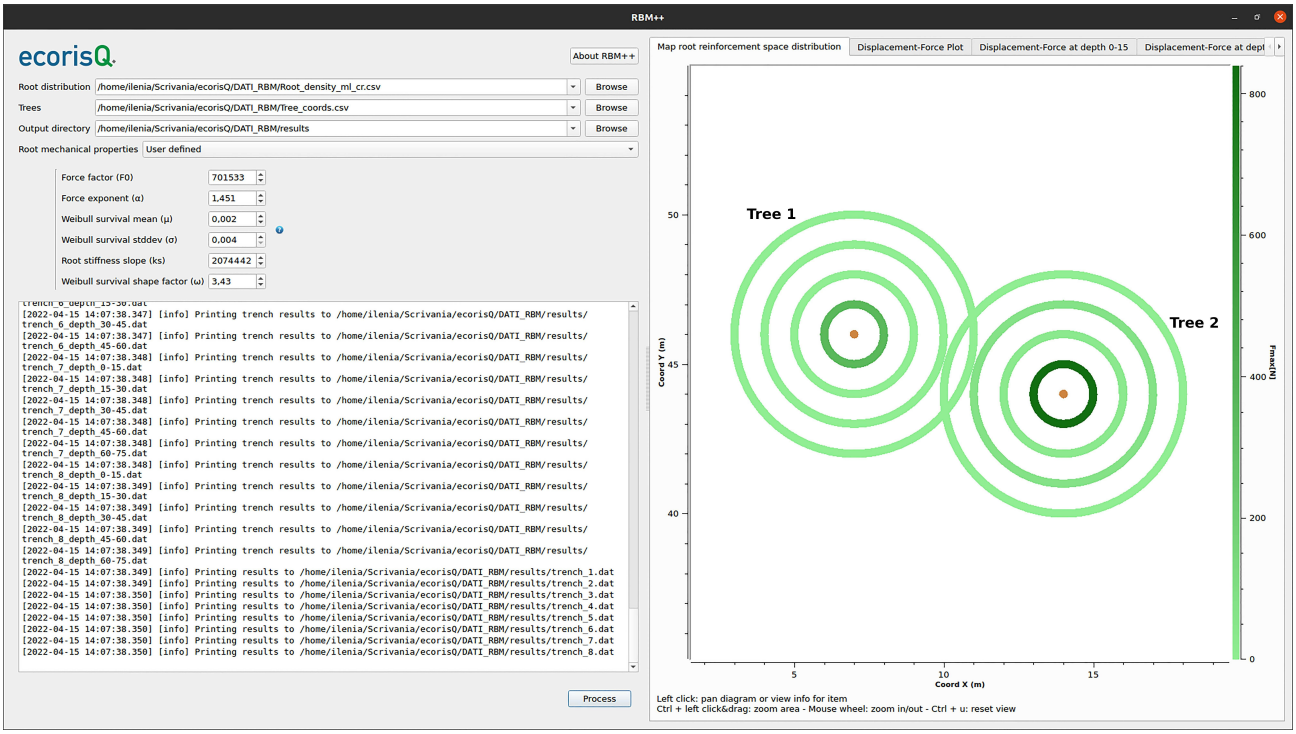

FIGURE 5.6: The Figure shows the Graphical User Interface of the RBM++ after the root reinforcement calculation. In the graph in the left window, the brown dots represent the tree diameters at 1.30 m, while the concentric circles in green represent the trenches at different distances from the stem. Relative to the trenches, the associated color intensity represents the estimated RR value, which can be verified by the force value bar displayed to the right of the graph.

Displacement-Force Plot The curve in Figure 5.7 shows the force-displacement relationship for all distances from plants where density was measured. The maximum observed value is for Trench 5, with RR equal to 898N. This value is almost twice as high as the next trench in force intensity, Trench 1, with 566N. Although these trenches refer to different trees, they are located at equal distances (1.5m from the tree stem), so the significant difference in value is due to root density. As observed in the analysis of root density (Figures 5.1 a and e), a higher number of roots was measured in the Trench 5 compared to Trench 1, in particular for roots belonging to diametric classes of 2-5mm and 11-15mm.

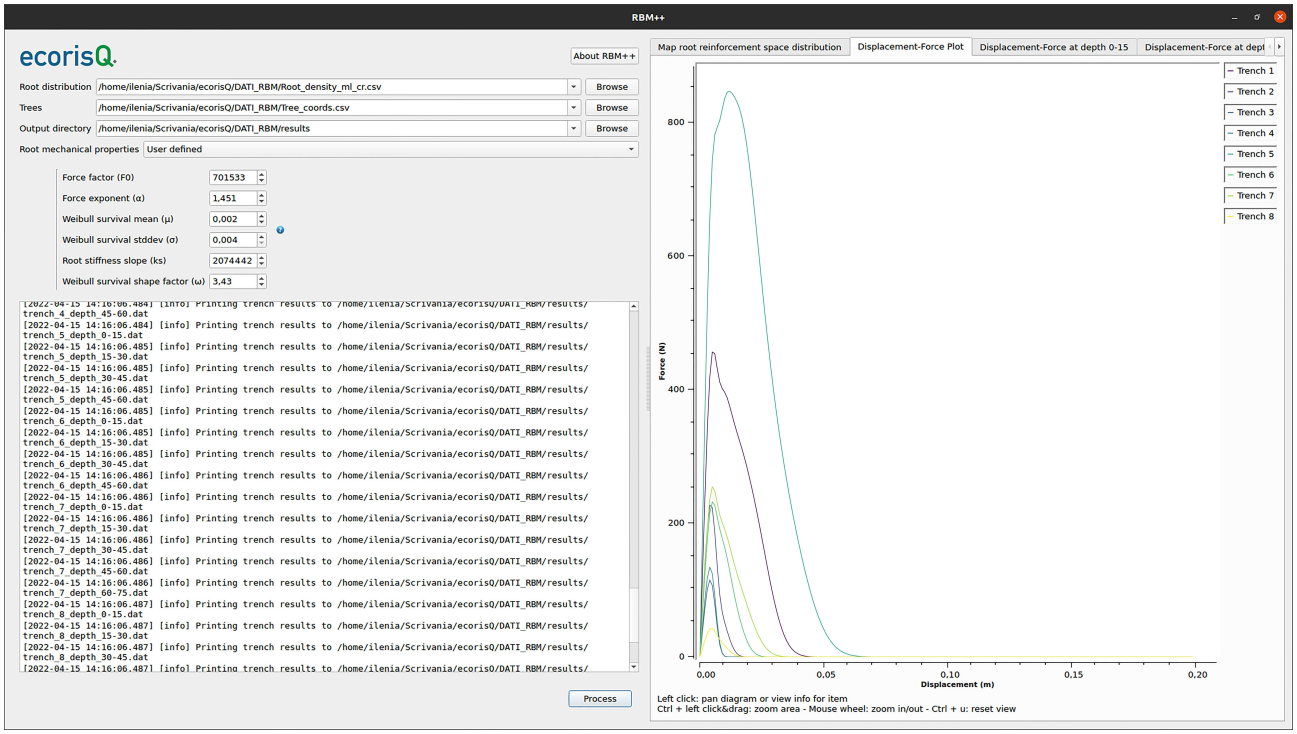

FIGURE 5.7: The Figure shows the Graphical User Interface of the RBM++ after the root reinforcement calculation is completed. In the left window graph, the force-displacement curves of each trench can be observed. In this case, the force and displacement values refer to the entire soil depth investigated. The curve's color is unique for each trench and can be checked on the right side of the window.

In both of the previous trenches, it is possible to observe two peaks on the curve that depend on the elasticity observed for the Japanese cedar and the root sizes belonging to the respective diametric classes.

Considering the remaining curves, it is possible to observe that Trench 7 and 6 show very similar maximum reinforcement values (Figure 5.8), 271N and 233N, respectively. From this observation, it can be stated that the trench farthest from the Tree 2 (Trench 7) provides a RR almost constant in space with a value equal to that estimated for the closest distance (Trench 6). In this case, it is evident that the higher number of roots, even if belonging to the smaller diametric classes, guarantees a higher reinforcement than the presence of coarse roots (Figure 5.1f and g).

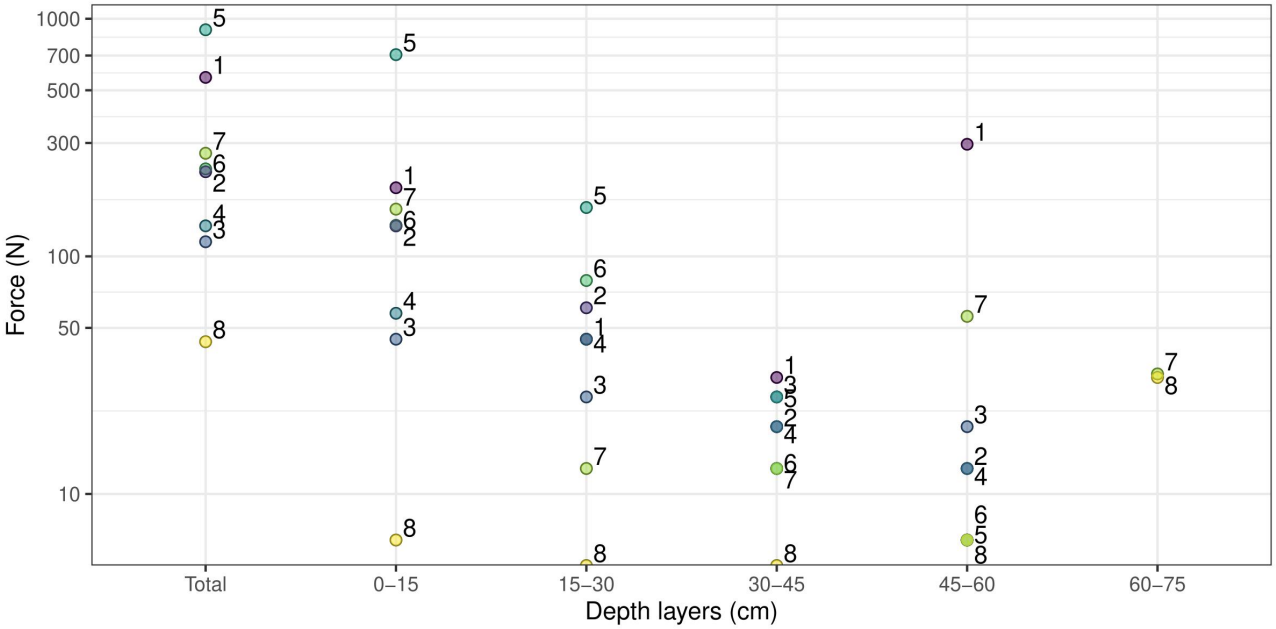

FIGURE 5.8: The graph in the Figure shows the maximum estimated RR values for each trench and soil depth layer. The number and color are distinctive for each Trench. Overlapping values can be observed through this visualization, allowing for a more detailed reinforcement assessment.

Relative to Trench 2, this shows very similar values to Trench 7 and 6 of 227N. Although there is a significant difference in the reinforcement on the closest trenches (Trench 1 and 5), this difference reduces significantly as the distance from the stem increases.

As for the remaining trenches, Trench 4 and Trench 3 show very similar reinforcement values, 134N and 115N, respectively, while the estimated reinforcement for Trench 8, 43N, is significantly reduced. The reduced reinforcement value again depends on the root number recorded in the vicinity of this plant, which is also very small compared to the other plant.

Displacement-Force at depth 0-15 Analyzing in detail the estimated reinforcement near the first 15 cm of soil (Figure 5.9), it is possible to observe that for all trenches, much of the total reinforcement is procured by roots located in this soil layer, confirming the observations of Genet et al. (2008). For example, in the case of Trench 5, a value of 705N is estimated, equivalent to three-quarters of the total reinforcement value observed previously (898N). The values in the vicinity of the other trenches continue to be significantly lower (Figure 5.8).

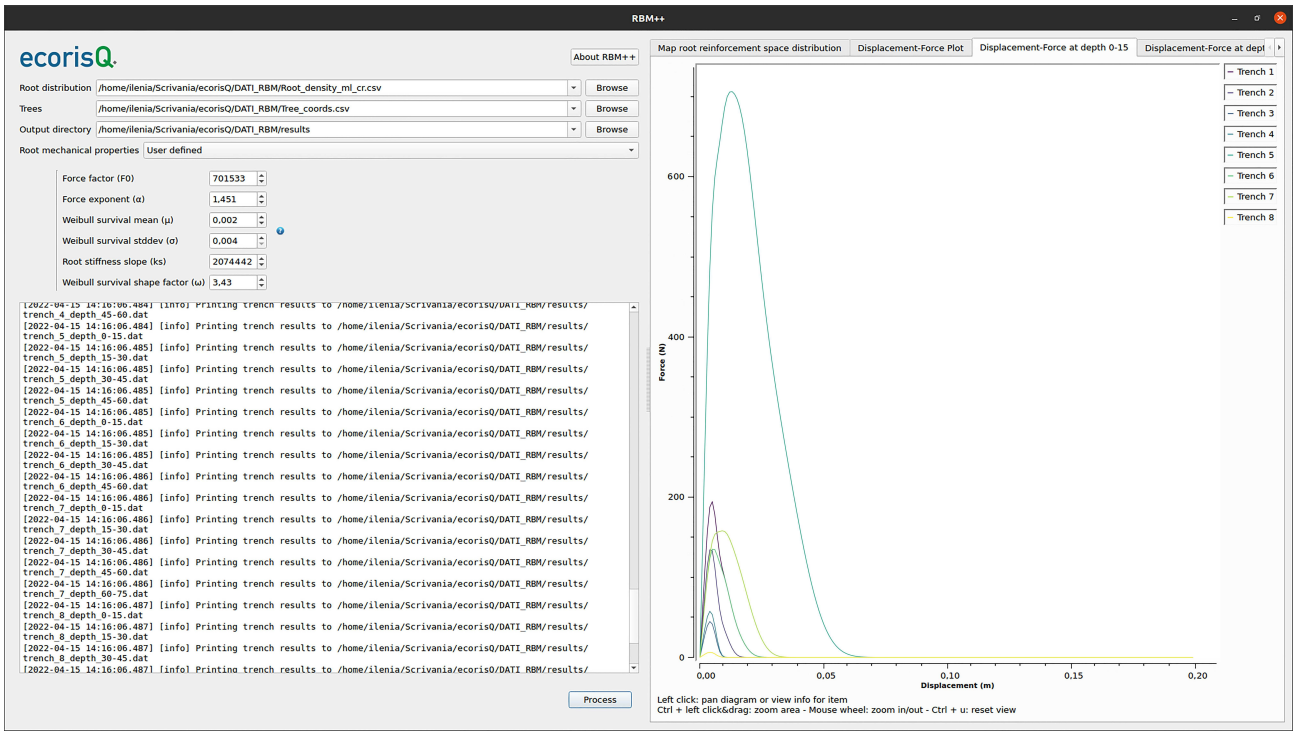

FIGURE 5.9: The Figure shows the Graphical User Interface of the RBM++ after the root reinforcement calculation is completed. In the left window graph, the force-displacement curves of each trench can be observed. In this case, the force and displacement values refer to the soil layer between the surface and 15cm. The curve's color is unique for each trench and can be checked on the right side of the window.

Displacement-Force at depth 15-30 Relative to the reinforcement shown at the depth layer of 15-30cm (Figure 5.10), different behavior of the various trenches can be observed. Trench 5 still shows the highest reinforcement value, equal to 160N, while Trench 6 shows a reinforcement value of 79N. About the Tree 1, the highest reinforcement value, equal to 60N, is observed in Trench 2, which slightly exceeds the trench closest to the plant, Trench 1, with 44N. In addition, the estimated value in the trench closest to the plant also corresponds to the one furthest from the plant, Trench 4 (Figure 5.8). From the root density graph (Figure 5.1 a and d), it is evident that in Trench 2 there are many small roots (class $\leq$2mm), whereas in Trench 1 there are less small roots and more large ones (class 6-10mm). Having more small roots guarantees a bigger reinforcement than having less but big roots.

The minimal reinforcement previously observed in Trench 8 is completely annulled at this depth.

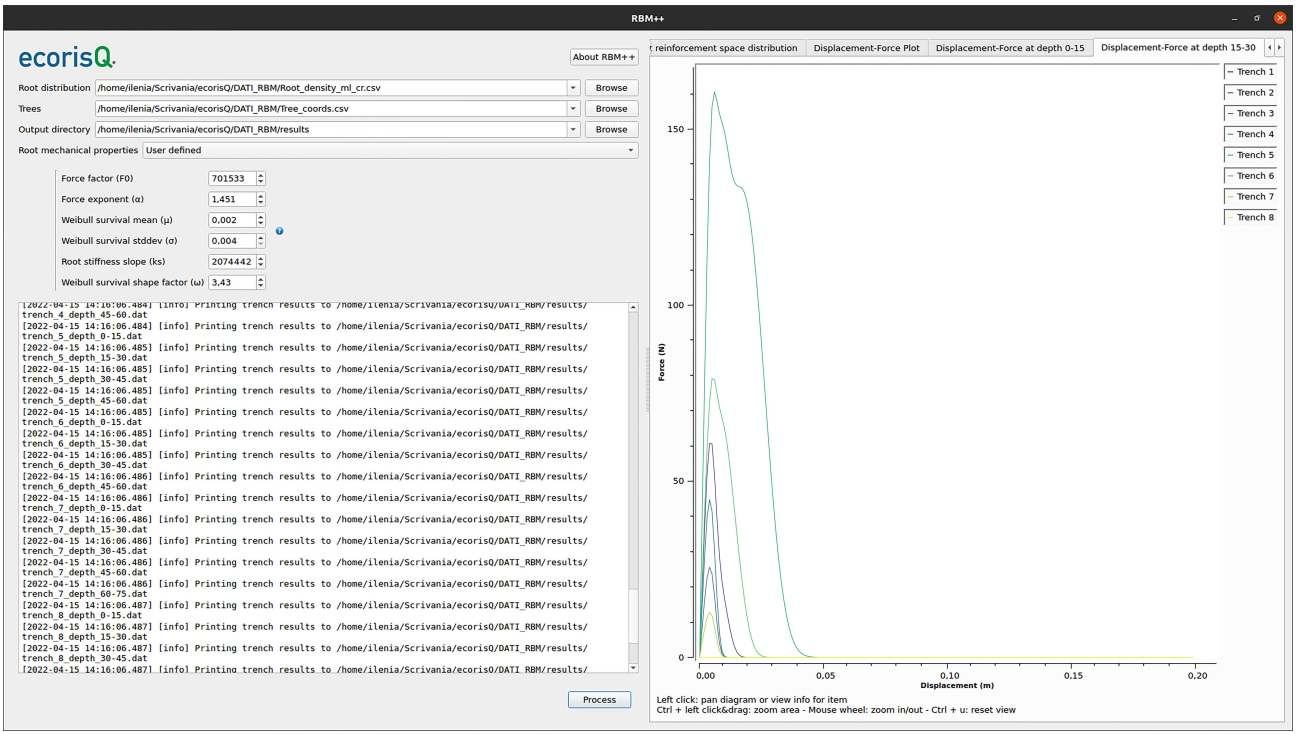

FIGURE 5.10: The Figure shows the Graphical User Interface of the RBM++ after the root reinforcement calculation is completed. In the left window graph, the force-displacement curves of each trench can be observed. In this case, the force and displacement values refer to the soil layer between 15cm and 30cm. The curve's color is unique for each trench and can be checked on the right side of the window.

Displacement-Force at depth 30-45 From the plot in Figure 5.11, it is observed that at this soil depth, the reinforcement in all trenches is negligible. The estimated reinforcements for the various trenches overlap, and their dependence on distance from the tree nullifies (Figure 5.8).

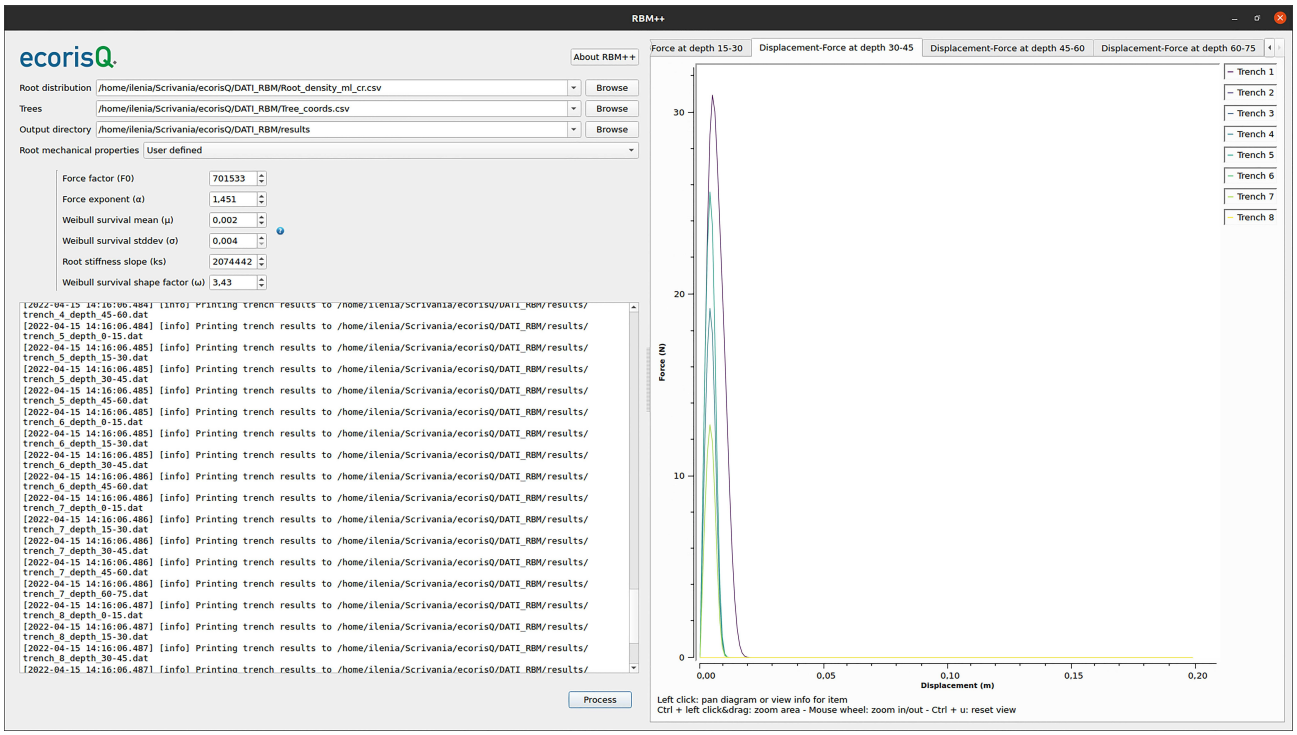

FIGURE 5.11: The Figure shows the Graphical User Interface of the RBM++ after the root reinforcement calculation is completed. In the left window graph, the force-displacement curves of each trench can be observed. In this case, the force and displacement values refer to the soil layer between 30cm and 45cm. The curve's color is unique for each trench and can be checked on the right side of the window.

Displacement-Force at depth 45-60 Although reinforcement values almost canceled out in the previous soil layer, it is observed that in Trench 1, the reinforcement increases again to a value of 296N. This value of RR depends mainly on some roots with a diameter of 5mm measured near this layer.

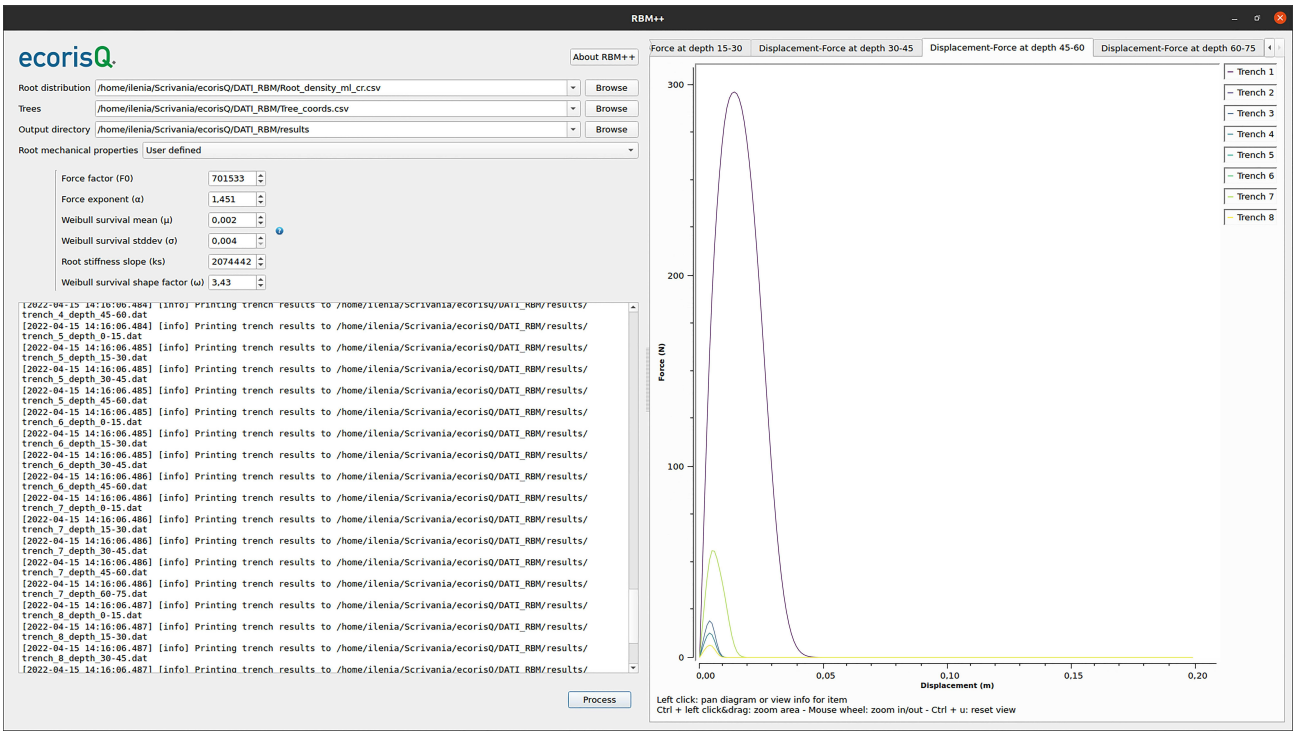

FIGURE 5.12: The Figure shows the Graphical User Interface of the RBM++ after the root reinforcement calculation is completed. In the left window graph, the force-displacement curves of each trench can be observed. In this case, the force and displacement values refer to the soil layer between 45cm and 60cm. The curve's color is unique for each trench and can be checked on the right side of the window.

Displacement-Force at depth 60-75 Minimal reinforcement values were measured in Trench 7 and 8 (Figure 5.13), albeit with negligible values.

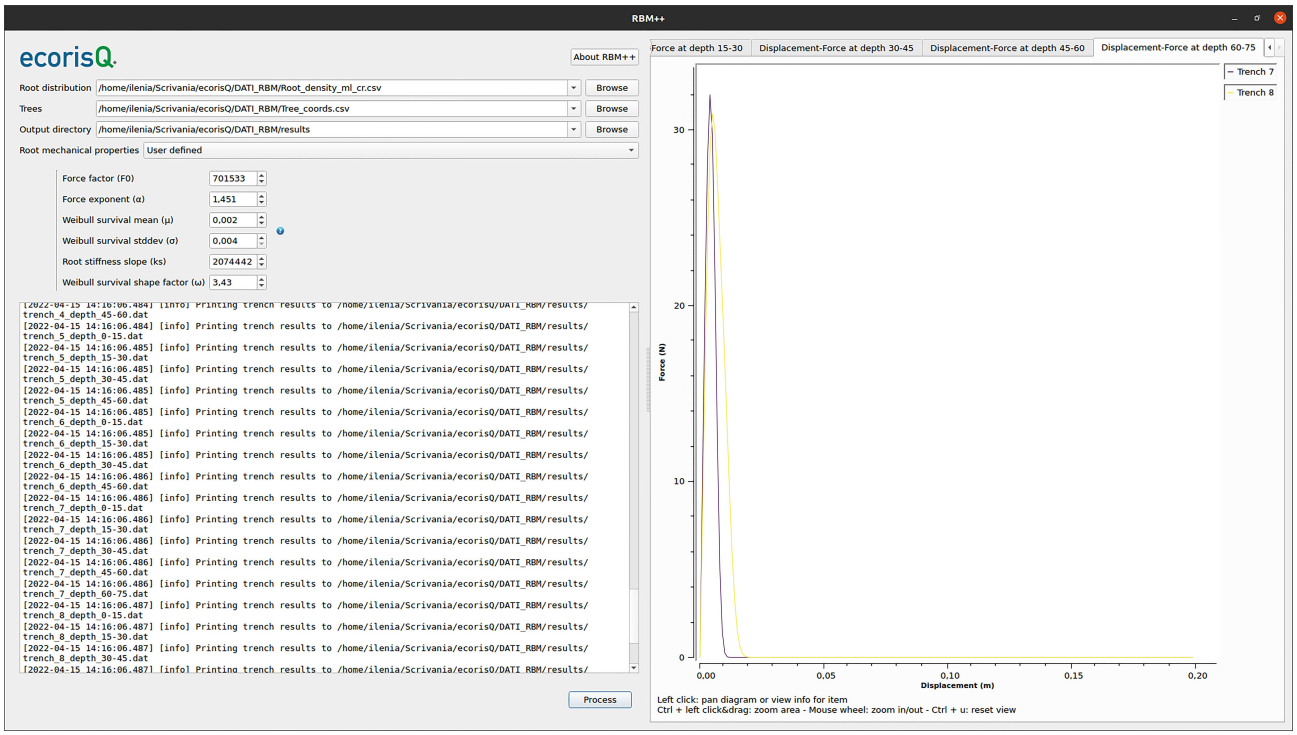

FIGURE 5.13: The Figure shows the Graphical User Interface of the RBM++ after the root reinforcement calculation is completed. In the left window graph, the force-displacement curves of each trench can be observed. In this case, the force and displacement values refer to the deeper soil layer investigated. The curve's color is unique for each trench and can be checked on the right side of the window.

5.1.3 General comment

The Japanese cedar is considered a suitable tree species for improving slope stability (Genet et al., 2008; Yamase et al., 2019) and, therefore, potentially ideal for use in reforestation aimed at direct soil protection on areas particularly susceptible to SLs. However, there is still insufficient information to assess how RR of this species can counter landslide events.

The analysis of RR performed for the two Japanese cedar trees confirms the observations highlighted by previous studies specific to this species.In particular, Fujimaki et al. (2007) and Genet et al. (2008) had observed that root density decreases with increasing depth and that most of the RR is warranted near the surface layers of the soil. Also in this study, the typical branched root system structure is highlighted by the root density graph in Figure 5.1, while the hypothesis of higher reinforcement values' activation in the surface layers of the soil is confirmed both by the curves obtained through the RBM++ software and by the comparison graph in Figure 5.8.

The typical trend of the curve representing the relationship between maximum tension force and root diameter confirms that the tensile force of the single root is more significant as the size of its diameters increases. However, at the root bundle scale, the root distribution becomes a determining factor for the total values of RR. Japanese cedar roots revealed considerable spatial variability in RR values, showing

the need for further studies to understand what physiological and environmental factors influence root distribution and, consequently, root reinforcement. Past studies have investigated the influence of the Japanese cedar tree age on the variation of reinforcement. In particular, Genet et al., 2008 observed that mature plants provide greater RR than younger ones and discussed the importance of forest management to preserve the protective effect in space and time. Regarding environmental factors, it is necessary to study how soil characteristics and possible competition for space and nutrients with neighboring plants affect the growth of root systems of this tree species. Therefore, it is necessary to increase the number of data available for root reinforcement mechanical characterization for this species and to study the correlations that these variations have in combination with the environmental conditions in which the trees are found.

To quantify RR under different environmental conditions, tools such as the RBM++ software could play a crucial supporting role in the rapid assessment and spatial analysis of RR, as well as in the a priori knowledge of the maximum values of force that can be activated in the event of SL triggering. The new information and assumptions can be applied in larger-scale studies to evaluate this species' effects on slope stability and identify proper forest management of Japanese cedar stands.

5.2 Local scale analysis: Rüdlingen artificial shallow landslide

Results from SOSlope about the analysis of Rüdlingen artificial SL show a strong influence of the temporal variability of rainfall intensity in the progressive development of all output data obtained from the simulation. In particular, fluctuations in the pore water pressure in fractures and macroporosity show an evident dependence on the rainfall trend (Figure 4.9).

In the following, the results obtained from simulating the SL with SOSlope are discussed and compared with observations made in the TRAMM project.

5.2.1 Soil stability assessment

When discussing slope stability, we generally refer to quantifying the representative parameter of that condition, the Factor of Safety (FoS), and look at how much the soil moves once triggering occurs. These two parameters, FoS and soil displacement are the main criteria that represent the triggering of SLs.

The following shows what has been obtained relative to these two main parameter for Rüdlingen artificial SL.

Factor of safety

Regarding the evaluation of slope stability through the quantification of FoS, the results obtained with SOSlope differ from those obtained from the application of the stability models shown in Askarinejad et al. (2012). Specifically, the minimum value of FoS quantified with SOSlope is 0.5, while the values calculated through the two models applied in TRAMM project are 0.76 for the 2D model and 0.83 for the 3D model, respectively. These differences depend on the equation implemented in SOSlope (equation 3.1), which is different from that of the 2D model and 3D model applied by Askarinejad et al. (2012). However, the main reason for this difference is the approach used to consider RR in the FoS estimation. SOSlope quantifies RR as a function of the tree positions, size, and species present in the investigated area. The other two models use a constant, spatially and temporally, and uniformly distributed value of root cohesion added to soil cohesion. The progressive root activation and the values reached through the analysis with SOSlope are shown in detail later in this section, while in Askarinejad et al. (2012) the values used are derived from the quantification made by Schwarz et al. (2012b) and therefore equal to 0.5kPa for BRR and 4kPa for LRR.

Soil displacement

Soil displacement results from the SOSlope analysis (Figure 5.14) show a SL shape similar to the one observed in the field in March 2009. Despite SOSlope limitation of being strongly constrained to the square shape of the input raster grid (see software

description in section 3.2), the general area is quite similar. Askarinejad et al. (2012) reports a measured landslide area of about 127 m^2, while the estimated unstable area from SOSlope is about 130 m^2. In both cases, simulated and real SL (Askarinejad et al., 2012; Schwarz et al., 2012b), the shape is related to the presence of trees on the left side of the instrumented area. However, the tree presence influenced not only the shape of the head of SL but also its progressive downslope movement. By analyzing the triggering process of the simulated SL, it was possible to observe that:

1. Soil movement starts 11h 56min after the beginning of the simulation (Figure 5.14b) in the central part of the area, showing displacement values of about 0.5cm. This small movement happens were there are no trees, and therefore no RR, and the simulated rainfall intensity is higher;

2. The effective triggering and greater soil movement (up to a maximum of 2m) occur after 2min, around 12h after the start of the simulation (Figure 5.14d).

3. After 2h from the triggering, the SL widening occurs in the left side (Figure 5.14e). This delay depends on the progressive root failure from trees located on the left side of the SL.

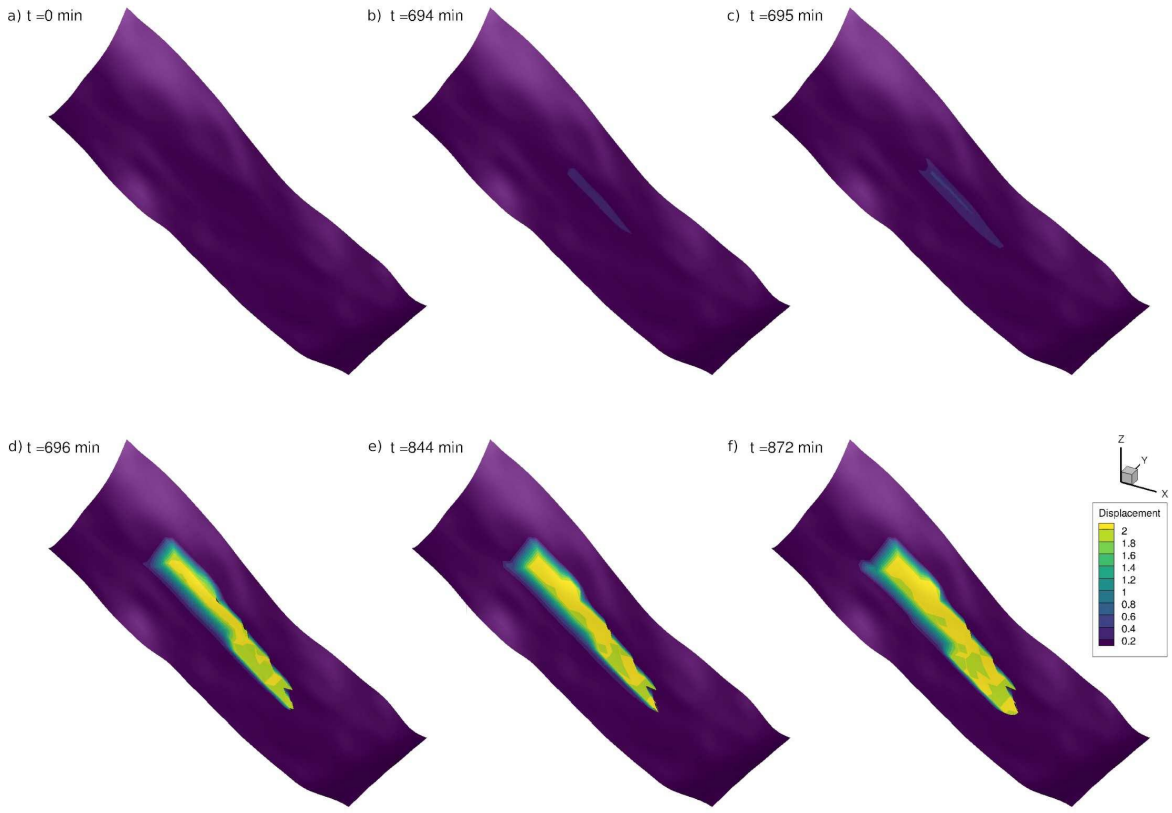

FIGURE 5.14: The Figure shows the key frames of the progressive soil movement obtained from the SOSlope simulation. Time (t) is expressed in consecutive minutes from the start of the test, while displacement values are expressed in meters.

Comparing observations in the simulated SL and what was reported by Askarinejad et al. (2012), it is possible to state that the initial soil movement in Figure 5.14 (b) could be assimilated to what was measured and reported in Figure 5.15. In fact, the Graph (a) shows a slow and small movement in the whole instrumented area. Considering that the rainfall data used in SOSlope does not consider the first hour of rain measured in the field, as stated before, it is possible to affirm that the triggering of the simulated SL occurs at the same time as it did in reality, i.e., at 15 hours after from the start of the test. The same can be said for the SL widening at its left side, corresponding to the last change in the curve trend in Figure 5.15 (a).

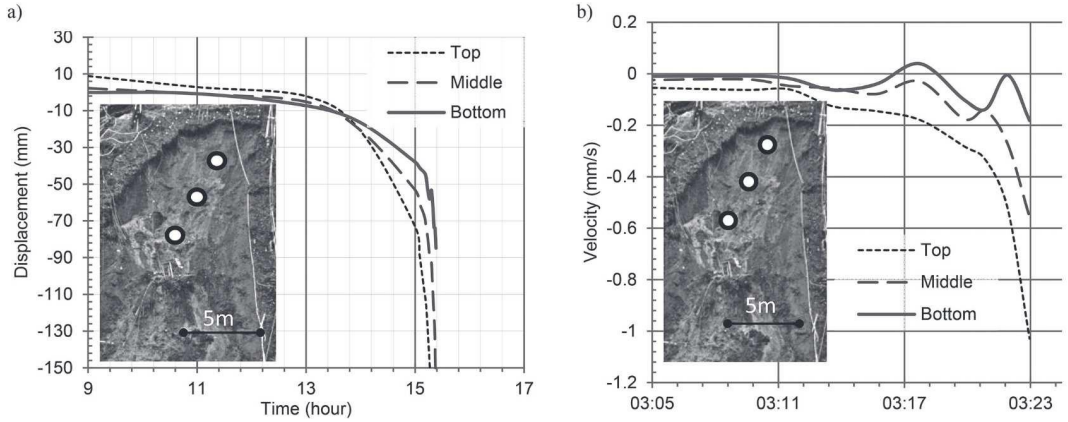

FIGURE 5.15: Soil displacement and velocity measured in the TRAMM project and published by Askarinejad et al. (2012). The three dots represent the investigated positions in the failure wedge for making the displacement and velocity graphs.

In general, it can be said that the progressive movement of the unstable soil mass reconstructed using SOSlope is quite similar to what was observed and measured in the field.

5.2.2 Root reinforcement activation

By analyzing in detail the values and spatial distribution of RR, its crucial role in the progressive initiation of SL was observed and confirmed.

Basal root reinforcement

The BRR is the reinforcement provided by tree roots that are vertically activated along with the soil profile. The BRR values estimated through SOSlope, considering the size and the tree species of the experimental site, showed a maximum value of 5.3kPa exerted by the largest tree (62 cm) localized in the upper part of the SL. Considering instead the whole area under analysis, the estimated average value of BRR is 0.40kPa, with a standard deviation of 0.59kPa.

Lateral root reinforcement

Relative to the LRR, SOSlope can provide different information related to the two different types of reinforcement (Table 3.4). The LRR is procured by roots that are activated horizontally and parallel to the soil surface. Generally, the LRR in tension develops in the head and sides of the unstable soil mass to counteract its movement by stretching until the root breakage. Conversely, the LRR in compression is activated to counteract the soil movement by contracting and finally breaking the roots located in the sides and at the foot of the SL.

In SOSlope simulation, the mobilized LRR in tension shows a maximum value of 23.43kPa again in the vicinity of the larger plant. The higher value of LRR compared to BRR is justified by what was observed and stated by Schwarz et al. (2012a). Reinforcement values ranging from 10kPa to almost 19kPa are shown on the left side of the landslide, confirming their activation to counteract the second ground motion discussed above. Considering the entire area under analysis, the mean value of LRR in tension is estimated to be 1.6kPa, with a standard deviation of 4.06 kPa.

Regarding the progressive activation of the LRR in tension, it was observed that:

1. Minimum values of LRR are activated in a small area on the upper right part of the instrumented area already 4 min after the start of the simulation (Figure 5.16b), remaining constant until 5h 45min after the phase in Figure 5.16 (c);

2. Regarding the point above, the LRR develops in space, increasing in intensity up to values of 3kPa after 7h 22min (Figure 5.16d), and again remaining constant until 9h 27min later (Figure 5.16e);

3. The LRR progressive increase occurs after 10h 32min (Figure 5.16g), with an increase in space and intensity, reaching values up to about 10kPa;

4. The LRR continues to increase in space and intensity, reaching the maximum value of RR activated, 19kPa, during the SL triggering at 11h 38min;

5. Remaining roots reactivate the RR in the lateral part at 12h 20min (Figure 5.16h), contrasting the lateral soil movements observed and reaching values up to 19kPa when the lateral part of the unstable mass also moves at 14h 5min (Figure 5.16i).

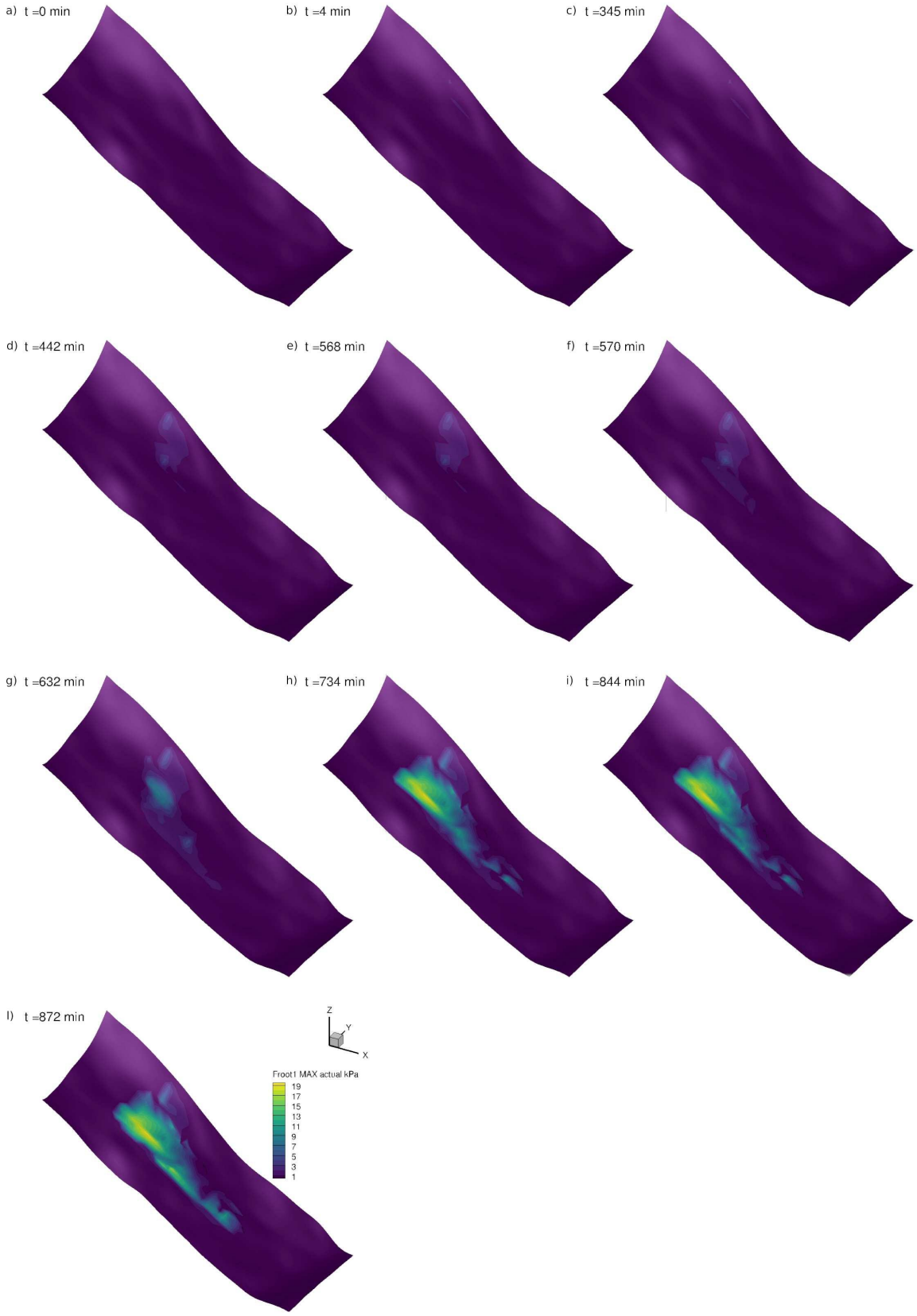

FIGURE 5.16: The figure shows the key frames of the progressive activation of LRR obtained from the SOSlope simulation. Time (t) is expressed in consecutive minutes from the start of the test, while RR values are expressed in kilopascal.

Regarding the mobilized LRR in compression, the maximum value reached is 1201.58kPa developed in the sides of the unstable mass, while considering the whole study area, the average value of LRR in compression is estimated to be 90.14kPa, with a standard deviation of 189.39kPa.

In general concerning the RR, only the LRR was quantified and discussed by Schwarz et al. (2012a) in the TRAMM project. Comparing results obtained with SOSlope and those presented in his paper (Figure 5.17), it is possible to observe good correspondence. The RR values are equivalent, and the spatial distribution of reinforcement is very similar between the two results. In particular, in the upper left area of both SLs the reinforcement distributed along the high side of the unstable soil mass show RR values greater than 10kPa.

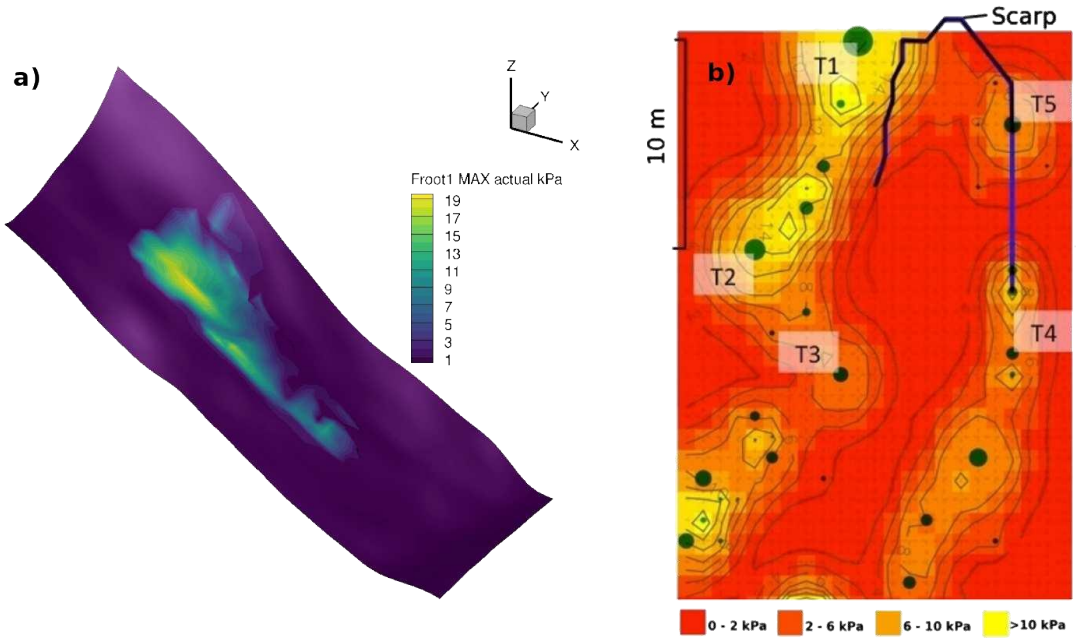

FIGURE 5.17: The two figures show the spatial distribution of root reinforcement values estimated through SOSlope (a) and calculated in the project TRAMM by Schwarz et al. (2012b) (b). In both figures, the areas in yellow represent the maximum values achieved, located at the upper left side of the landslide. The lower left side can also show good correspondence between the two outputs.

5.2.3 Hydrological dynamics analysis

The importance of hydrologic mechanisms in the initiation of SLs has already been discussed in the overview presented in chapter 2. Therefore, to have a complete view of the triggering phenomenon and to evaluate in detail the causes leading to the loss of stability of a slope, SOSlope provides output data referring to the main triggering hydrological mechanism, the increase of pore water pressure.

Pore water pressure

The hydrological module implemented in SOSlope applies a simplified empirical Dual-porosity model (Cohen and Schwarz, 2017), which allows reconstructing the evolution of water content and pressure distribution in both the soil matrix and macropores. The model considers a rapid increase in positive pore pressure in the preferential flow domain, i.e., macropores and fractures, and the slow decrease in soil suction matric by transferring water from macropores to the matrix. In view of this, the two different type of soil pressure are observed and discussed.

Before proceeding with the analysis of these two outputs, it is necessary to highlight another fundamental difference related to their starting conditions. In the case of water pressure in macropores and soil fractures, the starting condition (Figure 5.18a) involves null values of water pressure. Since the soil is generally dry, the voids are occupied mainly by air. In contrast, the starting condition in soil matric pressure is different. Following the soil suction effect, there is a water request from the soil matrix, thus promoting the development of negative pressure values. This condition is represented by the values assigned to the Van Genucthen parameters (Table 4.2). As the water content increases, also the pressure in the macropores and fractures increases assuming more significant positive values, while the increase in matric pressure promotes the reduction of the negative values that tends toward zero.

Starting from the analysis of pressure variability in the macroporosity and fractures, value variations reflect changes quite well in the intensity of simulated rainfall (see Figure 4.9). In detail, it was possible to observe that:

1. Pressure values begin to increase after 5 min from the start of the simulation (Figure 5.18b), probably due to an initial soil water content of about 0.2 m^3m^{-3} (see Table 4.2). As the rainfall simulation continues, the pressure increases rapidly until it reaches 4kPa in the upper part of the area and spreads progressively in space near the upper part of the instrumented area. In the lower areas, the pressure also increases after 15min from the beginning of the simulation (Figure 5.18c), continuing to increase in space after 30min (Figure 5.18d). This general increase in pore pressure corresponds precisely with the intensity peaks around 17mm/h during 30min of rainfall, shown in Figure 4.9.

2. After 37min from the start of the simulation (Figure 5.18f), it was possible to observe a reduction in pressure up to values of 2kPa in the main part of the investigated area, while values of 4kPa remained in the upper part. This variations depends on the rainfall intensity reduction up to 8mm/h.

3. Following the interruption of the simulated rainfall between about 2h 6min (Figure 5.18g) and 2h 36min (Figure 5.18h), pressure values decrease progressively until they annul.

4. After the rainfall stops, pressure restarts to increase after 7h 27min (Figure 5.18i) and reduces again at about 9h 9min (Figure 5.18m). Again, the reduction in pressure depends on the reduction in rainfall intensity in a period between Figure 5.18i and Figure 5.18m. However, in this case, the pressure does not fall down until 0kPa but remains with minimum values of 1.5kPa in the areas more in downslope and 2kPa in the upslope area.

5. The pressure increases again to values of 4kPa after 9h 35min (Figure 5.18n), which spread over the entire experimental area during the next 2 hours (11h 36min, Figure 5.18o). This moment corresponds with the triggering of the SL.

6. After triggering, the influence of rainfall intensity on pore water pressure is significantly lower. The pressure values decrease further after the second soil movement at about 14h, continuing to oscillate until the end of the simulation.

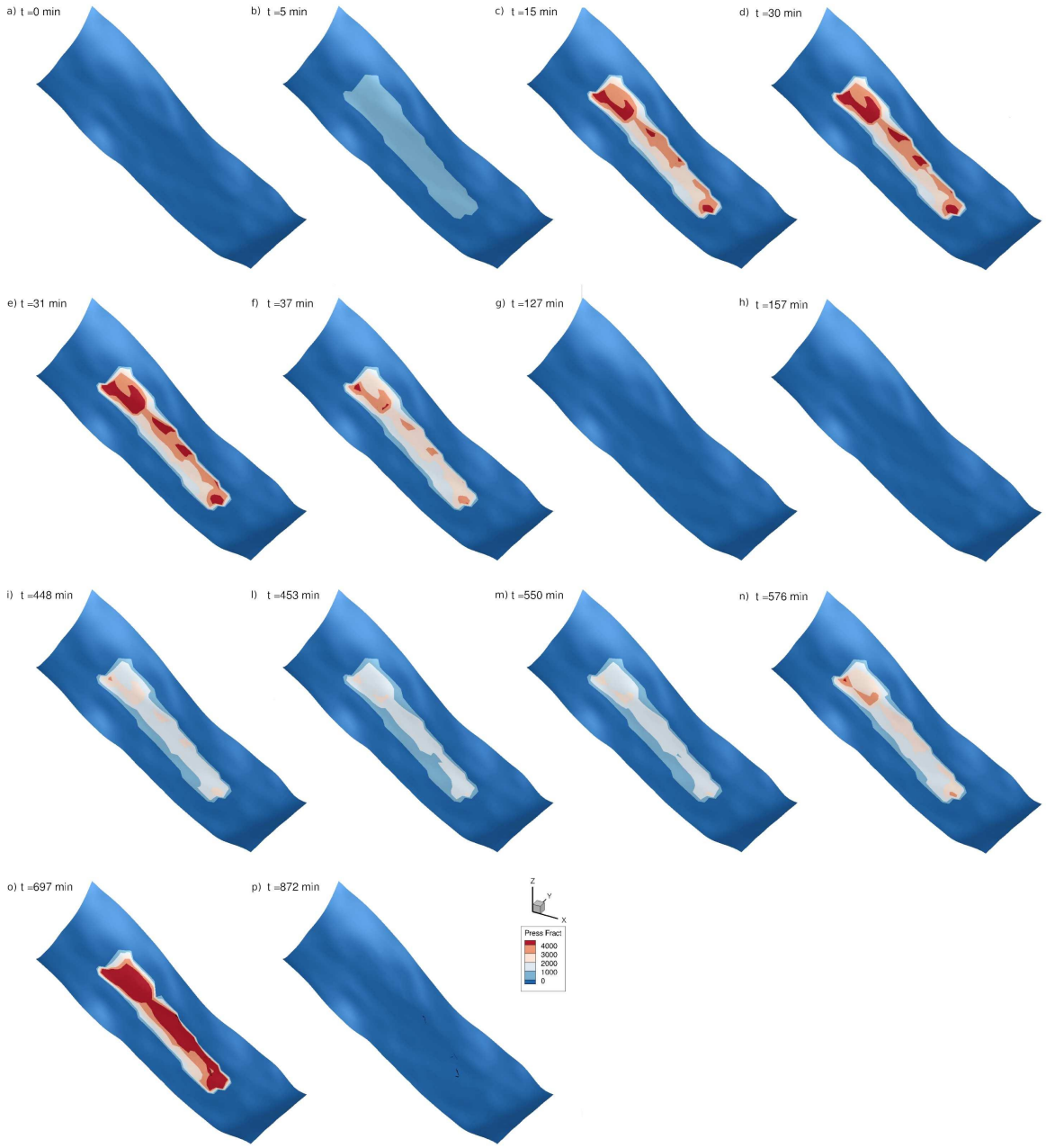

FIGURE 5.18: The figure shows the key frames of the progressive evolution of water pressure in macropores and fractures obtained from the SOSlope simulation. Time (t) is expressed in consecutive minutes from the start of the test, while pressure values are expressed in kilopascal.

Regarding the soil matric pressure, the presence of the initial soil water content highly influences pressure values over space.

Analyzing the evolution of this factor, it was possible to observe that:

1. at the start of the SOSlope simulation, pressure values are different over the investigated area, showing values of 11.4kPa at the upslope area and 14.2kPa in the remaining part. This condition stays constant until 2h 42min (Figure 5.19b) and then start to increase until values of 12kPa.

2. After about 3h 11min (Figure 5.19c) from the simulation start, matrix pressure values around 11kPa begin to develop also in the downslope part. This value spreads gradually in space until 3h 41min (Figure 5.19d). At the same time, the values in the whole area progressively increase.

3. After 4h 35min (Figure 5.19e), following a reduction in simulated rainfall intensity the soil matrix pressure also drops around values of 12kPa, before gradually increasing again when the rainfall intensity stabilizes.

4. At 5h 19min (Figure 5.19f), the pressure values are around 11.6kPa in the whole area, starting to become uniform at 11.4kPa. After 5h 49min (Figure 5.19g), the soil matrix pressure remains uniform and constant at 11.4kPa until the end of the simulation.

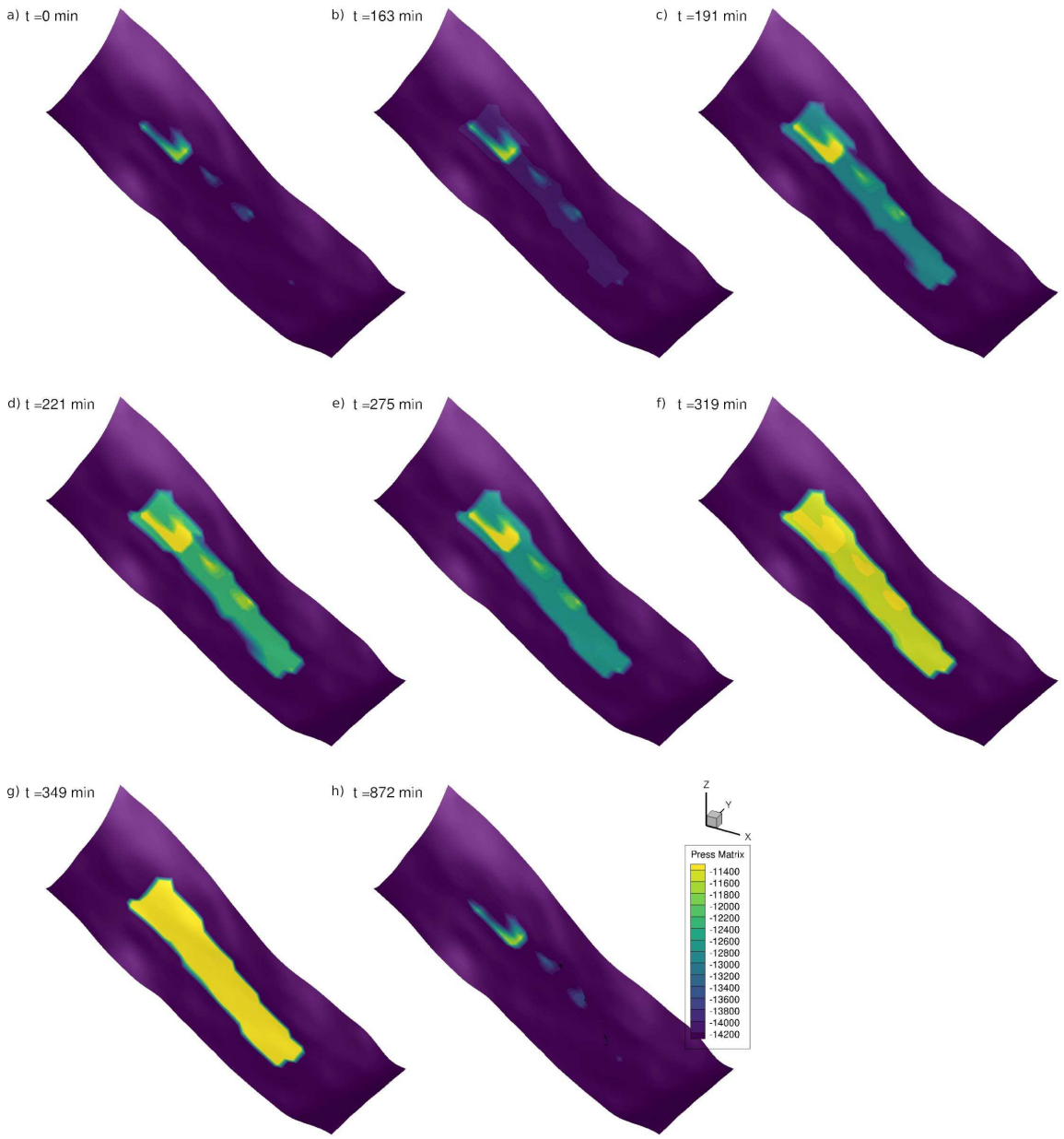

FIGURE 5.19: The figure shows the key frames of the progressive evolution of water pressure in the soil matrix obtained from the SOSlope simulation. Time (t) is expressed in consecutive minutes from the start of the test, while pressure values are expressed in kilopascal.

The graphs in Figure 5.20 show the position of key frames (vertical dashed lines) with respect to the evolution of simulated rainfall intensity. It is evident how variability in rainfall intensity influences the development of preferential flows that cause the significant fluctuation of water pressure values in soil macropores and fractures over time. This process demonstrates the good capacity of the soil to drain, a condition shown to be crucial during the October 2008 experiment in which no SL occurred. In this phase, pressure peaks coincide with rainfall intensity peaks. The achievement of stable pressure values occurs when pressure values in the soil matrix

also begin to increase. Once the matrix begins to saturate, the pressure of macropores and fractures no longer altogether cancel out. From this point on, the correlation between the evolution of pressure values in the macropores and rainfall intensity is no longer evident, while the influence of the soil matrix component comes into play.

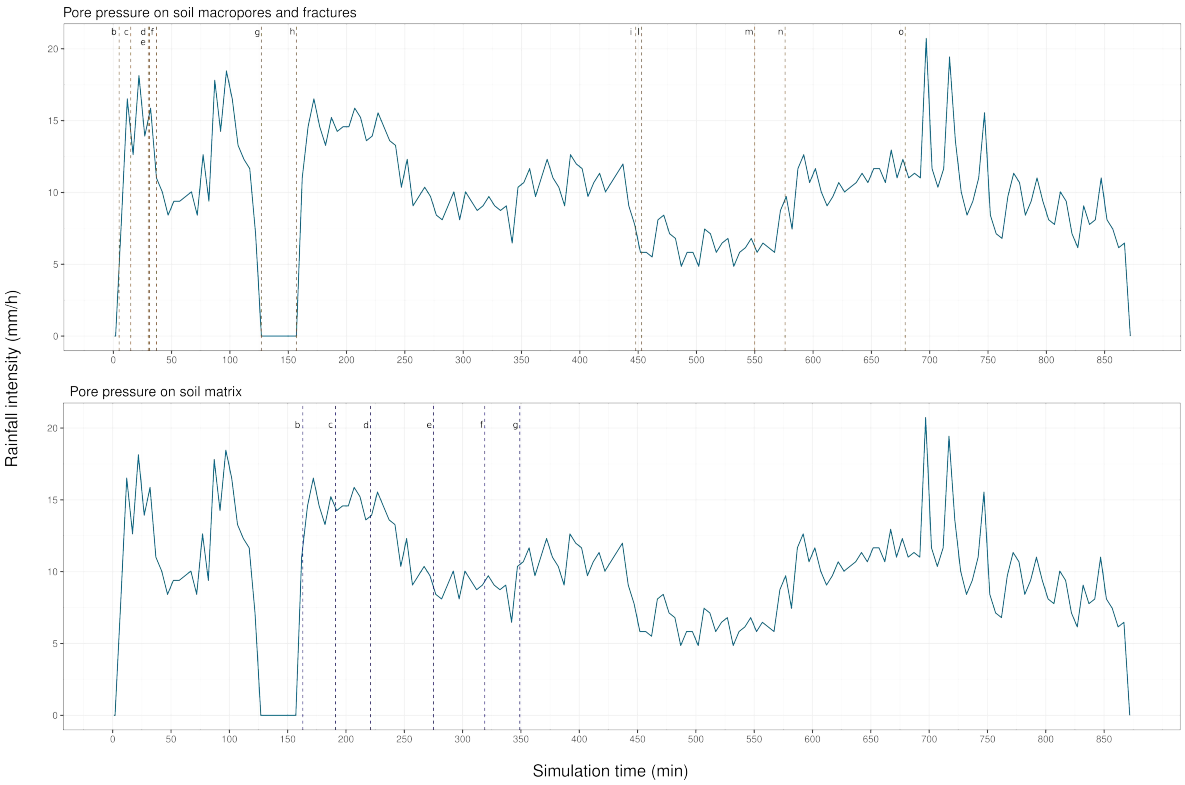

FIGURE 5.20: The two graphs show how the temporal variability of simulated rainfall intensity affected the evolution of the two types of pore pressure reconstructed through SOSlope. The solid blue line represents rainfall intensity values, while the dashed vertical lines represent key frames relative to the indicated letter. It is evident that while a specific moment of pressure evolution in the macropores and soil fractures is greatly influenced by intensity variation, e.g., pauses, increases, or decreases, the soil matrix pressure is less dependent on these variations.

5.2.4 Geotechnical dynamics analysis

Soil compression, like root compression, also plays a crucial role in counteracting downstream soil movement. The two mechanisms develop simultaneously, but Schwarz et al. (2015) observed that soil compression has no direct influence on the overall soil strength yet causes an increase in stiffness that acts as a delay factor in the SL initiation. This parameter was not investigated in the TRAMM project, as it is still poorly understood. However, since it is a mechanical process that affects the slope's stability by counteracting from the downslope area the movement of the unstable soil mass, SOSlope provides it as an output. Therefore, it was possible to proceed with its analysis and understanding.

Soil compression

Soil compression is a mechanical process still poorly studied and, therefore, rarely included in the SSM (see section 2.1.2).

Regarding the analysis performed in Rüdlingen, the results allowed us to observe:

1. the initial condition shows a general equilibrium in the investigated area and the presence of soil resistance forces in the upper part, probably due to the slope of the area and resulting from its frictional force. This condition remained stable for 7h (Figure 5.21b).

2. After 7h 20min (Figure 5.21c), at the center of the area it can be observed that compression forces are starting to develop with values of 15kPa. This condition remains constant until 9h 18min (Figure 5.21d).

3. After 10h 50min, soil forces start to change spatially. While in the upper part of the area, the tension forces increase in space, in the lower central part, the compressive soil forces begin to develop (Figure 5.21e).

4. At 11h 42min after the start of SOSlope simulation, the two areas, differentiated by activation of tension and compression forces, are still evident. After the SL triggering (Figure 5.21f), values around 30kPa develop on the right side and at the foot of the SL. This condition remains constant until the movement of the left side of the SL at 14h 9min (Figure 5.21g).

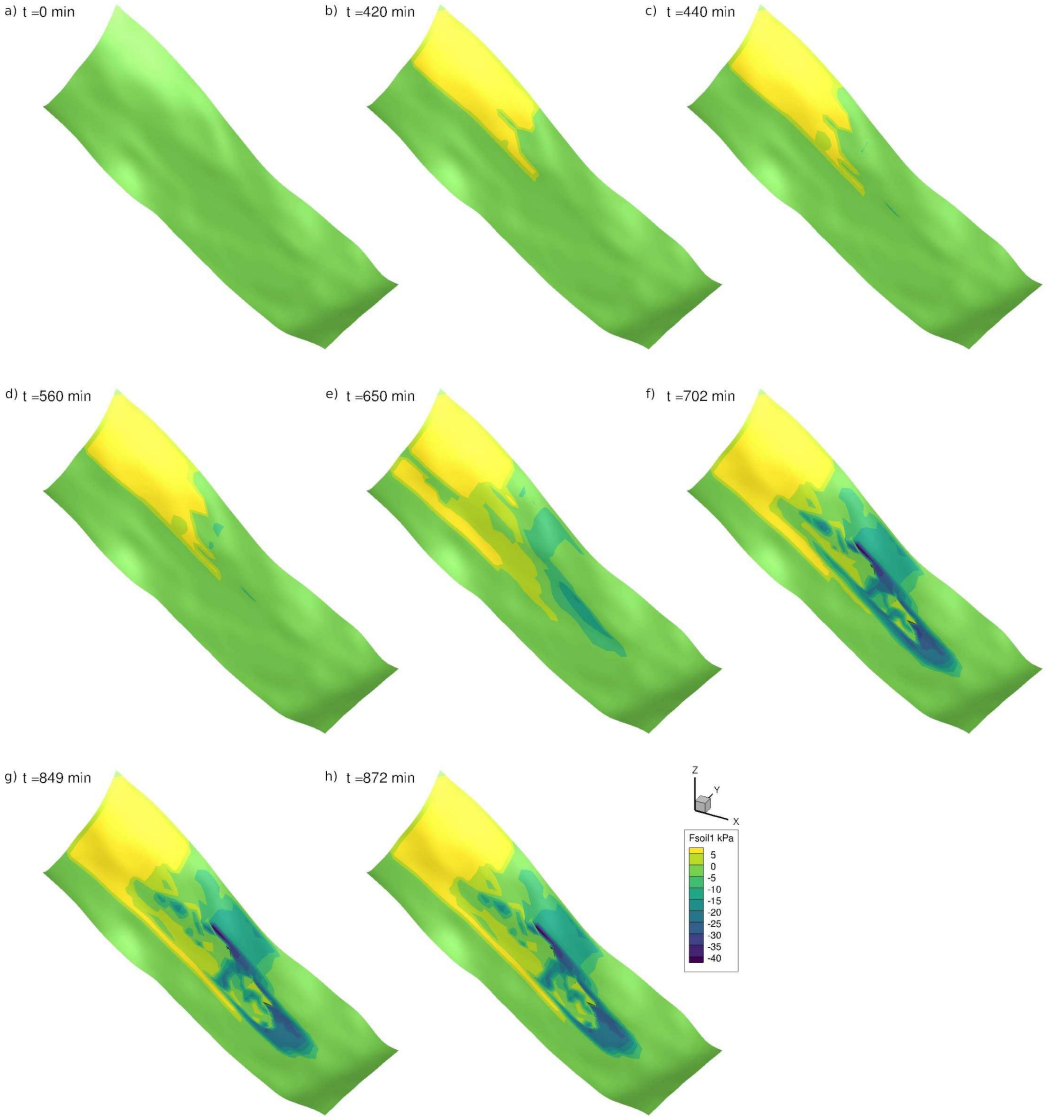

FIGURE 5.21: The figure shows the key frames of the progressive evolution of soil compression obtained from the SOSlope simulation. Time (t) is expressed in consecutive minutes from the start of the test, while pressure values are expressed in kilopascal (positive values represented tension forces, while negative values represented compression forces).

5.2.5 General comment

The need to study and analyze the complex interactions among the factors determining the stability of a vegetated slope requires applying tools capable of adequately considering each of these aspects. It was pointed out in the chapter 2 that generally, slope stability models best develop one specific aspect while greatly simplifying the rest. Generally, the aspect that has suffered most has been the root reinforcement so far. In contrast, SOSlope quantifies this factor by evaluating its influence and correlation with other hydro-mechanical factors (e.g., passive earth pressure, pore water pressure). Therefore, the application of SOSlope in this case study proved to be useful both in conducting a systemic analysis of the landslide event and in assessing in

detail the evolutionary dynamics of the single factor. The results obtained allow for the analysis of the different stages of stability variation and the hydrological causes that favored them. It was possible not only to know a maximum numerical value of root reinforcement activated to counteract soil movement but also to observe how this is activated in space and time. Hydraulic dynamics related to pore pressure are also detailed and separated into two main components: preferential flows in macropores and soil fractures, and water pressure soil matric. The added value of this study comes from verifying the correspondence of the results obtained from simulations with SOSlope with what happened and measured in the field as part of the TRAMM project. Comparison with field observations made it possible to validate the efficiency of the software and identify some of its limitations. Among them, the main one appears to be related to the strict dependence of the calculation process on the DEM grid structure, identifying each cell as a single calculation unit. This dependence is also reflected in the resolution of the final result, for example, the slight overestimation of the landslide surface obtained through SOSlope. Different solutions, such as using a triangular mesh, could probably improve the computational process in terms of time and the quality of the result. As discussed earlier, future developments should improve the computational capacity of slope stability models, ensuring that the complexity of the dynamics that come into play in vegetated slope stability can be preserved, but especially their reliability in analyses that do not involve event validation as in this case.

5.3 Regional scale analysis: Monviso's forest plan

The several results obtained from SlideforMAP elaboration have been used to realize analysis maps. From the whole Monviso zone, a smaller area in the municipality of Oncino is chosen as an sample area to show and explain the analysis method applied.

5.3.1 Risk analysis

Indicative map of shallow landslide hazard

The indicative map of SL hazard in Figure 5.22 shows the spatial variability of the failure probability values, indicating the most critical areas. However, it is fundamental to state that in the specific case of this analysis, the map shows an indicative condition because it displays just the failure probability referred to a return period of 100 years. Generally, a complete map of shallow landslide hazards must compare scenarios based on different return periods (1 year, 50, 100, and 300 years) and simulate the relative rainfall intensity.

The map in the following Figure was obtained by simulating the *100RT_W0* scenario.

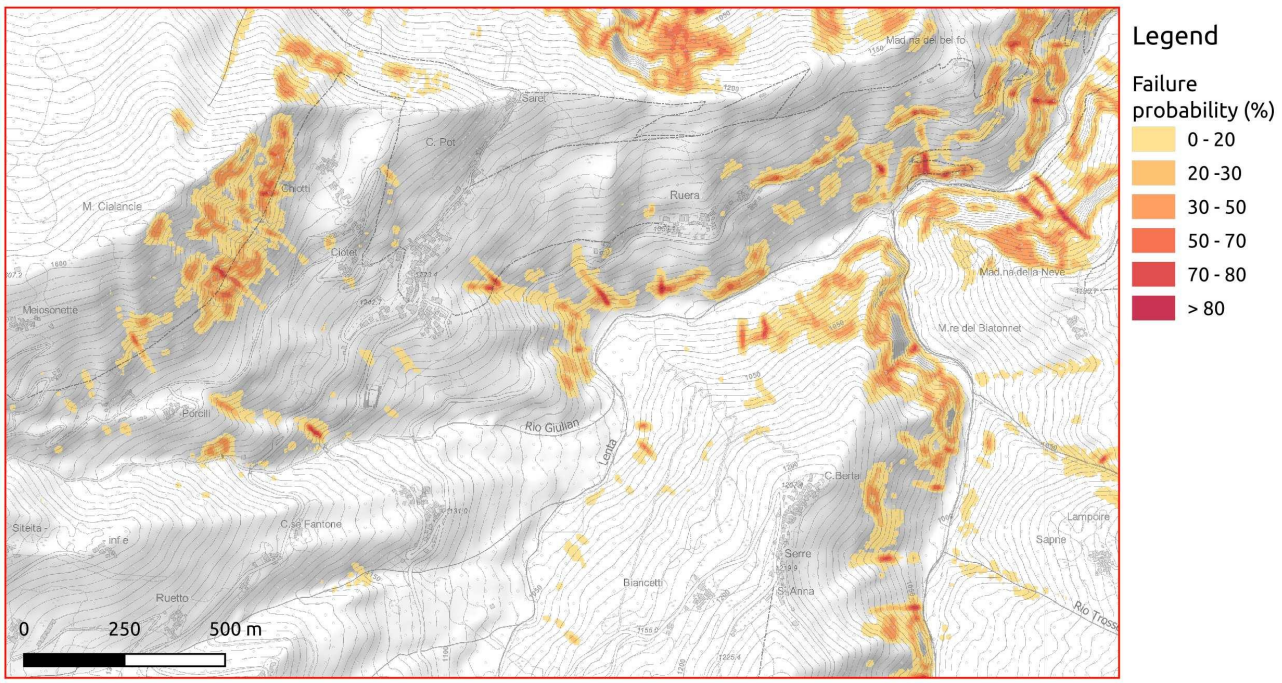

FIGURE 5.22: The map in Figure shows the probability of SL referring to the worst-case scenario *100RT_W0*. The color range represents the probability of slope failure expressed as a percentage. The probability of SLs occurrence increases as the red color becomes more intense. The areas identified are those potentially most susceptible due to morphology. In this scenario, the presence of vegetation is not considered.

The map highlights the critical role of morphology as a central factor in increasing an area's susceptibility to confirm SL occurrence. The typical valley morphology

present in the considered area promotes high probability values localized near areas of a higher slope, along watercourses, and near tributaries. The latter aspect is evidenced not only by the contour lines but also by the elongated shape of the area presenting the failure probability. Additionally, north of the area, it is possible to observe the critical role of roads in increased susceptibility. Infrastructures are elements prone to possible SLs trigger points. Changes in slope dynamics, mechanical and hydrological, caused by the construction and presence of infrastructure is a widely studied and discussed issue (Persichillo et al., 2017; Bordoni et al., 2018; Mauri et al., 2022).

In the following maps, as it will be further explained, it is possible to observe that forested areas actually present reduce SL probability values. However, in some critical areas, values of probability are still significant (small map in Figure 5.27).

Qualitative map of potential damage

The qualitative map of potential damages highlights the areas with a higher density of exposed elements, distinguished in this analysis in structures and infrastructures. This type of map allows observing the distribution of the elements in space; therefore, evaluating in detail how the occurrence of SL phenomena could affect both the land and the environment. For each type of element, a density map (also know as heat map) has been realized through the module *Kernel Density Estimation* in QGIS and considering buffers around the element with a distance from it of 300 m for structures and 100 m for infrastructures.

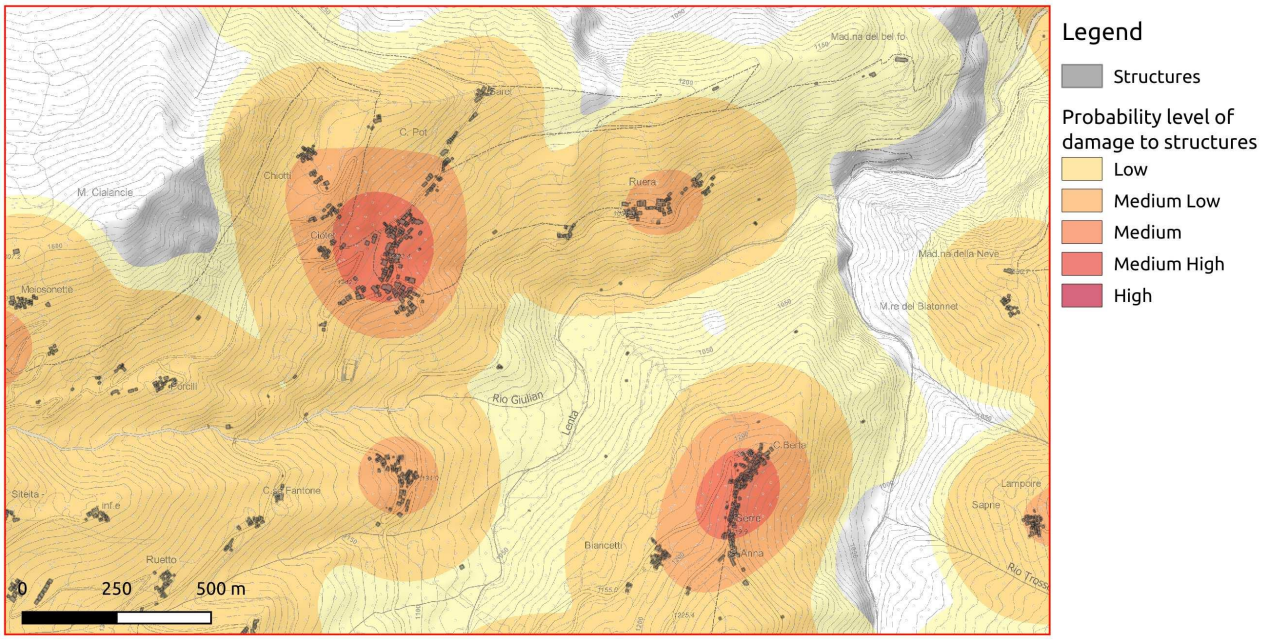

FIGURE 5.23: The map in the Figure shows the probability levels of damage to structures. The color intensity depends on the density of the structures in the specific area. This information helps to assess how spatially distributed the structures are.

As far as the sample area is concerned, the map of the structures in the Figure 5.23 shows the presence of four agglomerates located in the center of the area, of which two present considerable density with a value ≥ 100, while the other two less dense assume a value between 50-100. These values are indicative of the number of structures located in that area. The buffer area, which assumes a value between 10-and 50, shows that the presence of exposed elements is uniform in space.

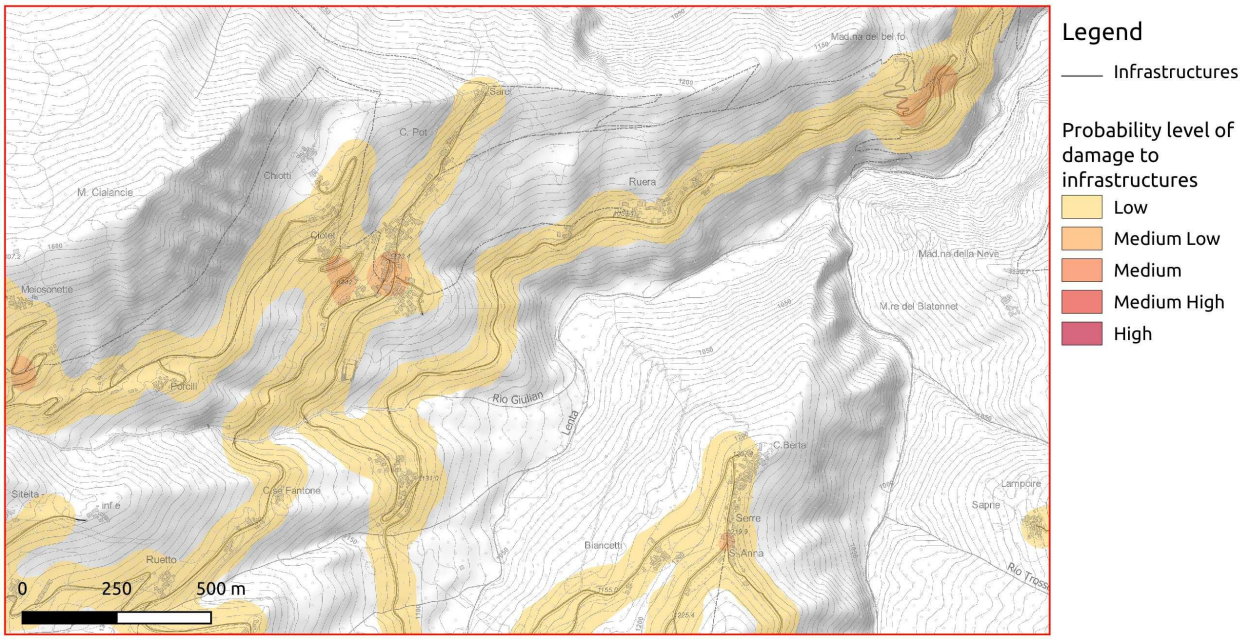

FIGURE 5.24: The map in the figure shows probability levels of damage to infrastructures. The color intensity depends on the density of the infrastructures in the specific area. This information helps to assess how spatially distributed the infrastructures are.

On the other hand, considering infrastructures, the map in the Figure 5.24 shows punctual areas where road sections are denser, assuming values generally of 15-30, and in the specific area near the built-up area of Ciatet, values of 30-45. In this case, the density is quantified by considering that closer road sections increase the risk and, therefore, the potential damage.

Priority map of the potential protection forest

Identifying areas at risk requires combining information concerning failure probability (Figure 5.22) and potential damages to structure and infrastructures (Figures 5.23 and 5.24). The areas that present specific risk values should be those in which the forest, if present, should assume a direct protective function as a priority. Where the forest is absent, it is possible to observe if the risk is localized in areas with different land use and evaluate the planning of specific interventions to reduce this risk.

Generally, a SL event-triggered upslope of a structure or agglomeration is considered riskier than the same event-triggered downslope. While upslope events would

cause direct damage by impacting structures, following the movement of the unstable soil mass driven by gravity, downslope events would cause indirect damage by causing a general loss of the slope stability. Considering this aspect, buffer areas upslope and downslope of the structures were distinguished by performing a geospatial analysis based on elevation. Combining all this information, the map in Figure 5.25 was realized.

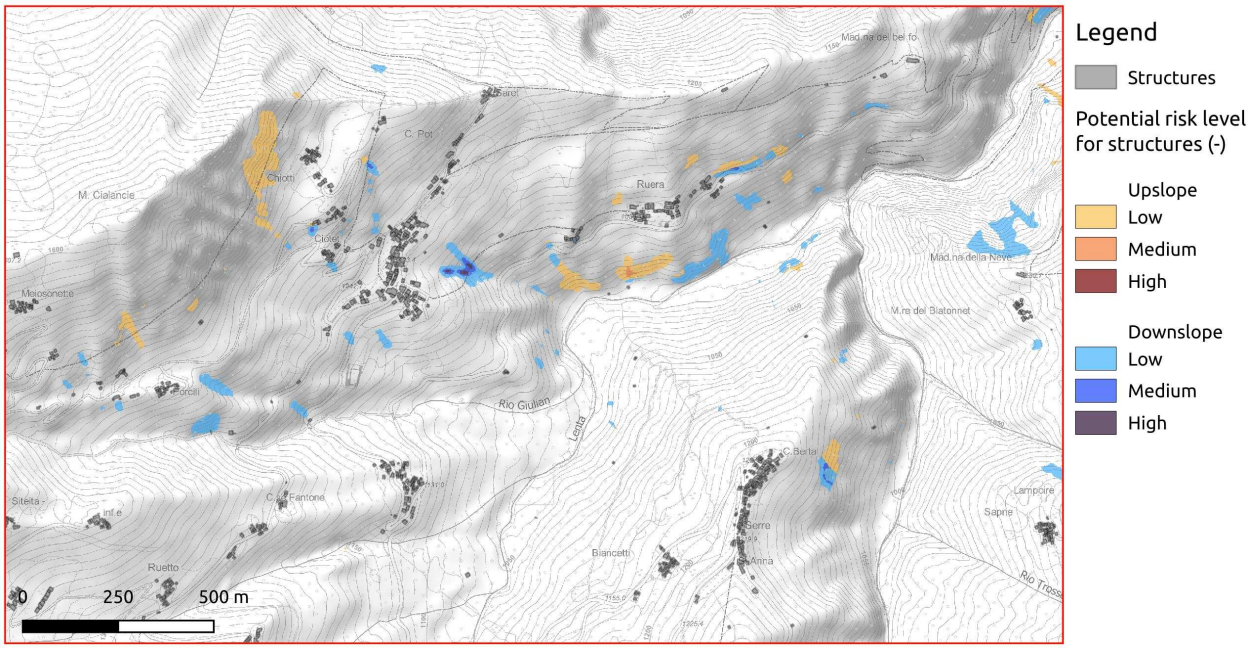

FIGURE 5.25: The map in the Figure identifies areas where it is possible to have a risk of a SL occurrence. The risk level depends on the failure probability value and exposed elements' density. In this case, considering structures, the risk level is distinguished depending on upslope and downslope location. Generally, an event occurring upslope of a structure or agglomeration is considered riskier than the same event occurring downslope, as it could cause direct damage due to gravity-driven movement of the unstable soil mass.

In quantifying damage near infrastructure, this distinction is not made, but the risk is calculated by multiplying the failure probability by the exposed elements (Figure 5.26).

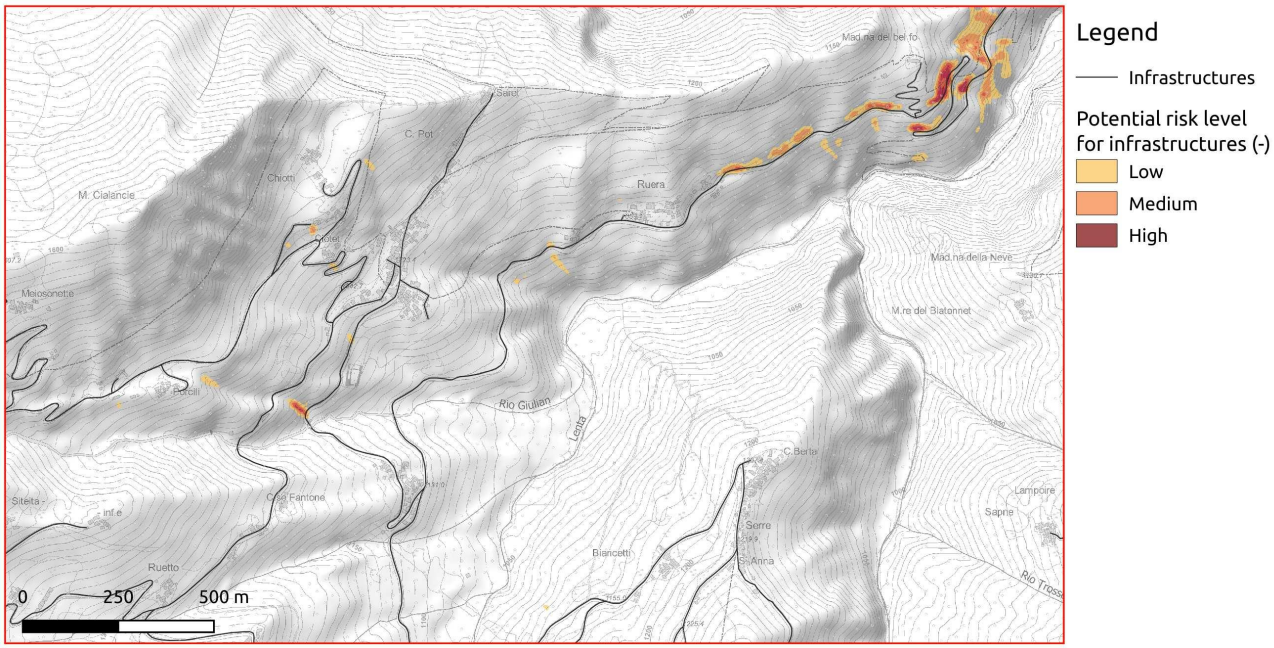

FIGURE 5.26: The map in the Figure identifies areas where it is possible to have a risk of a SL occurrence. The risk level depends on the failure probability value and exposed elements' density. Considering infrastructures, no distinction was made between upslope and downslope events. Since these are, in fact, linear elements, the damage caused in the case of SL would be identical.

Based on the worst-case scenario *100RT_W0*, this first part of the analysis allows assessing the most critical areas throughout the territory. The results obtained are combined with the forested scenarios to verify, through comparison of the forested areas, where it is necessary to intervene in order to improve soil protection.

5.3.2 Forest analysis

The forest is an essential element capable of providing stability to vegetated slopes. However, the presence of the forest does not always mean having adequate soil protection and, therefore, slope stability. This analysis identifies areas where it is necessary to intervene for improving or developing soil stability, also identifying priorities of silvicultural interventions.

Map of the actual forest protection effect In the map of the actual forest protection effect (scenario 100RT_Wa), it is possible to observe the areas in which the forest procures the reduction of slope failure probability. Probability failure reduction happens at localized points in the forest, providing reduction values generally around 30%. However, this reduction in values does not mean a total cancellation of the probability.

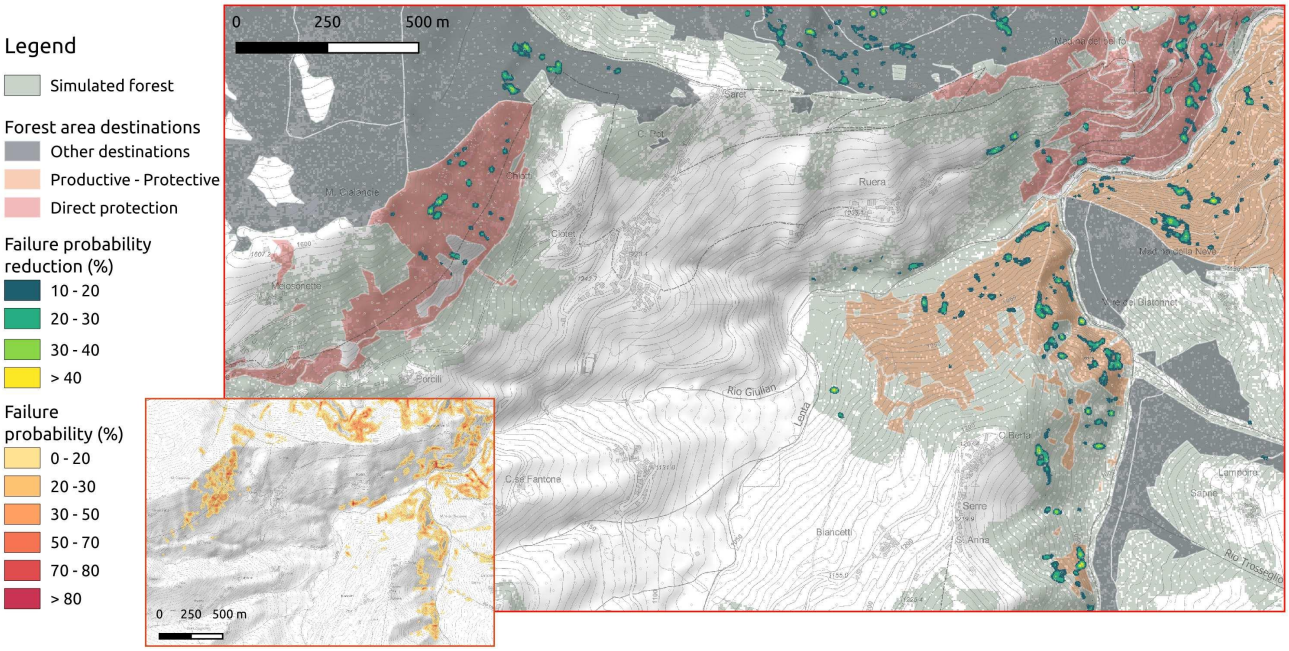

FIGURE 5.27: The map in the Figure shows the areas where the forest, considered with its current structure and composition, reduces the slope failure probability. As the areas tend to be yellow, the mitigation effect of the forest is more significant. However, it can be observed that there is not always a correlation between effective forest mitigation and the functional definition assigned to the stand. Although a specific forest area plays a direct soil protection role, this is generally not assigned to this function. The map in the small box below shows that although there is a protective effect of the current forest, this is not sufficient in some areas to nullify or reduce the probability of SLs occurrence.

Map of the ideal forest protection effect In the map of the ideal forest protection (scenario 100RT_Wi), it is possible to observe a significant reduction in the failure probability, both in terms of surface and values. The possibility of being able to guarantee in space an effective RR allows better results in the frequency and intensity mitigation of SL events. This condition can be defined as aiming for a more detailed silviculture.

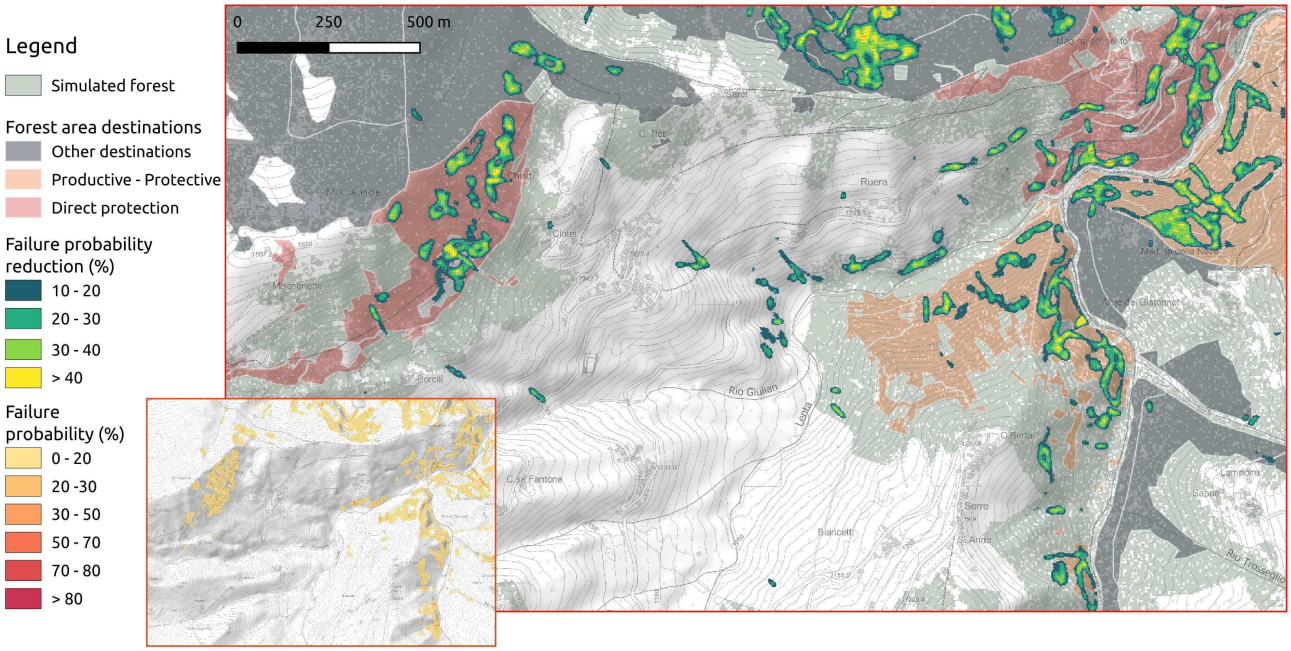

FIGURE 5.28: The map in the figure identifies areas where the potential forest, considering an ideal value of RR, reduces the probability of failure. As the areas tend to be yellow, the mitigation effect of the forest is more significant. The map at the bottom shows an overall significant reduction in the probability of initiation SLs. Areas still showing the red color identify points where the forest effect would never be able to limit the probability. In these areas, reasoning should be more related to identifying nature-based or classical engineering solutions.

Map of the protective value of the ideal forest The map of the protective value of the ideal forest highlights the areas where the protective effect is more urgent due to the presence of areas with high-risk exposure. The map is obtained by relating the ideal protective forest (Figure 5.30) to the map of potential damage, distinguished by upstream and downslope in the case of buildings. The indicative values obtained can be interpreted, for example, as a monetary amount that could be avoided in case of SL event if the forest is managed correctly. The map shows low protection values located in forested areas with a functional destination of direct protection (red areas) or protective-productive (orange areas). This aspect highlights the need for direct protection forests to be managed to ensure the protective effect in space and time.

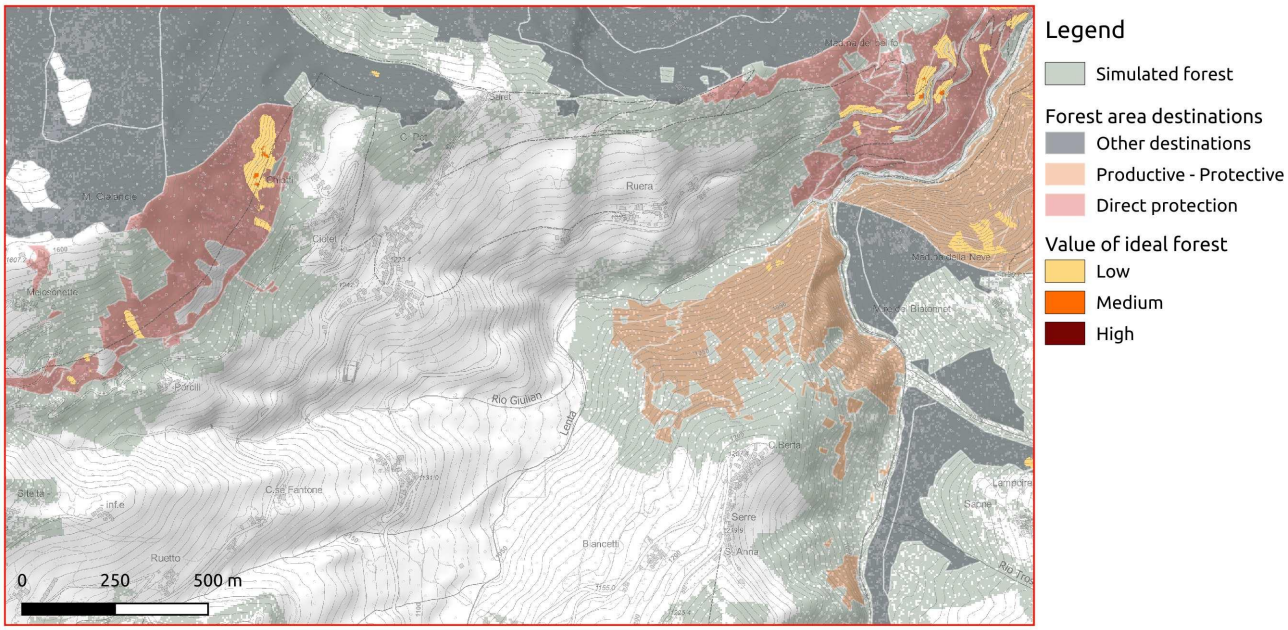

FIGURE 5.29: The map in the figure identifies areas where the protective effect is more urgent due to the presence of areas with high-risk exposure. Generally low protection values are located in forested areas with a functional destination of direct protection (red areas) or protective-productive (orange areas). This aspect highlights the need for direct protection forests to be managed aiming to preserve the protective effect in space and time.

Priority map of silvicultural interventions This map shows areas where the current forest protection is adequate and those where it is necessary to improve this effect. Specifically, the orange color highlights areas where the RR of the current forest is better than the ideal one, while the blue-yellow color range highlights areas that can be improved and identifies the priority and urgency of intervention. Multiplying the protective value of the ideal forest and the difference in probability between the ideal and current forest provides a valuable criterion for prioritizing forestry interventions.

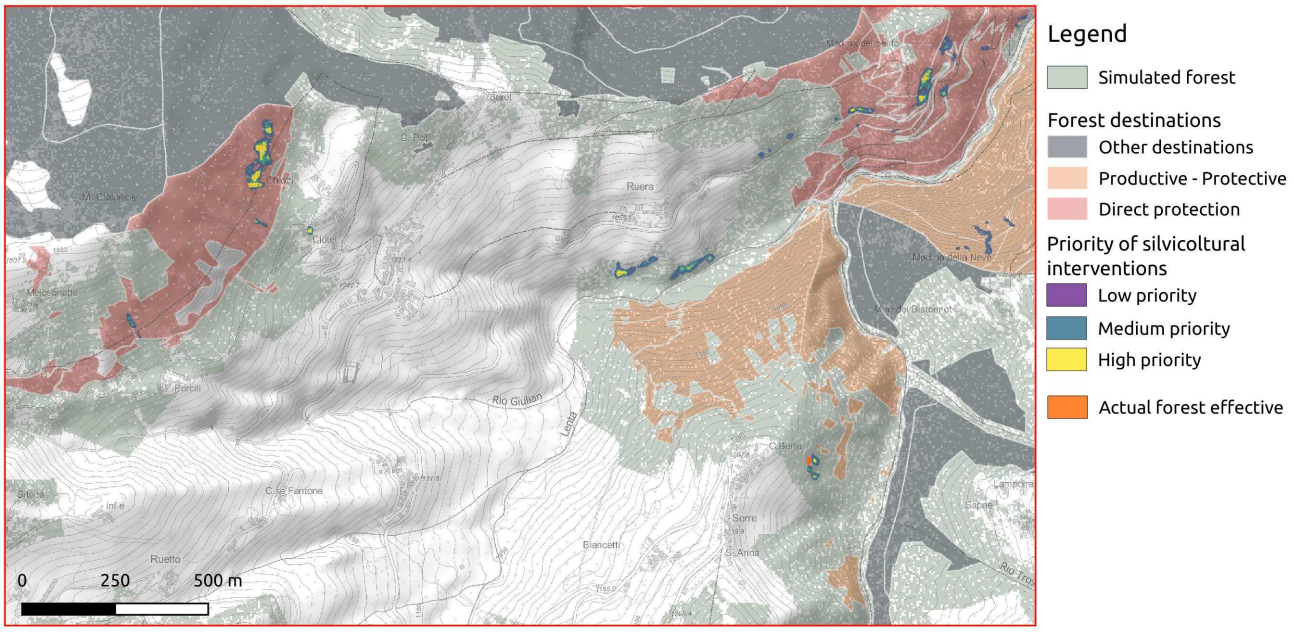

FIGURE 5.30: The map in the Figure shows different level of silvicoltural interventions priority. The level of priority, identified blue-yellow color range, depends on the urgency of managing that forested area aiming to improve root reinforcement and soil protection. However, there are also small areas where the current forest effect is still effective (orange areas).

This map also highlights the need for appropriate management of direct protection forests.

5.3.3 General comment

The analysis discussed in this section demonstrates an *ad-hoc* designed methodology for identifying areas prone to surface landslides. The reconstruction of scenarios based on statistically verified values of rainfall intensity, referring to different return periods, and different land cover conditions allow reconstructing and assessing a priori the degree of hazard and risk that could occur in a given area. From the analysis and comparison of the results obtained by the SlideforMAP software and rallied to the different scenarios, it is possible to assess the forest's actual contribution to soil stability and verify whether this mitigation effect is adequate or requires improvements. The high level of attention to considering forest structure and composition makes it possible to simulate scenarios in which interventions are expected to modify one or both of these factors, as well as to observe how these changes may affect the probability of occurrence of SLs. Indeed, the ability to perform parameterization at the scale of a single tree makes it possible to simulate silvicultural scenarios and identify appropriate small-scale management strategies (Zadelhoff et al., 2021a).

The methodology is adequate for the analysis of future, hypothetical scenarios necessary for accurate management of direct protection forests, which is currently based on more generic methodologies, e.g., applying RUSLE, or even on knowledge of inventoried events in the area under investigation. To the best of our knowledge,

no model can provide valuable indications for improving the effectiveness of the direct protection forest. Knowing precisely where interventions are needed, assessing the urgency depending on the probability and proximity to exposed elements, and simulating different hypothetical management scenarios become invaluable in informed forest planning aimed at mitigating this risk.

However, further applications and case studies are needed to identify potential points of improvement in both the methodology and the SlideforMAP software. For the latter, the most critical improvement concerns the need to collect new data on the mechanical characterization of RR of the most common forest species. In this way, the analysis could become part of the forest planning process in complex stands with different specific compositions, providing an essential improvement in identifying the correct silvicultural practices for managing direct protection forests.

Chapter 6

Conclusions

The objective of this research work was to create, validate, and apply multiscale analysis tools and methodologies for verifying the stability of vegetated slopes.

The state of the art analysis highlighted users' tendency to prefer simple models, as they are immediately understandable and based on easy-to-obtain information. However, these models have proven to be ineffective in quantifying and evaluating vegetation's mitigation effect because they usually assume constant and uniform values of root reinforcement in space and time. With the increase in computer knowledge and attention to vegetation's role in slope stability, new complex models were developed, but their use often remains limited to the research field. Therefore, to facilitate the use of these models, both in the academic and professional fields, new software model-based were developed and equipped with a user-friendly graphical interface. Following this purpose, this research proposes applying three software programs to investigate the dynamics of root reinforcement on three different scales of analysis.

Relative to the tree scale, the RBM++ software allows quick quantification and spatial evaluation of root reinforcement. Based on the model of root reinforcement implemented in recent slope stability models, the Root Bundle Model with Weibull function (RBMw), allows us to observe how the root reinforcement varies both as a function of distance from the tree stem, but mainly as a function of increasing depth in the soil. However, this first version of RBM++ is still constrained to preliminary processing to be done externally to the software, but necessary to quantify the mechanical parameters of the reinforcement. This limitation is already partly overcome by the possibility of using standardized root reinforcement values of some of the tree species. Future developments of RBM++ envision complete software autonomy in estimating reinforcement using little accessible information, e.g., tree size and root density, and becoming a valuable tool for initial field verification and quantification of root reinforcement.

Relative to the slope scale, the SOSlope software allows reconstruction and evaluation of slope hydro-mechanical dynamics, focusing on the progressive activation in space and time of root reinforcement. Its validation through the reconstruction of the Rüdlingen artificial landslide event demonstrated a good reconstruction of the

complex dynamics that led to the loss of soil stability. SOSlope is suitable for detailed analyses of susceptible areas, such as near structures or infrastructures, or in planning reforestation interventions to improve an area's stability. In the latter case, the software makes it possible to study the structure and composition of the planting and verify its efficiency. Future developments related to SOSlope concern the development of a new version that will provide *ad hoc* solutions to overcome the square grid of the digital terrain model with a mesh model, but above all, the inclusion of new tree species will be available for the calculation of root reinforcement.

Finally, considering the regional analysis scale, the SlideforMAP software made it possible to investigate the degree of susceptibility of the Monviso area to the occurrence of shallow landslides and quantify the actual contribution of forests to soil protection. The case study presents the first example of this software application in forest management decision-making. The innovative aspect of this methodology concerns the possibility of verifying and quantifying the protective effect of forests, guiding the identification of protection forest areas. Future developments of this methodology involve the application of further case studies that will allow both the software's validation and, more importantly, the refinement of the analysis methodology.

These three models and related methodologies can potentially become part of forest and land management decision-making processes to prevent and mitigate shallow landslide phenomena. However, their application implies that although they are software-based on complex physical models, simplifications and assumptions are inevitable. The already discussed difference between deterministic physically-based and probabilistic physically-based models originates from respective simplifications, which are inevitable to allow their application and computation in different contexts and scales of analysis. Moreover, although input data are generally readily available on the regional geographical website or the literature, some contexts must make assumptions based on weighted reasoning. An example is the lack of standardized root reinforcement values related to a specific tree species in the investigated area. The user's knowledge and experience will allow the user to identify among those available the one that most closely resembles the species present in the investigated area.

Another aspect not to be underestimated concerns that although the models can highlight potentially overlooked situations by applying simplified approaches of analysis and subjective evaluations, the results must be carefully interpreted by the user. The computational process does not consider local situations that produce objective evaluation errors. A common example is identifying potentially unstable areas near the change in slope at building construction cut-offs. In these cases, knowledge of the investigated area is essential for correctly interpreting information.

In conclusion, the introduction and application of these tools as part of future decision-making processes will make it possible both to know and quantify in detail the areas most susceptible to surface landslide phenomena, but more importantly,

to better manage the forest by identifying the silvicultural practices best suited to improve and ensure the protective effect of the soil over time and space.

Bibliography

Abe, Keita, Kenichi Soga, and Samila Bandara (Mar. 2014). "Material Point Method for Coupled Hydromechanical Problems". In: *Journal of Geotechnical and Geoenvironmental Engineering* 140.3, p. 04013033. ISSN: 1090-0241, 1943-5606. DOI: 10.1061/(ASCE)GT.1943-5606.0001011. URL: http://ascelibrary.org/doi/10.1061/%28ASCE%29GT.1943-5606.0001011 (visited on 05/26/2021).

Akca, Devrim, Armin Gruen, Amin Askarinejad, and Sarah M Springman (2011). "Photogrammetric monitoring of an artificially generated landslide". In: Publisher: Unpublished. DOI: 10.13140/RG.2.1.1084.5289. URL: http://rgdoi.net/10.13140/RG.2.1.1084.5289 (visited on 04/08/2022).

Andersen, S. and L. Andersen (Jan. 2010). "Modelling of landslides with the material-point method". In: *Computational Geosciences* 14.1, pp. 137–147. ISSN: 1420-0597, 1573-1499. DOI: 10.1007/s10596-009-9137-y. URL: http://link.springer.com/10.1007/s10596-009-9137-y (visited on 05/26/2021).

Arnone, E, D Caracciolo, L V Noto, F Preti, and R L Bras (2016a). "Modeling the hydrological and mechanical effect of roots on shallow landslides". In: *Water Resources Research*, p. 23. DOI: 10.1002/2015WR018227.. URL: https://agupubs.onlinelibrary.wiley.com/doi/pdf/10.1002/2015WR018227.

Arnone, E., Y. G. Dialynas, L. V. Noto, and R. L. Bras (Mar. 15, 2016b). "Accounting for soil parameter uncertainty in a physically based and distributed approach for rainfall-triggered landslides: Soil Parameter Uncertainty in Distributed Landslide Analysis". In: *Hydrological Processes* 30.6, pp. 927–944. ISSN: 08856087. DOI: 10.1002/hyp.10609. URL: https://onlinelibrary.wiley.com/doi/10.1002/hyp.10609 (visited on 09/07/2021).

Arnone, E., L.V. Noto, C. Lepore, and R.L. Bras (Oct. 2011). "Physically-based and distributed approach to analyze rainfall-triggered landslides at watershed scale". In: *Geomorphology* 133.3, pp. 121–131. ISSN: 0169555X. DOI: 10.1016/j.geomorph.2011.03.019. URL: https://linkinghub.elsevier.com/retrieve/pii/S0169555X11002637 (visited on 09/07/2021).

Arnone, Elisa, Antonio Francipane, Leonardo V. Noto, Antonino Scarbaci, and Goffredo La Loggia (Mar. 1, 2014). "Strategies investigation in using artificial neural network for landslide susceptibility mapping: application to a Sicilian catchment". In: *Journal of Hydroinformatics* 16.2, pp. 502–515. ISSN: 1464-7141, 1465-1734. DOI: 10.2166/hydro.2013.191. URL: https://iwaponline.com/jh/article/16/2/502/3497/Strategies-investigation-in-using-artificial (visited on 02/27/2022).

Askarinejad, A, F Casini, P Kienzler, and S M Springman (2011). *Comparison between the in situ and laboratory water retention curves for a silty sand*. TRAMM. CRC Press. ISBN: 978-0-415-60428-4 978-0-203-83401-5. URL: http://www.crcnetbase.com/doi/book/10.1201/b10526 (visited on 03/05/2021).

Askarinejad, Amin (2013). "Failure mechanisms in unsaturated silty sand slopes triggered by rainfall". Artwork Size: 1 Band Medium: application/pdf Pages: 1 Band. PhD thesis. ETH Zurich. DOI: 10.3929/ETHZ-A-010002526. URL: http://hdl.handle.net/20.500.11850/74159 (visited on 02/27/2022).

— (Nov. 2015). *Failure Mechanisms in Unsaturated Silty Sand Slopes Triggered by Rainfall*. vdf Hochschulverlag AG. ISBN: 978-3-7281-3676-3.

Askarinejad, Amin, Devrim Akca, and Sarah M. Springman (Sept. 2018). "Precursors of instability in a natural slope due to rainfall: a full-scale experiment". In: *Landslides* 15.9. TRAMM, pp. 1745–1759. ISSN: 1612-510X, 1612-5118. DOI: 10.1007/s10346-018-0994-0. URL: http://link.springer.com/10.1007/s10346-018-0994-0 (visited on 03/01/2021).

Askarinejad, Amin, Francesca Casini, Patrick Bischof, Alexander Beck, and Sarah M Springman (2012). "Rainfall induced instabilities: a field experiment on a silty sand slope in northern Switzerland". In: p. 22.

Askarinejad, Amin and Sarah M Springman (2017). "A Novel Technique to Monitor Subsurface Movements of Landslides". In: 00, p. 11.

Askarinejad, Amin and Sarah M. Springman (2021). "Water Exfiltration from Bedrock: A Drastic Landslide Triggering Mechanism". In: *Understanding and Reducing Landslide Disaster Risk*. Cham: Springer International Publishing, pp. 85–99. ISBN: 978-3-030-60712-8 978-3-030-60713-5. URL: http://link.springer.com/10.1007/978-3-030-60713-5_10 (visited on 01/17/2021).

Avolio, M. V., Salvatore Di Gregorio, Franco Mantovani, Alessandro Pasuto, Rocco Rongo, Sandro Silvano, and William Spataro (2000). "Simulation of the 1992 Tessina landslide by a cellular automata model and future hazard scenarios". In: *International Journal of Applied Earth Observation and Geoinformation* 2.1, pp. 41–50. ISSN: 0303-2434. DOI: https://doi.org/10.1016/S0303-2434(00)85025-4. URL: https://www.sciencedirect.com/science/article/pii/S0303243400850254.

Ayalew, Lulseged and Hiromitsu Yamagishi (Feb. 2005). "The application of GIS-based logistic regression for landslide susceptibility mapping in the Kakuda-Yahiko Mountains, Central Japan". In: *Geomorphology* 65.1, pp. 15–31. ISSN: 0169555X. DOI: 10.1016/j.geomorph.2004.06.010. URL: https://linkinghub.elsevier.com/retrieve/pii/S0169555X04001631 (visited on 07/14/2020).

Bak, Per, Chao Tang, and Kurt Wiesenfeld (1988). "Self-organized criticality". In: *Physical review A* 38.1, p. 364. DOI: https://doi.org/10.1103/PhysRevA.38.364.

Baum, Rex L., Jeffery A. Coe, Jonathan W. Godt, Edwin L. Harp, Mark E. Reid, William Z. Savage, William H. Schulz, Dianne L. Brien, Alan F. Chleborad, Jonathan P. McKenna, and John A. Michael (Dec. 2005). "Regional landslide-hazard assessment for Seattle, Washington, USA". In: *Landslides* 2.4, pp. 266–279. ISSN:

1612-510X, 1612-5118. DOI: 10.1007/s10346-005-0023-y. URL: http://link.springer.com/10.1007/s10346-005-0023-y (visited on 01/24/2020).

Baum, Rex L. and Jonathan W. Godt (Sept. 2010). "Early warning of rainfall-induced shallow landslides and debris flows in the USA". In: *Landslides* 7.3, pp. 259–272. ISSN: 1612-510X, 1612-5118. DOI: 10.1007/s10346-009-0177-0. URL: http://link.springer.com/10.1007/s10346-009-0177-0 (visited on 03/15/2021).

Baum, Rex L, William Z Savage, and Jonathan W Godt (2002). "TRIGRS—A Fortran Program for Transient Rainfall Infiltration and Grid-Based Regional Slope-Stability Analysis". In: p. 61. URL: https://citeseerx.ist.psu.edu/viewdoc/download?doi=10.1.1.593.6092&rep=rep1&type=pdf.

Beek, LUDOVICUS PETRUS HENRICUS van (2002). "Assessment of the influence of changes in land use and climate on landslide activity in a Mediterranean environment". PhD thesis. ISBN: 90-6809-329-0 (NGS). URL: https://core.ac.uk/download/pdf/39699985.pdf.

Benda, Lee and Thomas Dunne (Dec. 1997). "Stochastic forcing of sediment routing and storage in channel networks". In: *Water Resources Research* 33.12, pp. 2865–2880. ISSN: 00431397. DOI: 10.1029/97WR02387. URL: http://doi.wiley.com/10.1029/97WR02387 (visited on 02/17/2021).

Beven, Keith and Peter Germann (Oct. 1982). "Macropores and water flow in soils". In: *Water Resources Research* 18.5, pp. 1311–1325. ISSN: 00431397. DOI: 10.1029/WR018i005p01311. URL: http://doi.wiley.com/10.1029/WR018i005p01311 (visited on 02/25/2022).

Bischetti, Gian Battista, Enrico A. Chiaradia, Tommaso Simonato, Barbara Speziali, Barbara Vitali, Paolo Vullo, and Antonio Zocco (Dec. 2005). "Root Strength and Root Area Ratio of Forest Species in Lombardy (Northern Italy)". In: *Plant and Soil* 278.1, pp. 11–22. ISSN: 0032-079X, 1573-5036. DOI: 10.1007/s11104-005-0605-4. URL: http://link.springer.com/10.1007/s11104-005-0605-4 (visited on 02/03/2019).

Bischetti, Gian Battista, Giovanni De Cesare, Slobodan B. Mickovski, Hans Peter Rauch, Massimiliano Schwarz, and Rosemarie Stangl (Nov. 2021). "Design and temporal issues in Soil Bioengineering structures for the stabilisation of shallow soil movements". In: *Ecological Engineering* 169, p. 106309. ISSN: 09258574. DOI: 10.1016/j.ecoleng.2021.106309. URL: https://linkinghub.elsevier.com/retrieve/pii/S0925857421001646 (visited on 11/08/2021).

Bishop, Alan W (1955). *The use of the slip circle in the stability analysis of slopes*. https://doi.org/10.1680/geot.1955.5.1.7.

Bogaard, Thom A. and Roberto Greco (May 2016). "Landslide hydrology: from hydrology to pore pressure". In: *WIREs Water* 3.3, pp. 439–459. ISSN: 2049-1948, 2049-1948. DOI: 10.1002/wat2.1126. URL: https://onlinelibrary.wiley.com/doi/abs/10.1002/wat2.1126 (visited on 05/05/2021).

Bordoni, M., C. Meisina, R. Valentino, M. Bittelli, and S. Chersich (May 21, 2015). "Site-specific to local-scale shallow landslides triggering zones assessment using TRIGRS". In: *Natural Hazards and Earth System Sciences* 15.5, pp. 1025–1050. ISSN: 1684-9981. DOI: 10.5194/nhess-15-1025-2015. URL: https://nhess.copernicus.org/articles/15/1025/2015/ (visited on 03/03/2022).

Bordoni, Massimiliano, M Giuseppina Persichillo, Claudia Meisina, Stefano Crema, Marco Cavalli, Carlotta Bartelletti, Yuri Galanti, Michele Barsanti, Roberto Giannecchini, and Giacomo D'Amato Avanzi (2018). "Estimation of the susceptibility of a road network to shallow landslides with the integration of the sediment connectivity". In: *Natural Hazards and Earth System Sciences* 18.6, pp. 1735–1758.

Borga, Marco, Giancarlo Dalla Fontana, and Federico Cazorzi (Nov. 2002). "Analysis of topographic and climatic control on rainfall-triggered shallow landsliding using a quasi-dynamic wetness index". In: *Journal of Hydrology* 268.1, pp. 56–71. ISSN: 00221694. DOI: 10.1016/S0022-1694(02)00118-X. URL: https://linkinghub.elsevier.com/retrieve/pii/S002216940200118X (visited on 05/12/2021).

Borga, Marco, Fabrizio Tonelli, and Jacopo Selleroni (Dec. 2004). "A physically based model of the effects of forest roads on slope stability: effects of forest roads on slope stability". In: *Water Resources Research* 40.12. ISSN: 00431397. DOI: 10.1029/2004WR003238. URL: http://doi.wiley.com/10.1029/2004WR003238 (visited on 03/12/2022).

Bourrier, Franck, François Kneib, Bruno Chareyre, and Thierry Fourcaud (Dec. 2013). "Discrete modeling of granular soils reinforcement by plant roots". In: *Ecological Engineering* 61, pp. 646–657. ISSN: 09258574. DOI: 10.1016/j.ecoleng.2013.05.002. URL: https://linkinghub.elsevier.com/retrieve/pii/S0925857413001936 (visited on 01/09/2022).

Breiman, Leo, Jerome Friedman, Charles J Stone, and Richard A Olshen (1984). *Classification and regression trees*. https://doi.org/10.1201/9781315139470.

Brenning, A. (Nov. 7, 2005). "Spatial prediction models for landslide hazards: review, comparison and evaluation". In: *Natural Hazards and Earth System Science* 5.6, pp. 853–862. ISSN: 1684-9981. DOI: 10.5194/nhess-5-853-2005. URL: http://www.nat-hazards-earth-syst-sci.net/5/853/2005/ (visited on 07/13/2020).

Burroughs, E R (Apr. 1985). "Landslide hazard rating for portions of the Oregon Coast Range". In: *Proceedings of Symposium Sponsored by Committee on Watershed Management, Irrigation Drainage Div., ASCE. Denver, CO: ASCE Convention, April 30–May 1*, pp. 132–139. URL: https://forest.moscowfsl.wsu.edu/engr/library/Burroughs/Burroughs1985a/1985a.html.

Burton, A. and J. C. Bathurst (Aug. 1998). "Physically based modelling of shallow landslide sediment yield at a catchment scale". In: *Environmental Geology* 35.2, pp. 89–99. ISSN: 0943-0105, 1432-0495. DOI: 10.1007/s002540050296. URL: http://link.springer.com/10.1007/s002540050296 (visited on 12/29/2019).

Camargo, Júlia, Raquel Quadros Velloso, and Euripedes A. Vargas (Dec. 2016). "Numerical limit analysis of three-dimensional slope stability problems in catchment areas". In: *Acta Geotechnica* 11.6, pp. 1369–1383. ISSN: 1861-1125, 1861-1133. DOI: 10.1007/s11440-016-0459-3. URL: http://link.springer.com/10.1007/s11440-016-0459-3 (visited on 05/14/2021).

Camarretta, Nicolò, Peter A. Harrison, Tanya Bailey, Brad Potts, Arko Lucieer, Neil Davidson, and Mark Hunt (July 2020). "Monitoring forest structure to guide adaptive management of forest restoration: a review of remote sensing approaches". In: *New Forests* 51.4, pp. 573–596. ISSN: 0169-4286, 1573-5095. DOI: 10.1007/s11056-019-09754-5. URL: http://link.springer.com/10.1007/s11056-019-09754-5 (visited on 02/24/2022).

Capparelli, Giovanna and Pasquale Versace (Mar. 2011). "FLaIR and SUSHI: two mathematical models for early warning of landslides induced by rainfall". In: *Landslides* 8.1, pp. 67–79. ISSN: 1612-510X, 1612-5118. DOI: 10.1007/s10346-010-0228-6. URL: http://link.springer.com/10.1007/s10346-010-0228-6 (visited on 01/06/2020).

Carrara, Alberto (June 1983). "Multivariate models for landslide hazard evaluation". In: *Journal of the International Association for Mathematical Geology* 15.3, pp. 403–426. ISSN: 0020-5958, 1573-8868. DOI: 10.1007/BF01031290. URL: http://link.springer.com/10.1007/BF01031290 (visited on 02/27/2022).

Casini, F, L Colombo, C Jommi, and Sarah M Springman (2009). "Large shear box for analysing strength mobilisation in unsaturated conditions". In: *Scientific Conference: From shear bands to rapid flow*. Institute for Geotechnical Engineering (IGT).

Chen, Chunshu, Yuanyou Xia, and Victor Mwango Bowa (Jan. 2017). "Slope stability analysis by polar slice method in rotational failure mechanism". In: *Computers and Geotechnics* 81, pp. 188–194. ISSN: 0266352X. DOI: 10.1016/j.compgeo.2016.08.016. URL: https://linkinghub.elsevier.com/retrieve/pii/S0266352X16301847 (visited on 11/05/2020).

Chen, Jian, Jian-Hua Yin, and C F Lee (2003). "Upper bound limit analysis of slope stability using rigid finite elements and nonlinear programming". In: p. 13. DOI: https://doi.org/10.1139/t03-032.

Chen, Wai-Fah (2007). *Limit analysis and soil plasticity*. J. Ross publishing.

Chen, Zu-Yu and Chang-Ming Shao (1988). "Evaluation of minimum factor of safety in slope stability analysis". In: 25, p. 17. DOI: https://doi.org/10.1139/t88-084. URL: http://www.geoeng.iwhr.com/ytgcyjs/rootfiles/2015/10/28/1445241321868136-1445565535447269.pdf.

Chirico, Giovanni B., Marco Borga, Paolo Tarolli, Riccardo Rigon, and Federico Preti (2013). "Role of Vegetation on Slope Stability under Transient Unsaturated Conditions". In: *Procedia Environmental Sciences* 19, pp. 932–941. ISSN: 18780296. DOI: 10.1016/j.proenv.2013.06.103. URL: https://linkinghub.elsevier.com/retrieve/pii/S1878029613003733 (visited on 03/15/2022).

Ciervo, F., G. Rianna, P. Mercogliano, and M. N. Papa (June 2017). "Effects of climate change on shallow landslides in a small coastal catchment in southern Italy". In: *Landslides* 14.3, pp. 1043–1055. ISSN: 1612-510X, 1612-5118. DOI: 10.1007/s10346-016-0743-1. URL: http://link.springer.com/10.1007/s10346-016-0743-1 (visited on 01/17/2021).

Cislaghi, Alessio, Enrico Antonio Chiaradia, and Gian Battista Bischetti (Sept. 30, 2017). "Including root reinforcement variability in a probabilistic 3D stability model: Root reinforcement variability in a probabilistic 3-D stability model". In: *Earth Surface Processes and Landforms* 42.12, pp. 1789–1806. ISSN: 01979337. DOI: 10.1002/esp.4127. URL: http://doi.wiley.com/10.1002/esp.4127 (visited on 07/28/2020).

Cislaghi, Alessio, Denis Cohen, Eric Gasser, Gian Battista Bischetti, and Massimiliano Schwarz (Mar. 2019). "Field Measurements of Passive Earth Forces in Steep, Shallow, Landslide-Prone Areas". In: *Journal of Geophysical Research: Earth Surface* 124.3, pp. 838–866. ISSN: 2169-9003, 2169-9011. DOI: 10.1029/2017JF004557. URL: https://onlinelibrary.wiley.com/doi/abs/10.1029/2017JF004557 (visited on 01/17/2021).

Cohen, D., P. Lehmann, and D. Or (2009). "Fiber Bundle Model for Multiscale Modeling of Hydromechanical Triggering of Shallow Landslides". In: *Water Resources Research* 45.10. ISSN: 1944-7973. DOI: 10.1029/2009WR007889.

Cohen, D., M. Schwarz, and D. Or (Aug. 2011). "An Analytical Fiber Bundle Model for Pullout Mechanics of Root Bundles". In: *Journal of Geophysical Research* 116 (F3). ISSN: 0148-0227. DOI: 10.1029/2010JF001886.

Cohen, Denis and Massimiliano Schwarz (Aug. 17, 2017). "Tree-root control of shallow landslides". In: *Earth Surface Dynamics* 5.3, pp. 451–477. ISSN: 2196-632X. DOI: 10.5194/esurf-5-451-2017. URL: https://esurf.copernicus.org/articles/5/451/2017/ (visited on 05/16/2021).

Conte, Enrico, Luigi Pugliese, and Antonello Troncone (Nov. 2020). "Post-failure analysis of the Maierato landslide using the material point method". In: *Engineering Geology* 277, p. 105788. ISSN: 00137952. DOI: 10.1016/j.enggeo.2020.105788. URL: https://linkinghub.elsevier.com/retrieve/pii/S0013795220304518 (visited on 05/26/2021).

Crozier, Michael J (2010). "Deciphering the effect of climate change on landslide activity: A review". In: *Geomorphology* 124.3-4, pp. 260–267. DOI: 10.1016/j.geomorph.2010.04.009.

Cundall, P. A. and O. D. L. Strack (Mar. 1979). "A discrete numerical model for granular assemblies". In: *Géotechnique* 29.1, pp. 47–65. ISSN: 0016-8505, 1751-7656. DOI: 10.1680/geot.1979.29.1.47. URL: http://www.icevirtuallibrary.com/doi/10.1680/geot.1979.29.1.47 (visited on 02/10/2020).

Dazio, Emanuele (Plinio Rinaldo), Marco Conedera, and Massimiliano Schwarz (May 2018). "Impact of different chestnut coppice managements on root reinforcement and shallow landslide susceptibility". In: *Forest Ecology and Management* 417, pp. 63–

76. ISSN: 03781127. DOI: 10.1016/j.foreco.2018.02.031. URL: https://linkinghub.elsevier.com/retrieve/pii/S0378112717320996 (visited on 09/09/2021).

Docker, B.B. and T.C.T. Hubble (Aug. 2008). "Quantifying Root-Reinforcement of River Bank Soils by Four Australian Tree Species". In: *Geomorphology* 100.3, pp. 401–418. ISSN: 0169555X. DOI: 10.1016/j.geomorph.2008.01.009.

D'Odorico, Paolo and Sergio Fagherazzi (Sept. 2003). "A probabilistic model of rainfall-triggered shallow landslides in hollows: A long-term analysis". In: *Water Resources Research* 39.9. ISSN: 00431397. DOI: 10.1029/2002WR001595. URL: http://doi.wiley.com/10.1029/2002WR001595 (visited on 01/17/2021).

Dorren, L (2014). "FINT—Find Individual Trees User Manual". In: *EcorisQ: Genève, Switzerland*.

Dorren, Luuk and Massimiliano Schwarz (2016). "Quantifying the stabilizing effect of forests on shallow landslide-prone slopes". In: *Ecosystem-Based Disaster Risk Reduction and Adaptation in Practice*. Springer, pp. 255–270. URL: https://www.researchgate.net/profile/Karen_Sudmeier-Rieux/publication/311487489_Ecosystem-BasedDisasterRiskReduction/links/5848994408aeda696825e888/Ecosystem-Based-Disaster-Risk-Reduction.pdf#page=272.

Drucker, D. C. and W. Prager (1952). "Soil mechanics and plastic analysis or limit design". In: *Quarterly of Applied Mathematics* 10.2, pp. 157–165. ISSN: 0033-569X, 1552-4485. DOI: 10.1090/qam/48291. URL: https://www.ams.org/qam/1952-10-02/S0033-569X-1952-48291-2/ (visited on 02/27/2022).

Duncan, James Michael (July 1996). "State of the Art: Limit Equilibrium and Finite-Element Analysis of Slopes". In: *Journal of Geotechnical Engineering* 122.7, pp. 577–596. ISSN: 0733-9410, 1944-8368. DOI: 10.1061/(ASCE)0733-9410(1996)122:7(577).

Dunne, T (1991). "Stochastic aspects of the relations between climate, hydrology and landform evolution". In: *Transactions of Japanese Geomorphological Union* 12, pp. 1–24. ISSN: 0389-1755. URL: http://jgu.jp/en/publication.html.

Dupuy, L., T. Fourcaud, and A. Stokes (June 2005). "A numerical investigation into factors affecting the anchorage of roots in tension". In: *European Journal of Soil Science* 56.3, pp. 319–327. ISSN: 1351-0754, 1365-2389. DOI: 10.1111/j.1365-2389.2004.00666.x. URL: https://onlinelibrary.wiley.com/doi/10.1111/j.1365-2389.2004.00666.x (visited on 03/01/2022).

Dupuy, Lionel X, Thierry Fourcaud, Patrick Lac, and Alexia Stokes (2007). "A generic 3D finite element model of tree anchorage integrating soil mechanics and real root system architecture". In: *American Journal of Botany* 94.9, pp. 1506–1514.

D'Ambrosio, D., S. Di Gregorio, and G. Iovine (Dec. 31, 2003). "Simulating debris flows through a hexagonal cellular automata model: SCIDDICA S_{3-hex}". In: *Natural Hazards and Earth System Sciences* 3.6, pp. 545–559. ISSN: 1684-9981. DOI: 10.5194/nhess-3-545-2003. URL: https://nhess.copernicus.org/articles/3/545/2003/ (visited on 11/20/2020).

Ekanayake, Jagath C., Michael Marden, Alex J. Watson, and Donna Rowan (1997). *Tree roots and slope stability: a comparison between Pinus radiata and*.

Ekanayake, Jagath C and Christopher J Phillips (1999). "A method for stability analysis of vegetated hillslopes: an energy approach". In: 36, p. 13.

Ewen, John, Geoff Parkin, and Patrick Enda O'Connell (2000). "SHETRAN: distributed river basin flow and transport modeling system". In: *Journal of hydrologic engineering* 5.3, pp. 250–258. DOI: 10.1061/(ASCE)1084-0699(2000)5:3(250).

Fairfield, John and Pierre Leymarie (1991). "Drainage networks from grid digital elevation models". In: *Water resources research* 27.5, pp. 709–717.

Falaschi, F., F. Giacomelli, P. R. Federici, A. Puccinelli, G. D'Amato Avanzi, A. Pochini, and A. Ribolini (Sept. 2009). "Logistic regression versus artificial neural networks: landslide susceptibility evaluation in a sample area of the Serchio River valley, Italy". In: *Natural Hazards* 50.3, pp. 551–569. ISSN: 0921-030X, 1573-0840. DOI: 10.1007/s11069-009-9356-5. URL: http://link.springer.com/10.1007/s11069-009-9356-5 (visited on 07/13/2020).

Fannin, RJ, A Eliadorani, and JMT Wilkinson (2005). "Shear strength of cohesionless soils at low stress". In: *Géotechnique* 55.6, pp. 467–478.

Felicísimo, Ángel M., Aurora Cuartero, Juan Remondo, and Elia Quirós (Apr. 2013). "Mapping landslide susceptibility with logistic regression, multiple adaptive regression splines, classification and regression trees, and maximum entropy methods: a comparative study". In: *Landslides* 10.2, pp. 175–189. ISSN: 1612-510X, 1612-5118. DOI: 10.1007/s10346-012-0320-1. URL: http://link.springer.com/10.1007/s10346-012-0320-1 (visited on 01/20/2021).

Fischer, C, J López, and SM Springman (2003). "Remediation of an eroded steep slope in weathered sandstone after a major rainstorm". In: *International conference on landslides, Hong Kong*. Vol. 8. 10.

Fourcaud, Thierry, Jin-Nan Ji, Zhi-Qiang Zhang, and Alexia Stokes (2008). "Understanding the impact of root morphology on overturning mechanisms: a modelling approach". In: *Annals of Botany* 101.8, pp. 1267–1280.

Freeman, T Graham (1991). "Calculating catchment area with divergent flow based on a regular grid". In: *Computers & geosciences* 17.3, pp. 413–422.

Frydman, S and V Operstein (2001). "Numerical simulation of direct shear of root-reinforced soil". In: *Proceedings of the Institution of Civil Engineers-Ground Improvement* 5.1, pp. 41–48.

Fujimaki, Reiji, Ryunosuke Tateno, and Naoko Tokuchi (Apr. 2007). "Root development across a chronosequence in a Japanese cedar (*Cryptomeria japonica* D. Don) plantation". In: *Journal of Forest Research* 12.2, pp. 96–102. ISSN: 1341-6979, 1610-7403. DOI: 10.1007/s10310-006-0256-1. URL: https://www.tandfonline.com/doi/full/10.1007/s10310-006-0256-1 (visited on 04/20/2020).

Gambazzi, F and B Suski (2009). "Electrical Resistivity Tomography Rüdlingen". In: *Internernal Tramm meeting. ETH Zurich, Switzerland*.

Gariano, S.L., G. Rianna, O. Petrucci, and F. Guzzetti (Oct. 2017). "Assessing future changes in the occurrence of rainfall-induced landslides at a regional scale". In: *Science of The Total Environment* 596-597, pp. 417–426. ISSN: 00489697. DOI: 10.1016/j.scitotenv.2017.03.103. URL: https://linkinghub.elsevier.com/retrieve/pii/S0048969717306150 (visited on 04/10/2020).

Gehring, Eric, Marco Conedera, Janet Maringer, Filippo Giadrossich, Enrico Guastini, and Massimiliano Schwarz (Dec. 2019). "Shallow landslide disposition in burnt European beech (Fagus sylvatica L.) forests". In: *Scientific Reports* 9.1, p. 8638. ISSN: 2045-2322. DOI: 10.1038/s41598-019-45073-7. URL: http://www.nature.com/articles/s41598-019-45073-7 (visited on 06/10/2022).

Genet, Marie, Nomessi Kokutse, Alexia Stokes, Thierry Fourcaud, Xiaohu Cai, Jinnan Ji, and Slobodan Mickovski (Oct. 2008). "Root reinforcement in plantations of Cryptomeria japonica D. Don: effect of tree age and stand structure on slope stability". In: *Forest Ecology and Management* 256.8, pp. 1517–1526. ISSN: 03781127. DOI: 10.1016/j.foreco.2008.05.050. URL: https://linkinghub.elsevier.com/retrieve/pii/S037811270800457X (visited on 06/29/2022).

Genet, Marie, Alexia Stokes, Thierry Fourcaud, Xiaohu Cai, and Yuanchang Lu (2006). *Disaster Mitigation of Debris Flows, Slope Failures and Landslides 535 Soil Fixation by Tree Roots: Changes in Root Reinforcement Parameters with*.

Genet, Marie, Alexia Stokes, Thierry Fourcaud, and Joanne E. Norris (Mar. 2010). "The influence of plant diversity on slope stability in a moist evergreen deciduous forest". In: *Ecological Engineering* 36.3, pp. 265–275. ISSN: 09258574. DOI: 10.1016/j.ecoleng.2009.05.018. URL: https://linkinghub.elsevier.com/retrieve/pii/S0925857409001591 (visited on 12/15/2019).

Ghestem, Murielle, Roy C. Sidle, and Alexia Stokes (Nov. 2011). "The Influence of Plant Root Systems on Subsurface Flow: Implications for Slope Stability". In: *BioScience* 61.11, pp. 869–879. ISSN: 1525-3244, 0006-3568. DOI: 10.1525/bio.2011.61.11.6. URL: https://academic.oup.com/bioscience/article-lookup/doi/10.1525/bio.2011.61.11.6 (visited on 05/14/2021).

Giadrossich, F, F Preti, E Guastini, and P Vannocci (2010). "Metodologie sperimentali per l'esecuzione di prove di taglio diretto su terre rinforzate con radici (Experimental methodologies for the direct shear tests on soils reinforced by roots)". In: *Geologia tecnica & ambientale* 4, pp. 5–12.

Giadrossich, F., M. Schwarz, D. Cohen, A. Cislaghi, C. Vergani, T. Hubble, C. Phillips, and A. Stokes (Dec. 1, 2017). "Methods to measure the mechanical behaviour of tree roots: A review". In: *Ecological Engineering*. Soil Bio- and Eco-Engineering: The Use of Vegetation to Improve Slope Stability - Proceedings of the Fourth International Conference 109, pp. 256–271. ISSN: 0925-8574. DOI: 10.1016/j.ecoleng.2017.08.032. URL: http://www.sciencedirect.com/science/article/pii/S0925857417305025 (visited on 01/31/2019).

Giadrossich, F., M. Schwarz, D. Cohen, F. Preti, and D. Or (June 2013). "Mechanical interactions between neighbouring roots during pullout tests". In: *Plant and Soil*

367.1, pp. 391–406. ISSN: 0032-079X, 1573-5036. DOI: 10.1007/s11104-012-1475-1. URL: http://link.springer.com/10.1007/s11104-012-1475-1 (visited on 11/11/2019).

Giadrossich, Filippo, Denis Cohen, Massimiliano Schwarz, Antonio Ganga, Roberto Marrosu, Mario Pirastru, and Gian Franco Capra (2019). "Large roots dominate the contribution of trees to slope stability". In: *Earth Surface Processes and Landforms* 44.8, pp. 1602–1609. ISSN: 1096-9837. DOI: 10.1002/esp.4597. URL: https://onlinelibrary.wiley.com/doi/abs/10.1002/esp.4597 (visited on 05/21/2020).

Giadrossich, Filippo, Massimiliano Schwarz, Michael Marden, Roberto Marrosu, and Chris Phillips (Aug. 11, 2020). "Minimum representative root distribution sampling for calculating slope stability in Pinus radiata D.Don plantations in New Zealand". In: *New Zealand Journal of Forestry Science* 50. ISSN: 1179-5395. DOI: 10.33494/nzjfs502020x68x. URL: http://nzjforestryscience.nz/index.php/nzjfs/article/view/68 (visited on 05/16/2021).

Glade, Thomas (Apr. 2003). "Landslide occurrence as a response to land use change: a review of evidence from New Zealand". In: *CATENA* 51.3, pp. 297–314. ISSN: 03418162. DOI: 10.1016/S0341-8162(02)00170-4. URL: https://linkinghub.elsevier.com/retrieve/pii/S0341816202001704 (visited on 03/14/2022).

Godt, J.W., R.L. Baum, W.Z. Savage, D. Salciarini, W.H. Schulz, and E.L. Harp (Dec. 2008). "Transient deterministic shallow landslide modeling: Requirements for susceptibility and hazard assessments in a GIS framework". In: *Engineering Geology* 102.3, pp. 214–226. ISSN: 00137952. DOI: 10.1016/j.enggeo.2008.03.019. URL: https://linkinghub.elsevier.com/retrieve/pii/S0013795208001853 (visited on 04/28/2019).

Gray, Donald H (1974). "Reinforcement and stabilization of soil by vegetation". In: *Journal of the Geotechnical Engineering Division* 100.6, pp. 695–699.

Gray, Donald H and Harukazu Ohashi (1983). "Mechanics of fiber reinforcement in sand". In: *Journal of geotechnical engineering* 109.3, pp. 335–353.

Greenwood, John R. (June 2006). "SLIP4EX – A Program for Routine Slope Stability Analysis to Include the Effects of Vegetation, Reinforcement and Hydrological Changes". In: *Geotechnical and Geological Engineering* 24.3, pp. 449–465. ISSN: 0960-3182, 1573-1529. DOI: 10.1007/s10706-005-4156-5. URL: http://link.springer.com/10.1007/s10706-005-4156-5 (visited on 05/30/2021).

Griffiths, D.V., Jinsong Huang, and Gordon A. Fenton (June 2011). "Probabilistic infinite slope analysis". In: *Computers and Geotechnics* 38.4, pp. 577–584. ISSN: 0266352X. DOI: 10.1016/j.compgeo.2011.03.006. URL: https://linkinghub.elsevier.com/retrieve/pii/S0266352X11000474 (visited on 02/11/2020).

Guzzetti, F., M. Cardinali, P. Reichenbach, and A. Carrara (Mar. 30, 2000). "Comparing Landslide Maps: A Case Study in the Upper Tiber River Basin, Central Italy". In: *Environmental Management* 25.3, pp. 247–263. ISSN: 0364-152X, 1432-1009. DOI: 10.1007/s002679910020. URL: http://link.springer.com/10.1007/s002679910020 (visited on 07/13/2020).

Guzzetti, Fausto, Silvia Peruccacci, Mauro Rossi, and Colin P. Stark (Feb. 2008). "The rainfall intensity–duration control of shallow landslides and debris flows: an update". In: *Landslides* 5.1, pp. 3–17. ISSN: 1612-510X, 1612-5118. DOI: 10.1007/s10346-007-0112-1. URL: http://link.springer.com/10.1007/s10346-007-0112-1 (visited on 05/12/2020).

Hammond, Carol (1992). *Level I stability analysis (LISA) documentation for version 2.0*. Vol. 285. US Department of Agriculture, Forest Service, Intermountain Research Station.

Hergarten, S. (2003). "Landslides, sandpiles, and self-organized criticality". In: *Natural Hazards and Earth System Science* 3.6, pp. 505–514. ISSN: 1684-9981. DOI: 10.5194/nhess-3-505-2003. URL: http://www.nat-hazards-earth-syst-sci.net/3/505/2003/ (visited on 07/09/2020).

Hergarten, Stefan (2013). "SOC in landslides". In: *Self-Organized Criticality Systems*, pp. 379–401.

Hergarten, Stefan and Horst J. Neugebauer (1998). "Self-Organized Criticality in a Landslide Model". In: *Geophysical Research Letters* 25.6, pp. 801–804. ISSN: 1944-8007. DOI: 10.1029/98GL50419.

Hosmer, David W and Stanley Lemeshow (2000). "Applied Logistic Regression, John Wiley & Sons". In: *New York*.

Hubble, TCT, BB Docker, and ID Rutherfurd (2010). "The role of riparian trees in maintaining riverbank stability: a review of Australian experience and practice". In: *Ecological Engineering* 36.3, pp. 292–304. DOI: https://doi.org/10.1016/j.ecoleng.2009.04.006.

Istanbulluoglu, Erkan (2005). "Vegetation-modulated landscape evolution: Effects of vegetation on landscape processes, drainage density, and topography". In: *Journal of Geophysical Research* 110 (F2). ISSN: 0148-0227. DOI: 10.1029/2004JF000249. URL: http://doi.wiley.com/10.1029/2004JF000249 (visited on 02/03/2019).

Ji, Jinnan, Zhun Mao, Wenbin Qu, and Zhiqiang Zhang (2020). "Energy-based fibre bundle model algorithms to predict soil reinforcement by roots". In: *Plant and Soil* 446.1, pp. 307–329. ISSN: 0032-079X, 1573-5036. DOI: 10.1007/s11104-019-04327-z. URL: http://link.springer.com/10.1007/s11104-019-04327-z (visited on 03/16/2020).

Jones, Haydon, Peter Clough, Barbara Hock, and Chris Phillips (2008). "Economic costs of hill country erosion and benefits of mitigation in New Zealand: Review and recommendation of approach". In: *SCION, December*.

Kim, Junghwan, Kwangwoo Lee, Sangseom Jeong, and Gwangseob Kim (Nov. 2014). "GIS-based prediction method of landslide susceptibility using a rainfall infiltration-groundwater flow model". In: *Engineering Geology* 182, pp. 63–78. ISSN: 00137952. DOI: 10.1016/j.enggeo.2014.09.001. URL: https://linkinghub.elsevier.com/retrieve/pii/S0013795214002348 (visited on 05/12/2020).

Kirkby, MJ and Darrell Weyman (1972). *Measurements of contributing area in very small drainage basins*. Department of Geography, University of Bristol.

Kokutse, Nomessi, Thierry Fourcaud, Kouami Kokou, Kouma Neglo, and P Lac (2006). "3D Numerical Modelling and Analysis of the Influence of Forest Structure on Hill Slopes Stability". In: p. 7.

Koopialipoor, Mohammadreza, Danial Jahed Armaghani, Ahmadreza Hedayat, Aminaton Marto, and Behrouz Gordan (July 2019). "Applying various hybrid intelligent systems to evaluate and predict slope stability under static and dynamic conditions". In: *Soft Computing* 23.14, pp. 5913–5929. ISSN: 1432-7643, 1433-7479. DOI: 10.1007/s00500-018-3253-3. URL: http://link.springer.com/10.1007/s00500-018-3253-3 (visited on 01/07/2020).

Kramer, Steven Lawrence (1996). *Geotechnical earthquake engineering*. Pearson Education India.

Lanni, C., J. J. McDonnell, and R. Rigon (Dec. 15, 2011). "On the relative role of upslope and downslope topography for describing water flow path and storage dynamics: a theoretical analysis". In: *Hydrological Processes* 25.25, pp. 3909–3923. ISSN: 08856087. DOI: 10.1002/hyp.8263. URL: http://doi.wiley.com/10.1002/hyp.8263 (visited on 05/10/2021).

Lehmann, Peter, Francesca Gambazzi, Barbara Suski, Ludovic Baron, Amin Askarinejad, Sarah M. Springman, Klaus Holliger, and Dani Or (Dec. 2013). "Evolution of soil wetting patterns preceding a hydrologically induced landslide inferred from electrical resistivity survey and point measurements of volumetric water content and pore water pressure: EVOLUTION OF WETTING PATTERNS PRECEDING A RAPID LANDSLIDE". In: *Water Resources Research* 49.12, pp. 7992–8004. ISSN: 00431397. DOI: 10.1002/2013WR014560. URL: http://doi.wiley.com/10.1002/2013WR014560 (visited on 02/03/2019).

Lepore, C., E. Arnone, L. V. Noto, G. Sivandran, and R. L. Bras (Sept. 3, 2013). "Physically based modeling of rainfall-triggered landslides: a case study in the Luquillo forest, Puerto Rico". In: *Hydrology and Earth System Sciences* 17.9, pp. 3371–3387. ISSN: 1607-7938. DOI: 10.5194/hess-17-3371-2013. URL: https://hess.copernicus.org/articles/17/3371/2013/ (visited on 09/29/2021).

Leshchinsky, Ben and Spencer Ambauen (Oct. 2015). "Limit Equilibrium and Limit Analysis: Comparison of Benchmark Slope Stability Problems". In: *Journal of Geotechnical and Geoenvironmental Engineering* 141.10, p. 04015043. ISSN: 1090-0241, 1943-5606. DOI: 10.1061/(ASCE)GT.1943-5606.0001347. URL: http://ascelibrary.org/doi/10.1061/%28ASCE%29GT.1943-5606.0001347 (visited on 02/27/2022).

Liang, Wei-Li, Ken'ichirou Kosugi, and Takahisa Mizuyama (Nov. 2007). "Heterogeneous Soil Water Dynamics around a Tree Growing on a Steep Hillslope". In: *Vadose Zone Journal* 6.4, pp. 879–889. ISSN: 15391663. DOI: 10.2136/vzj2007.0029. URL: http://doi.wiley.com/10.2136/vzj2007.0029 (visited on 01/17/2021).

Likos, William J., Ning Lu, and Jonathan W. Godt (Apr. 2014). "Hysteresis and Uncertainty in Soil Water-Retention Curve Parameters". In: *Journal of Geotechnical and Geoenvironmental Engineering* 140.4, p. 04013050. ISSN: 1090-0241, 1943-5606.

DOI: 10.1061/(ASCE)GT.1943-5606.0001071. URL: https://ascelibrary.org/doi/10.1061/%28ASCE%29GT.1943-5606.0001071 (visited on 07/04/2022).

Lin, Der-Guey, Bor-Shun Huang, and Shin-Hwei Lin (Aug. 2010). "3-D numerical investigations into the shear strength of the soil–root system of Makino bamboo and its effect on slope stability". In: *Ecological Engineering* 36.8, pp. 992–1006. ISSN: 09258574. DOI: 10.1016/j.ecoleng.2010.04.005. URL: https://linkinghub.elsevier.com/retrieve/pii/S0925857410000765 (visited on 12/15/2019).

Liu, Y.H., Z.Z. Cen, and B.Y. Xu (June 1995). "A numerical method for plastic limit analysis of 3-D structures". In: *International Journal of Solids and Structures* 32.12, pp. 1645–1658. ISSN: 00207683. DOI: 10.1016/0020-7683(94)00230-T. URL: https://linkinghub.elsevier.com/retrieve/pii/002076839400230T (visited on 05/16/2021).

Liucci, Luisa, Laura Melelli, Cristian Suteanu, and Francesco Ponziani (Aug. 2017). "The role of topography in the scaling distribution of landslide areas: A cellular automata modeling approach". In: *Geomorphology* 290, pp. 236–249. ISSN: 0169555X. DOI: 10.1016/j.geomorph.2017.04.017. URL: https://linkinghub.elsevier.com/retrieve/pii/S0169555X17301642 (visited on 05/16/2021).

Loades, K.W., A.G. Bengough, M.F. Bransby, and P.D. Hallett (Mar. 2010). "Planting density influence on fibrous root reinforcement of soils". In: *Ecological Engineering* 36.3, pp. 276–284. ISSN: 09258574. DOI: 10.1016/j.ecoleng.2009.02.005. URL: https://linkinghub.elsevier.com/retrieve/pii/S0925857409001050 (visited on 01/29/2019).

Lu, Ning and Jonathan Godt (Nov. 2008). "Infinite Slope Stability under Steady Unsaturated Seepage Conditions: INFINITE SLOPE STABILITY". In: *Water Resources Research* 44.11. ISSN: 00431397. DOI: 10.1029/2008WR006976.

Lu, Ning, Jonathan W. Godt, and David T. Wu (2010). "A closed-form equation for effective stress in unsaturated soil". In: *Water Resources Research* 46.5. ISSN: 1944-7973. DOI: 10.1029/2009WR008646. URL: https://agupubs.onlinelibrary.wiley.com/doi/abs/10.1029/2009WR008646 (visited on 02/03/2019).

Malamud, Bruce D., Donald L. Turcotte, Fausto Guzzetti, and Paola Reichenbach (June 2004). "Landslide inventories and their statistical properties". In: *Earth Surface Processes and Landforms* 29.6, pp. 687–711. ISSN: 0197-9337, 1096-9837. DOI: 10.1002/esp.1064. URL: http://doi.wiley.com/10.1002/esp.1064 (visited on 07/13/2020).

Mao, Zhun, Franck Bourrier, Alexia Stokes, and Thierry Fourcaud (Feb. 2014a). "Three-dimensional modelling of slope stability in heterogeneous montane forest ecosystems". In: *Ecological Modelling* 273, pp. 11–22. ISSN: 03043800. DOI: 10.1016/j.ecolmodel.2013.10.017. URL: https://linkinghub.elsevier.com/retrieve/pii/S0304380013004845 (visited on 12/26/2021).

Mao, Zhun, Ming Yang, Franck Bourrier, and Thierry Fourcaud (Aug. 2014b). "Evaluation of root reinforcement models using numerical modelling approaches".

In: *Plant and Soil* 381.1, pp. 249–270. ISSN: 0032-079X, 1573-5036. DOI: 10.1007/s11104-014-2116-7. URL: http://link.springer.com/10.1007/s11104-014-2116-7 (visited on 01/06/2022).

Mauri, Luca, Eugenio Straffelini, and Paolo Tarolli (2022). "Multi-temporal modeling of road-induced overland flow alterations in a terraced landscape characterized by shallow landslides". In: *International Soil and Water Conservation Research* 10.2, pp. 240–253.

McColl, Samuel T. (2015). "Landslide Causes and Triggers". In: *Landslide Hazards, Risks and Disasters*. Elsevier, pp. 17–42. ISBN: 978-0-12-396452-6. DOI: 10.1016/B978-0-12-396452-6.00002-1. URL: https://linkinghub.elsevier.com/retrieve/pii/B9780123964526000021 (visited on 06/05/2020).

Michalowski, Radoslaw L and Aigen Zhao (1996). "Failure of fiber-reinforced granular soils". In: *Journal of geotechnical engineering* 122.3, pp. 226–234.

Mickovski, S. B., A. G. Bengough, M. F. Bransby, M. C. R. Davies, P. D. Hallett, and R. Sonnenberg (2007). "Material stiffness, branching pattern and soil matric potential affect the pullout resistance of model root systems". In: *European Journal of Soil Science* 58.6, pp. 1471–1481. ISSN: 1365-2389. DOI: 10.1111/j.1365-2389.2007.00953.x. URL: https://onlinelibrary.wiley.com/doi/abs/10.1111/j.1365-2389.2007.00953.x (visited on 12/16/2019).

Mickovski, Slobodan B. (May 9, 2021). "Sustainable Geotechnics—Theory, Practice, and Applications". In: *Sustainability* 13.9, p. 5286. ISSN: 2071-1050. DOI: 10.3390/su13095286. URL: https://www.mdpi.com/2071-1050/13/9/5286 (visited on 05/16/2021).

Mickovski, Slobodan B., Alexia Stokes, Rens van Beek, Murielle Ghestem, and Thierry Fourcaud (Oct. 2011). "Simulation of direct shear tests on rooted and non-rooted soil using finite element analysis". In: *Ecological Engineering* 37.10, pp. 1523–1532. ISSN: 09258574. DOI: 10.1016/j.ecoleng.2011.06.001. URL: https://linkinghub.elsevier.com/retrieve/pii/S0925857411001790 (visited on 01/09/2022).

Milledge, D. G., D. V. Griffiths, S. N. Lane, and J. Warburton (2012). "Limits on the validity of infinite length assumptions for modelling shallow landslides". In: *Earth Surface Processes and Landforms* 37.11, pp. 1158–1166. ISSN: 1096-9837. DOI: 10.1002/esp.3235. URL: https://onlinelibrary.wiley.com/doi/abs/10.1002/esp.3235 (visited on 12/13/2021).

Milledge, David G., Dino Bellugi, Jim A. McKean, Alexander L. Densmore, and William E. Dietrich (Nov. 2014). "A multidimensional stability model for predicting shallow landslide size and shape across landscapes: predicting landslide size and shape". In: *Journal of Geophysical Research: Earth Surface* 119.11, pp. 2481–2504. ISSN: 21699003. DOI: 10.1002/2014JF003135. URL: http://doi.wiley.com/10.1002/2014JF003135 (visited on 04/17/2019).

Montgomery, David R and John M Buffington (1997). "Channel-reach morphology in mountain drainage basins". In: *Geological Society of America Bulletin* 109.5, pp. 596–

611. URL: https://doi.org/10.1130/0016-7606(1997)109<0596:CRMIMD>2.3.CO;2.

Montgomery, David R. and William E. Dietrich (Apr. 1994). "A physically based model for the topographic control on shallow landsliding". In: *Water Resources Research* 30.4, pp. 1153–1171. ISSN: 00431397. DOI: 10.1029/93WR02979. URL: http://doi.wiley.com/10.1029/93WR02979 (visited on 05/11/2021).

Montgomery, David R., William E. Dietrich, and John T. Heffner (Dec. 2002). "Piezometric response in shallow bedrock at CB1: Implications for runoff generation and landsliding". In: *Water Resources Research* 38.12, pp. 10–1–10–18. ISSN: 00431397. DOI: 10.1029/2002WR001429. URL: http://doi.wiley.com/10.1029/2002WR001429 (visited on 09/24/2020).

Montgomery, David R., Kevin M. Schmidt, William E. Dietrich, and Jim McKean (Mar. 2009). "Instrumental record of debris flow initiation during natural rainfall: Implications for modeling slope stability". In: *Journal of Geophysical Research: Earth Surface* 114 (F1). ISSN: 2156-2202. DOI: 10.1029/2008JF001078. URL: https://agupubs.onlinelibrary.wiley.com/doi/abs/10.1029/2008JF001078 (visited on 04/28/2019).

Montgomery, David R, Kevin M Schmidt, Harvey M Greenberg, and William E Dietrich (2000). "Forest clearing and regional landsliding". In: p. 4. URL: https://people.wou.edu/~taylors/g473/AEG2016/8_montgomery_etal_2000_forestry_landsliding.pdf.

Montrasio, L. and R. Valentino (Oct. 21, 2008). "A model for triggering mechanisms of shallow landslides". In: *Natural Hazards and Earth System Sciences* 8.5, pp. 1149–1159. ISSN: 1684-9981. DOI: 10.5194/nhess-8-1149-2008. URL: https://nhess.copernicus.org/articles/8/1149/2008/ (visited on 03/03/2022).

Montrasio, L., R. Valentino, and G. L. Losi (July 2011). "Towards a real-time susceptibility assessment of rainfall-induced shallow landslides on a regional scale". In: *Natural Hazards and Earth System Science* 11.7, pp. 1927–1947. ISSN: 1684-9981. DOI: 10.5194/nhess-11-1927-2011. URL: http://www.nat-hazards-earth-syst-sci.net/11/1927/2011/ (visited on 02/04/2020).

Moos, Christine, Peter Bebi, Frank Graf, Josias Mattli, Christian Rickli, and Massimiliano Schwarz (2016). "How Does Forest Structure Affect Root Reinforcement and Susceptibility to Shallow Landslides?" In: *Earth Surface Processes and Landforms* 41.7, pp. 951–960. ISSN: 1096-9837. DOI: 10.1002/esp.3887.

Moos, Christine, Peter Bebi, Massimiliano Schwarz, Markus Stoffel, Karen Sudmeier-Rieux, and Luuk Dorren (Feb. 2018). "Ecosystem-based disaster risk reduction in mountains". In: *Earth-Science Reviews* 177, pp. 497–513. ISSN: 00128252. DOI: 10.1016/j.earscirev.2017.12.011. URL: https://linkinghub.elsevier.com/retrieve/pii/S0012825217303446 (visited on 05/26/2020).

Morgenstern, NR u and V Eo Price (1965). "The analysis of the stability of general slip surfaces". In: *Geotechnique* 15.1, pp. 79–93.

Morrison, IM and JR Greenwood (1989). "Assumptions in simplified slope stability analysis by the method of slices". In: *Geotechnique* 39.3, pp. 503–509. DOI: https://doi.org/10.1680/geot.1989.39.3.503.

Munjiza, A., D.R.J. Owen, and N. Bicanic (Feb. 1995). "A combined finite-discrete element method in transient dynamics of fracturing solids". In: *Engineering Computations* 12.2, pp. 145–174. ISSN: 0264-4401. DOI: 10.1108/02644409510799532. URL: https://www.emerald.com/insight/content/doi/10.1108/02644409510799532/full/html (visited on 02/10/2020).

Murgia, Ilenia, Filippo Giadrossich, Zhun Mao, Denis Cohen, GianFranco Capra, and Massimiliano Schwarz (Accepted). "Modeling shallow landslides and root reinforcement: a review". In: *Ecological Engineering*.

Murgia, Ilenia, Filippo Giadrossich, Marco Niccolini, Federico Preti, Yamuna Giambastiani, Gian Franco Capra, and Denis Cohen (2021). "Using SlideforMAP and SOSlope to identify susceptible areas to shallow landslides in the Foreste Casentinesi National Park (Tuscany, Italy)". In: *EGU General Assembly Conference Abstracts*, EGU21–14454. URL: https://ui.adsabs.harvard.edu/abs/2021EGUGA..2314454M/abstract.

Nandi, A. and A. Shakoor (Jan. 2010). "A GIS-based landslide susceptibility evaluation using bivariate and multivariate statistical analyses". In: *Engineering Geology* 110.1, pp. 11–20. ISSN: 00137952. DOI: 10.1016/j.enggeo.2009.10.001. URL: https://linkinghub.elsevier.com/retrieve/pii/S0013795209002646 (visited on 07/14/2020).

Nefeslioglu, H A, E Sezer, C Gokceoglu, A S Bozkir, and T Y Duman (2009). "Assessment of Landslide Susceptibility by Decision Trees in the Metropolitan Area of Istanbul, Turkey". In: *Mathematical Problems in Engineering*, p. 16. DOI: https://doi.org/10.1155/2010/901095.

Nefeslioglu, H.A., C. Gokceoglu, and H. Sonmez (Apr. 2008). "An assessment on the use of logistic regression and artificial neural networks with different sampling strategies for the preparation of landslide susceptibility maps". In: *Engineering Geology* 97.3, pp. 171–191. ISSN: 00137952. DOI: 10.1016/j.enggeo.2008.01.004. URL: https://linkinghub.elsevier.com/retrieve/pii/S0013795208000148 (visited on 07/14/2020).

Neuville, Romain, Jordan Steven Bates, and François Jonard (Jan. 20, 2021). "Estimating Forest Structure from UAV-Mounted LiDAR Point Cloud Using Machine Learning". In: *Remote Sensing* 13.3, p. 352. ISSN: 2072-4292. DOI: 10.3390/rs13030352. URL: https://www.mdpi.com/2072-4292/13/3/352 (visited on 02/24/2022).

Nimmo, JR (2009). *Vadose Water*. https://wwwrcamnl.wr.usgs.gov/uzf/abs_pubs/papers/nimmo.09.vadosewater.eiw.pdf.

O'Callaghan, John F and David M Mark (1984). "The extraction of drainage networks from digital elevation data". In: *Computer vision, graphics, and image processing* 28.3, pp. 323–344.

Olami, Zeev, Hans Jacob S. Feder, and Kim Christensen (Feb. 24, 1992). "Self-organized criticality in a continuous, nonconservative cellular automaton modeling earthquakes". In: *Physical Review Letters* 68.8, pp. 1244–1247. ISSN: 0031-9007. DOI: 10.1103/PhysRevLett.68.1244. URL: https://link.aps.org/doi/10.1103/PhysRevLett.68.1244 (visited on 07/10/2020).

O'Loughlin, Colin Lockhart (1972). "Investigation of the stability of the steepland forest soils in the coast mountains, southwest British Columbia". PhD thesis. University of British Columbia.

Pack, Robert T, David G Tarboton, and Craig N Goodwin (1998). "The SINMAP approach to terrain stability mapping". In: URL: https://digitalcommons.usu.edu/cee_facpub/2583/.

Park, Hyuck Jin, Jung Hyun Lee, and Ik Woo (July 2013). "Assessment of rainfall-induced shallow landslide susceptibility using a GIS-based probabilistic approach". In: *Engineering Geology* 161, pp. 1–15. ISSN: 00137952. DOI: 10.1016/j.enggeo.2013.04.011. URL: https://linkinghub.elsevier.com/retrieve/pii/S0013795213001361 (visited on 12/22/2021).

Pelletier, Jon D., Bruce D. Malamud, Troy Blodgett, and Donald L. Turcotte (Dec. 1997). "Scale-invariance of soil moisture variability and its implications for the frequency-size distribution of landslides". In: *Engineering Geology* 48.3, pp. 255–268. ISSN: 00137952. DOI: 10.1016/S0013-7952(97)00041-0. URL: https://linkinghub.elsevier.com/retrieve/pii/S0013795297000410 (visited on 11/20/2020).

Penna, D., H. J. van Meerveld, O. Oliviero, G. Zuecco, R. S. Assendelft, G. Dalla Fontana, and M. Borga (Apr. 15, 2015). "Seasonal changes in runoff generation in a small forested mountain catchment". In: *Hydrological Processes* 29.8, pp. 2027–2042. ISSN: 08856087. DOI: 10.1002/hyp.10347. URL: https://onlinelibrary.wiley.com/doi/10.1002/hyp.10347 (visited on 03/15/2022).

Persichillo, Maria Giuseppina, Massimiliano Bordoni, and Claudia Meisina (Jan. 2017). "The role of land use changes in the distribution of shallow landslides". In: *Science of The Total Environment* 574, pp. 924–937. ISSN: 00489697. DOI: 10.1016/j.scitotenv.2016.09.125. URL: https://linkinghub.elsevier.com/retrieve/pii/S0048969716320551 (visited on 03/14/2022).

Phillips, Chris, Tristram Hales, Hugh Smith, and Les Basher (Dec. 2021). "Shallow landslides and vegetation at the catchment scale: A perspective". In: *Ecological Engineering* 173, p. 106436. ISSN: 09258574. DOI: 10.1016/j.ecoleng.2021.106436. URL: https://linkinghub.elsevier.com/retrieve/pii/S0925857421002913 (visited on 03/13/2022).

Piegari, E., V. Cataudella, R. Di Maio, L. Milano, and M. Nicodemi (2006). "A cellular automaton for the factor of safety field in landslides modeling". In: *Geophysical Research Letters* 33.1. ISSN: 1944-8007. DOI: 10.1029/2005GL024759. URL: https://agupubs.onlinelibrary.wiley.com/doi/abs/10.1029/2005GL024759 (visited on 12/15/2019).

Pollen, Natasha (2007). "Temporal and spatial variability in root reinforcement of streambanks: accounting for soil shear strength and moisture". In: *Catena* 69.3, pp. 197–205.

Pollen, Natasha and Andrew Simon (2005). "Estimating the Mechanical Effects of Riparian Vegetation on Stream Bank Stability Using a Fiber Bundle Model". In: *Water Resources Research* 41.7. ISSN: 1944-7973. DOI: 10.1029/2004WR003801.

Pollen-Bankhead, Natasha and Andrew Simon (Apr. 2010). "Hydrologic and hydraulic effects of riparian root networks on streambank stability: Is mechanical root-reinforcement the whole story?" In: *Geomorphology* 116.3, pp. 353–362. ISSN: 0169555X. DOI: 10.1016/j.geomorph.2009.11.013. URL: https://linkinghub.elsevier.com/retrieve/pii/S0169555X09004875 (visited on 05/11/2020).

Preti, Federico (Dec. 2013). "Forest protection and protection forest: Tree root degradation over hydrological shallow landslides triggering". In: *Ecological Engineering* 61, pp. 633–645. ISSN: 09258574. DOI: 10.1016/j.ecoleng.2012.11.009. URL: https://linkinghub.elsevier.com/retrieve/pii/S0925857412003503 (visited on 04/11/2020).

Rajapakse, Ruwan (Jan. 1, 2016). "26 - Geotechnical engineering software". In: *Geotechnical Engineering Calculations and Rules of Thumb (Second Edition)*. Ed. by Ruwan Rajapakse. Butterworth-Heinemann, pp. 269–276. ISBN: 978-0-12-804698-2. DOI: 10.1016/B978-0-12-804698-2.00026-X. URL: http://www.sciencedirect.com/science/article/pii/B978012804698200026X (visited on 12/24/2019).

Ran, Qihua, Yanyan Hong, Wei Li, and Jihui Gao (Aug. 2018). "A modelling study of rainfall-induced shallow landslide mechanisms under different rainfall characteristics". In: *Journal of Hydrology* 563, pp. 790–801. ISSN: 00221694. DOI: 10.1016/j.jhydrol.2018.06.040. URL: https://linkinghub.elsevier.com/retrieve/pii/S0022169418304621 (visited on 05/13/2020).

Rapp, Bastian E. (Jan. 2017). "Chapter 32 - Finite Element Method". In: *Microfluidics: Modelling, Mechanics and Mathematics*. Ed. by Bastian E. Rapp. Micro and Nano Technologies. Oxford: Elsevier, pp. 655–678. ISBN: 978-1-4557-3141-1. DOI: 10.1016/B978-1-4557-3141-1.50032-0. URL: http://www.sciencedirect.com/science/article/pii/B9781455731411500320 (visited on 12/24/2019).

Reginatto, G M P, M Maccarini, M Kobiyama, R A R Higashi, A Grando, C W Corseuil, and M L Caramez (2012). "SHALSTAB application to identify the susceptible areas of shallow landslide in Cunha river watershed, Rio Dos Cedros City SC, Brasil". In: p. 6. URL: http://mtc-m16c.sid.inpe.br/col/sid.inpe.br/mtc-m18/2012/05.16.20.05/doc/034.pdf.

Reichenbach, P., C. Busca, A. C. Mondini, and M. Rossi (Dec. 2014). "The Influence of Land Use Change on Landslide Susceptibility Zonation: The Briga Catchment Test Site (Messina, Italy)". In: *Environmental Management* 54.6, pp. 1372–1384. ISSN: 0364-152X, 1432-1009. DOI: 10.1007/s00267-014-0357-0. URL: http://link.springer.com/10.1007/s00267-014-0357-0 (visited on 10/19/2021).

Reichenbach, Paola, Mauro Rossi, Bruce D. Malamud, Monika Mihir, and Fausto Guzzetti (May 2018). "A review of statistically-based landslide susceptibility models". In: *Earth-Science Reviews* 180, pp. 60–91. ISSN: 00128252. DOI: 10.1016/j.earscirev.2018.03.001. URL: https://linkinghub.elsevier.com/retrieve/pii/S0012825217305652 (visited on 03/18/2021).

Reneau, SL and WE Dietrich (1987). "Size and location of colluvial landslides in a steep forested landscape". In: *IAHS-AISH publication* 165, pp. 39–48.

Rickli, Christian and Frank Graf (2009). "Effects of forests on shallow landslides – case studies in Switzerland". In: p. 13. URL: https://www.researchgate.net/profile/Christian-Rickli/publication/228691482_Effects_of_forests_on_shallow_landslides_-_Case_studies_in_Switzerland/links/0912f51125389149320000000/Effects-of-forests-on-shallow-landslides-Case-studies-in-Switzerland.pdf.

Riestenberg, Mary M and Susan Sovonick-Dunford (1983). "The role of woody vegetation in stabilizing slopes in the Cincinnati area, Ohio". In: *Geological Society of America Bulletin* 94.4, pp. 506–518.

Roering, Joshua J, Kevin M Schmidt, Jonathan D Stock, William E Dietrich, and David R Montgomery (Apr. 1, 2003). "Shallow landsliding, root reinforcement, and the spatial distribution of trees in the Oregon Coast Range". In: *Canadian Geotechnical Journal* 40.2, pp. 237–253. ISSN: 0008-3674, 1208-6010. DOI: 10.1139/t02-113. URL: http://www.nrcresearchpress.com/doi/10.1139/t02-113 (visited on 05/26/2020).

Rossi, G., F. Catani, L. Leoni, S. Segoni, and V. Tofani (Jan. 25, 2013). "HIRESSS: a physically based slope stability simulator for HPC applications". In: *Natural Hazards and Earth System Sciences* 13.1, pp. 151–166. ISSN: 1684-9981. DOI: 10.5194/nhess-13-151-2013. URL: https://nhess.copernicus.org/articles/13/151/2013/ (visited on 12/05/2020).

Rossi, Mauro, Fausto Guzzetti, Paola Reichenbach, Alessandro Cesare Mondini, and Silvia Peruccacci (Jan. 2010). "Optimal landslide susceptibility zonation based on multiple forecasts". In: *Geomorphology* 114.3, pp. 129–142. ISSN: 0169555X. DOI: 10.1016/j.geomorph.2009.06.020. URL: https://linkinghub.elsevier.com/retrieve/pii/S0169555X0900258X (visited on 07/13/2020).

Ruette, J. von von, P. Lehmann, and D. Or (2013). "Rainfall-triggered shallow landslides at catchment scale: Threshold mechanics-based modeling for abruptness and localization". In: *Water Resources Research* 49.10, pp. 6266–6285. ISSN: 1944-7973. DOI: 10.1002/wrcr.20418. URL: https://agupubs.onlinelibrary.wiley.com/doi/abs/10.1002/wrcr.20418 (visited on 12/10/2019).

Ruette, Jonas von, Andreas Papritz, Peter Lehmann, Christian Rickli, and Dani Or (Oct. 2011). "Spatial statistical modeling of shallow landslides—Validating predictions for different landslide inventories and rainfall events". In: *Geomorphology* 133.1, pp. 11–22. ISSN: 0169555X. DOI: 10.1016/j.geomorph.2011.06.010.

URL: https://linkinghub.elsevier.com/retrieve/pii/S0169555X11002984 (visited on 07/13/2020).

Salciarini, Diana, Jonathan W. Godt, William Z. Savage, Rex L. Baum, and Pietro Conversini (Dec. 2008). "Modeling landslide recurrence in Seattle, Washington, USA". In: *Engineering Geology* 102.3, pp. 227–237. ISSN: 00137952. DOI: 10.1016/j.enggeo.2008.03.013. URL: https://linkinghub.elsevier.com/retrieve/pii/S0013795208001865 (visited on 03/03/2022).

Salciarini, Diana, Jonathan W. Godt, William Z. Savage, Pietro Conversini, Rex L. Baum, and John A. Michael (Sept. 2006). "Modeling regional initiation of rainfall-induced shallow landslides in the eastern Umbria Region of central Italy". In: *Landslides* 3.3, pp. 181–194. ISSN: 1612-510X, 1612-5118. DOI: 10.1007/s10346-006-0037-0. URL: http://link.springer.com/10.1007/s10346-006-0037-0 (visited on 03/03/2022).

Sanavia, L., F. Pesavento, and B. A. Schrefler (Mar. 2006). "Finite element analysis of non-isothermal multiphase geomaterials with application to strain localization simulation". In: *Computational Mechanics* 37.4, pp. 331–348. ISSN: 0178-7675, 1432-0924. DOI: 10.1007/s00466-005-0673-6. URL: http://link.springer.com/10.1007/s00466-005-0673-6 (visited on 03/01/2022).

Sanavia, Lorenzo, Bertrand Francois, Roberto Bortolotto, Loris Luison, and Lyesse Laloui (2008). "Finite element modeling of thermo-elasto-plastic water saturated porous materials". In: p. 19. URL: https://www.researchgate.net/publication/37462650.

Savage, WZ, JW Godt, and RL Baum (2004). "Modeling time-dependent areal slope stability". In: *Landslides-Evaluation and Stabilization, Proceedings of the 9th International Symposium on Landslides, edited by: Lacerda, WA, Erlich, M., Fontoura, SAB, and Sayao, ASF, AA Balkema Publishers, London*. Vol. 1, pp. 23–36.

Schmidt, Jochen (2001). "The role of mass movements for slope evolution - conceptual approaches and model applications in the Bonn area". In: p. 313. URL: https://bonndoc.ulb.uni-bonn.de/xmlui/handle/20.500.11811/1725.

Schmidt, K M, J J Roering, J D Stock, W E Dietrich, D R Montgomery, and T Schaub (2001). "The variability of root cohesion as an influence on shallow landslide susceptibility in the Oregon Coast Range". In: 38, p. 30. DOI: https://doi.org/10.1139/t01-031.

Schwarz, M., D. Cohen, and D. Or (June 2011). "Pullout tests of root analogs and natural root bundles in soil: Experiments and modeling". In: *Journal of Geophysical Research: Earth Surface* 116 (F2). ISSN: 01480227. DOI: 10.1029/2010JF001753. URL: http://doi.wiley.com/10.1029/2010JF001753 (visited on 01/29/2019).

— (Oct. 2012a). "Spatial characterization of root reinforcement at stand scale: Theory and case study". In: *Geomorphology* 171-172, pp. 190–200. ISSN: 0169555X. DOI: 10.1016/j.geomorph.2012.05.020. URL: https://linkinghub.elsevier.com/retrieve/pii/S0169555X12002577 (visited on 01/31/2019).

Schwarz, M., F. Giadrossich, and D. Cohen (Nov. 6, 2013). "Modeling root reinforcement using a root-failure Weibull survival function". In: *Hydrology and Earth System Sciences* 17.11, pp. 4367–4377. ISSN: 1607-7938. DOI: 10.5194/hess-17-4367-2013. URL: https://hess.copernicus.org/articles/17/4367/2013/ (visited on 01/06/2022).

Schwarz, M., P. Lehmann, and D. Or (2010). "Quantifying Lateral Root Reinforcement in Steep Slopes – from a Bundle of Roots to Tree Stands". In: *Earth Surface Processes and Landforms* 35.3, pp. 354–367. ISSN: 1096-9837. DOI: 10.1002/esp.1927.

Schwarz, M., A. Rist, D. Cohen, F. Giadrossich, P. Egorov, D. Büttner, M. Stolz, and J.-J. Thormann (2015). "Root reinforcement of soils under compression". In: *Journal of Geophysical Research: Earth Surface* 120.10, pp. 2103–2120. ISSN: 2169-9011. DOI: 10.1002/2015JF003632. URL: https://agupubs.onlinelibrary.wiley.com/doi/abs/10.1002/2015JF003632 (visited on 10/29/2019).

Schwarz, Massimiliano, Jean-Jacques Thormann, Kaspar Zürcher, and Karin Feller (2012b). "Quantifying root reinforcement in protection forests: implications for slope stability and forest management". In: p. 12.

Segre, Enrico, Istituto di Cosmogeofisica, CNR, Torino, Italy, Chiara Deangeli, Dipartimento di Georisorse e Territorio, Politecnico, Torino, and Italy (Feb. 1995). "Cellular Automaton for Realistic Modelling of Landslides". In: *arXiv:comp-gas/9407002*. URL: http://arxiv.org/abs/comp-gas/9407002 (visited on 12/27/2019).

Seibert, Jan and Brian L McGlynn (2007). "A new triangular multiple flow direction algorithm for computing upslope areas from gridded digital elevation models". In: *Water resources research* 43.4.

Selby, MJ (1993). *Hillslope Materials and Processes Oxford Univ.Press*.

Shao, Wei, Thom Bogaard, Mark Bakker, and Matteo Berti (Dec. 2016). "The influence of preferential flow on pressure propagation and landslide triggering of the Rocca Pitigliana landslide". In: *Journal of Hydrology* 543, pp. 360–372. ISSN: 00221694. DOI: 10.1016/j.jhydrol.2016.10.015. URL: https://linkinghub.elsevier.com/retrieve/pii/S0022169416306588 (visited on 05/12/2021).

Sidle, Roy C. and Thom A. Bogaard (Aug. 2016). "Dynamic earth system and ecological controls of rainfall-initiated landslides". In: *Earth-Science Reviews* 159, pp. 275–291. ISSN: 00128252. DOI: 10.1016/j.earscirev.2016.05.013. URL: https://linkinghub.elsevier.com/retrieve/pii/S0012825216301015 (visited on 02/25/2022).

Sidle, Roy C. and Hirotaka Ochiai (2006). *Landslides: processes, prediction and land use*. Water resources monograph 18. Washington (D.C.): American geophysical union. ISBN: 978-0-87590-322-4.

Silva-protect project in Switzerland (2016). https://www.bafu.admin.ch/bafu/de/home/themen/naturgefahren/fachinformationen/naturgefahrensituation-und-raumnutzung/gefahrengrundlagen/silvaprotect-ch.html. Accessed: 2022-02-22.

Simoni, Silvia, Fabrizio Zanotti, Giacomo Bertoldi, and Riccardo Rigon (2008). "Modelling the probability of occurrence of shallow landslides and channelized debris flows using GEOtop-FS". In: *Hydrological Processes* 22.4, pp. 532–545. ISSN: 1099-1085. DOI: 10.1002/hyp.6886. URL: https://onlinelibrary.wiley.com/doi/abs/10.1002/hyp.6886 (visited on 12/29/2019).

Springman, Sarah, Peter Kienzler, Francesca Casini, and Amin Askarinejad (2009). "Landslide triggering experiment in a steep forested slope in Switzerland". In: TRAMM, p. 4.

Spyrakos, Constantine C (1994). *Finite Element Modeling*. West Virginia Univ. Press.

Stokes, Alexia, Grant B. Douglas, Thierry Fourcaud, Filippo Giadrossich, Clayton Gillies, Thomas Hubble, John H. Kim, Kenneth W. Loades, Zhun Mao, Ian R. McIvor, Slobodan B. Mickovski, Stephen Mitchell, Normaniza Osman, Chris Phillips, Jean Poesen, Dave Polster, Federico Preti, Pierre Raymond, Freddy Rey, Massimiliano Schwarz, and Lawrence R. Walker (Apr. 2014). "Ecological mitigation of hillslope instability: ten key issues facing researchers and practitioners". In: *Plant and Soil* 377.1, pp. 1–23. ISSN: 0032-079X, 1573-5036. DOI: 10.1007/s11104-014-2044-6. URL: http://link.springer.com/10.1007/s11104-014-2044-6 (visited on 12/14/2021).

Sulsky, Deborah, Zhen Chen, and Howard L Schreyer (1994). "A particle method for history-dependent materials". In: *Computer methods in applied mechanics and engineering* 118.1-2, pp. 179–196. DOI: https://doi.org/10.1016/0045-7825(94)90112-0.

Swanson, Frederick J and Douglas N Swanston (1977). "Complex mass-movement terrains in the western Cascade Range, Oregon". In: *Reviews in Engineering Geology* 3, pp. 113–124. URL: https://andrewsforest.oregonstate.edu/sites/default/files/lter/pubs/pdf/pub521.pdf.

Świtała, BM (2016). *Analysis of slope stabilisation with soil bioengineering methods*. URL: https://epub.boku.ac.at/obvbokhs/content/structure/1931600?lang=de.

Süzen, Mehmet Lütfi and Vedat Doyuran (Mar. 1, 2004a). "A comparison of the GIS based landslide susceptibility assessment methods: multivariate versus bivariate". In: *Environmental Geology* 45.5, pp. 665–679. ISSN: 0943-0105, 1432-0495. DOI: 10.1007/s00254-003-0917-8. URL: http://link.springer.com/10.1007/s00254-003-0917-8 (visited on 07/16/2020).

— (Feb. 2004b). "Data driven bivariate landslide susceptibility assessment using geographical information systems: a method and application to Asarsuyu catchment, Turkey". In: *Engineering Geology* 71.3, pp. 303–321. ISSN: 00137952. DOI: 10.1016/S0013-7952(03)00143-1. URL: https://linkinghub.elsevier.com/retrieve/pii/S0013795203001431 (visited on 07/14/2020).

Tamagnini, R (2004). "An extended Cam-clay model for unsaturated soils with hydraulic hysteresis". In: *Géotechnique* 54.3, pp. 223–228. DOI: https://doi.org/10.1680/geot.2004.54.3.223.

Tarboton, David G (1997). "A new method for the determination of flow directions and upslope areas in grid digital elevation models". In: *Water resources research* 33.2, pp. 309–319.

Terzaghi, K (1943). "1943, Theoretical Soil Mechanics, John Wiley & Sons, New York". In.

Thomas, Robert E. and Natasha Pollen-Bankhead (Jan. 2010). "Modeling root-reinforcement with a fiber-bundle model and Monte Carlo simulation". In: *Ecological Engineering* 36.1, pp. 47–61. ISSN: 09258574. DOI: 10.1016/j.ecoleng.2009.09.008. URL: https://linkinghub.elsevier.com/retrieve/pii/S092585740900250X (visited on 05/11/2020).

Tofani, V, G. Bicocchi, G. Rossi, S. Segoni, M. D'Ambrosio, N. Casagli, and F. Catani (Apr. 2017). "Soil characterization for shallow landslides modeling: a case study in the Northern Apennines (Central Italy)". In: *Landslides* 14.2, pp. 755–770. ISSN: 1612-510X, 1612-5118. DOI: 10.1007/s10346-017-0809-8. URL: http://link.springer.com/10.1007/s10346-017-0809-8 (visited on 03/20/2021).

United State Geological Survey, USGS (2004). https://pubs.usgs.gov/fs/2004/3072/pdf/fs2004-3072.pdf. Accessed: 2022-02-22.

Vapnik, Vladimir (2013). *The nature of statistical learning theory*. Springer science & business media.

Vergani, C, F Giadrossich, P Buckley, M Conedera, M Pividori, F Salbitano, Hs Rauch, R Lovreglio, and M Schwarz (Apr. 2017a). "Root reinforcement dynamics of European coppice woodlands and their effect on shallow landslides: A review". In: *Earth-Science Reviews* 167, pp. 88–102. ISSN: 00128252. DOI: 10.1016/j.earscirev.2017.02.002. URL: https://linkinghub.elsevier.com/retrieve/pii/S0012825216301611 (visited on 01/29/2019).

Vergani, Chiara, Massimiliano Schwarz, Mattia Soldati, Andrea Corda, Filippo Giadrossich, Enrico A. Chiaradia, Paola Morando, and Chiara Bassanelli (Aug. 2016). "Root reinforcement dynamics in subalpine spruce forests following timber harvest: a case study in Canton Schwyz, Switzerland". In: *CATENA* 143, pp. 275–288. ISSN: 03418162. DOI: 10.1016/j.catena.2016.03.038. URL: https://linkinghub.elsevier.com/retrieve/pii/S0341816216301175 (visited on 03/18/2022).

Vergani, Chiara, Mario Werlen, Marco Conedera, Denis Cohen, and Massimiliano Schwarz (Sept. 2017b). "Investigation of root reinforcement decay after a forest fire in a Scots pine (Pinus sylvestris) protection forest". In: *Forest Ecology and Management* 400, pp. 339–352. ISSN: 03781127. DOI: 10.1016/j.foreco.2017.06.005. URL: https://linkinghub.elsevier.com/retrieve/pii/S0378112716312646 (visited on 09/28/2019).

Vertessy, RA, WRJ Dawes, L Zhang, TJ Hatton, and J Walker (1996). "Catchment-scale hydrologic modelling to assess the water and salt balance behaviour of eucalypt plantations". In.

Waldron, LJ (1977). "The shear resistance of root-permeated homogeneous and stratified soil". In: *Soil Science Society of America Journal* 41.5, pp. 843–849. DOI: https://doi.org/10.2136/sssaj1977.03615995004100050005x.

Waldron, LJ and Suren Dakessian (1981). "Soil reinforcement by roots: calculation of increased soil shear resistance from root properties". In: *Soil science* 132.6, pp. 427–435.

Wu, Tien H (1976). *Investigation of landslides on prince of Wales Island, Alaska*. Ohio State University.

Wu, Tien H., William P. McKinnell III, and Douglas N. Swanston (Feb. 1979). "Strength of Tree Roots and Landslides on Prince of Wales Island, Alaska". In: *Canadian Geotechnical Journal* 16.1, pp. 19–33. ISSN: 0008-3674, 1208-6010. DOI: 10.1139/t79-003.

Wu, Weimin and Roy C. Sidle (Aug. 1995). "A Distributed Slope Stability Model for Steep Forested Basins". In: *Water Resources Research* 31.8, pp. 2097–2110. ISSN: 00431397. DOI: 10.1029/95WR01136. URL: http://doi.wiley.com/10.1029/95WR01136 (visited on 05/30/2021).

Yamase, Keitaro, Toko Tanikawa, Masako Dannoura, Chikage Todo, Tomonori Yamamoto, Hidetoshi Ikeno, Mizue Ohashi, Kenji Aono, Ryuusei Doi, and Yasuhiro Hirano (Dec. 2019). "Estimating slope stability by lateral root reinforcement in thinned and unthinned stands of Cryptomeria japonica using ground-penetrating radar". In: *CATENA* 183, p. 104227. ISSN: 03418162. DOI: 10.1016/j.catena.2019.104227. URL: https://linkinghub.elsevier.com/retrieve/pii/S0341816219303698 (visited on 04/20/2020).

Yeon, Young-Kwang, Jong-Gyu Han, and Keun Ho Ryu (Nov. 2010). "Landslide susceptibility mapping in Injae, Korea, using a decision tree". In: *Engineering Geology* 116.3. CART, pp. 274–283. ISSN: 00137952. DOI: 10.1016/j.enggeo.2010.09.009. URL: https://linkinghub.elsevier.com/retrieve/pii/S0013795210001857 (visited on 01/19/2021).

Yildiz, A., F. Graf, C. Rickli, and S.M. Springman (July 2018). "Determination of the shearing behaviour of root-permeated soils with a large-scale direct shear apparatus". In: *CATENA* 166, pp. 98–113. ISSN: 03418162. DOI: 10.1016/j.catena.2018.03.022. URL: https://linkinghub.elsevier.com/retrieve/pii/S0341816218301048 (visited on 01/17/2021).

Yilmaz, Işık (June 2009). "Landslide susceptibility mapping using frequency ratio, logistic regression, artificial neural networks and their comparison: A case study from Kat landslides (Tokat—Turkey)". In: *Computers & Geosciences* 35.6, pp. 1125–1138. ISSN: 00983004. DOI: 10.1016/j.cageo.2008.08.007. URL: https://linkinghub.elsevier.com/retrieve/pii/S0098300408002665 (visited on 07/14/2020).

Yu, H. S., R. Salgado, S. W. Sloan, and J. M. Kim (Jan. 1998). "Limit Analysis versus Limit Equilibrium for Slope Stability". In: *Journal of Geotechnical and Geoenvironmental Engineering* 124.1, pp. 1–11. ISSN: 1090-0241, 1943-5606. DOI: 10.1061/

(ASCE)1090-0241(1998)124:1(1). URL: http://ascelibrary.org/doi/10.1061/%28ASCE%291090-0241%281998%29124%3A1%281%29 (visited on 05/17/2021).

Zadelhoff, Feiko Bernard van, Adel Albaba, Denis Cohen, Chris Phillips, Bettina Schaefli, Lucas Karel Agnes Dorren, and Massimiliano Schwarz (May 25, 2021a). *Introducing SlideforMap; a probabilistic finite slope approach for modelling shallow landslide probability in forested situations*. preprint. Landslides and Debris Flows Hazards. DOI: 10.5194/nhess-2021-140. URL: https://nhess.copernicus.org/preprints/nhess-2021-140/ (visited on 08/25/2021).

— (2021b). "Introducing SlideforMap; a probabilistic finite slope approach for modelling shallow landslide probability in forested situations". In: *Natural Hazards and Earth System Sciences Discussions*, pp. 1–33.

Zheng, Wenbo, Xiaoying Zhuang, Dwayne D. Tannant, Yongchang Cai, and Samuel Nunoo (Sept. 2014). "Unified continuum/discontinuum modeling framework for slope stability assessment". In: *Engineering Geology* 179, pp. 90–101. ISSN: 00137952. DOI: 10.1016/j.enggeo.2014.06.014. URL: https://linkinghub.elsevier.com/retrieve/pii/S0013795214001471 (visited on 03/01/2022).

Zhou, Yue, David Watts, Yuhui Li, and Xiaoping Cheng (Apr. 1998). "A case study of effect of lateral roots of Pinus yunnanensis on shallow soil reinforcement". In: *Forest Ecology and Management* 103.2, pp. 107–120. ISSN: 03781127. DOI: 10.1016/S0378-1127(97)00216-8. URL: https://linkinghub.elsevier.com/retrieve/pii/S0378112797002168 (visited on 10/29/2019).

Zhu, H., L.M. Zhang, T. Xiao, and X.Y. Li (May 2017). "Enhancement of slope stability by vegetation considering uncertainties in root distribution". In: *Computers and Geotechnics* 85, pp. 84–89. ISSN: 0266352X. DOI: 10.1016/j.compgeo.2016.12.027. URL: https://linkinghub.elsevier.com/retrieve/pii/S0266352X16303342 (visited on 06/07/2020).

Ziemer, Robert R (1981). "The Role of Vegetation in the Stability of Forested Slopes". In: p. 13. URL: https://www.fs.fed.us/psw/publications/ziemer/ZiemerIUFRO1981.PDF.

Świtała, B. M., A. Askarinejad, W. Wu, and S. M. Springman (May 2018). "Experimental validation of a coupled hydro-mechanical model for vegetated soil". In: *Géotechnique* 68.5, pp. 375–385. ISSN: 0016-8505, 1751-7656. DOI: 10.1680/jgeot.16.P.233. URL: https://www.icevirtuallibrary.com/doi/10.1680/jgeot.16.P.233 (visited on 06/01/2020).

Świtała, Barbara Maria, Wei Wu, and Shun Wang (Aug. 2019). "Implementation of a coupled hydro-mechanical model for root-reinforced soils in finite element code". In: *Computers and Geotechnics* 112, pp. 197–203. ISSN: 0266352X. DOI: 10.1016/j.compgeo.2019.04.015. URL: https://linkinghub.elsevier.com/retrieve/pii/S0266352X1930117X (visited on 03/01/2022).

La borsa di dottorato è stata cofinanziata con risorse del
Programma Operativo Nazionale Ricerca e Innovazione 2014-2020 (CCI 2014IT16M2OP005),
Fondo Sociale Europeo, Azione I.1 “Dottorati Innovativi con caratterizzazione Industriale”

UNIONE EUROPEA
Fondo Sociale Europeo